DLR-IB-RM-OP-2022-06

Benchmarking and Validation for Nonlinear Mode Analysis

Master's thesis

Niklas Fittkau

Deutsches Zentrum für Luft- und Raumfahrt
Institut für Robotik und Mechatronik

Deutsches Zentrum
DLR für Luft- und Raumfahrt

HEINZ NIXDORF INSTITUT
UNIVERSITÄT PADERBORN

Master Thesis

Industrial Engineering in Mechanical Engineering

Benchmarking and Validation for Nonlinear Mode Analysis

submitted by

Niklas Fittkau
Matriculation No.: 7129324

Supervisors:

Prof. Dr.-Ing. habil. Ansgar Trächtler (UPB)
Prof. Dr.-Ing. Alin Albu-Schäffer (DLR)
Dr.-Ing. Julia Timmermann (UPB)
M.Sc. Annika Schmidt (DLR)
M.Sc. Arne Sachtler (DLR)

Paderborn, 28.10.2022

Master Thesis

Benchmarking and Validation for Nonlinear Mode Analysis
on: 28.10.2022

Heinz Nixdorf Institut
Universität Paderborn
Regelungstechnik und Mechatronik
Prof. Dr.-Ing. habil. Ansgar Trächtler (UPB)
Fürstenallee 11
33102 Paderborn

Deutsches Zentrum für Luft- und Raumfahrt e.V.
Institut für Robotik und Mechatronik
Prof. Dr.-Ing. Alin Albu-Schäffer
Münchener Str. 20
82234 Weßling

Benchmarking and Validation for Nonlinear Mode Analysis

Master Thesis Topic Proposal for Niklas Fittkau

Annika Schmidt and Arne Sachtler

January 12, 2022

1 Project Background

Although seemingly easy, recreating the stability and energy efficiency of mammalian locomotion is still a major challenge for robotics. Especially for highly-dynamic gaits, such as running or hopping, correctly orchestrating the interaction of all limbs and supporting a continuous movement is needed to achieve stable motions. For this, mammals do not only rely on control through the Central Nervous System, but have also evolved in a way that their body dynamics are optimized to support the locomotion in the encountered environment in an energy efficient manner [1]. Analogously, it has been shown for robotics that inherently stable and energy efficient motions can be achieved when exploiting the intrinsic dynamics of a system [2]. Building upon this knowledge, Gan and Remy [3] have shown that even different gaits can be realized on a conceptual quadruped with elastic legs and that the choice of gait depends on the desired locomotion speed [4].
One way to characterize intrinsic dynamics is through mode analysis. Linear systems exhibit linear eigemodes, i.e., every oscillation of linear second-order conservative systems can be decomposed into the sum of base oscillations along the eigenmodes. This property is called superposition of eigenmodes. As a consequence these eigenmodes have useful properties. In particular, the eigenspaces associated to the eigenmodes of the system are invariant with respect to the system dynamics. When the system is oscillating on an eigenmode, it will indefinitely continue to do so, i.e., its state will stay within the eigenspace. These linear eigenmodes provide continuous families of structured oscillations for every energy level.
However, the eigenmode analysis is only possible for linear dynamical systems. In recent works, the notion of nonlinear eigenmodes has been introduced to the robotics community [5, 6, 7]. These publications aim at extending the notion of (linear) eigenmodes to nonlinear systems. It turns out that not all of the properties of linear eigenmodes can be kept in this process. More particularly, the superposition principle is dropped from nonlinear eigenmodes. A nonlinear eigenmode can be thought of a curved version of eigenspaces called eigenmanifolds. Just like eigenspaces, eigenmanifolds are subspaces of the state space containing the equilibrium, which are invariant with respect to the system dynamics. They can be thought of as continuous families of natural oscillations, which contain an oscillation for every energy level.

Figure 1: The quadruped Bert is equipped with elasticity in the joints. The goal is to exploit the natural dynamics of the system to perform locomotion.

With the goal to investigate the nonlinear normal modes and their use for quadrupedal locomotion, the German Aerospace Center has developed Bert [8], which is depicted in Fig. 1. In simulation and corresponding hardware setup, it serves as test platform to identify (nonlinear) normal modes and to develop control strategies that ideally support these inherent dynamics. This research is being carried out under the supervision of Prof. Dr. Alin Albu-Schäffer in a cooperation between TU Munich and DLR.

2 Goals

The next goals for our project are the derivation of the nonlinear normal modes for the quadruped Bert. For this purpose, a tool has already been developed, which is capable of analyzing serial robots. However, in a first step the tool needs to be extended to be applicable to parallel kinematics. In this context, it is especially interesting to investigate how different parameters such as mass distribution, spring stiffness, kinematics or damping influence the normal modes. In order to take a step, individual feet need to be lifted, which causes the system to exhibit hybrid dynamics. To match the phases of the swing and stance phases of different legs, it could be investigated how the mechanics of the system need to be adjusted so that periodic modal oscillations arise that can be exploited for locomotion. Another goal would be to examine how different modes can be combined to generate an overall gait pattern. It would also be interesting to inspect the stability and robustness of individual modes in order to scope their suitability for locomotion. Eventually the validity of derived nonlinear normal modes should be cross-checked with a multi-body simulation, i.e., Gazebo, and the corresponding hardware of the robot.
Within the suggested master thesis, not all of the above mentioned goals need to be achieved and the focus will depend on individual capability and interest.

3 Skills

- fluent in English and German
- basic knowledge of (non-)linear mode theory
- practical experience with robotic hardware and distributed systems
- good programming skills with matlab
- basic programming skills with python/C++
- knowledge of Linux and git
- general understanding of multi-body dynamics
- LaTeX
- independent problem solving
- critical thinking ability

Topic approved

(date, signature, institutional stamp)

References

[1] H. Geyer and H. Herr, "A muscle-reflex model that encodes principles of legged mechanics produces human walking dynamics and muscle activities," *IEEE Transactions on neural systems and rehabilitation engineering*, vol. 18, no. 3, pp. 263–273, 2010.

[2] N. Kashiri, A. Abate, S. J. Abram, A. Albu-Schaffer, P. J. Clary, M. Daley, S. Faraji, R. Furnemont, M. Garabini, H. Geyer, A. M. Grabowski, J. Hurst, J. Malzahn, G. Mathijssen, D. Remy, W. Roozing, M. Shahbazi, S. N. Simha, J.-B. Song, N. Smit-Anseeuw, S. Stramigioli, B. Vanderborght, Y. Yesilevskiy, and N. Tsagarakis, "An overview on principles for energy efficient robot locomotion," *Frontiers in Robotics and AI*, vol. 5, no. 129, 2018.

[3] Z. Gan and C. D. Remy, "A passive dynamic quadruped that moves in a large variety of gaits," in *IEEE/RSJ International Conference on Intelligent Robots and Systems*, pp. 4876–4881, 2014.

[4] W. Xi, Y. Yesilevskiy, and C. D. Remy, "Selecting gaits for economical locomotion of legged robots," *The International Journal of Robotics Research*, vol. 35, no. 9, pp. 1140–1154, 2016.

[5] A. Albu-Schäffer and C. Della Santina, "A review on nonlinear modes in conservative mechanical systems," *Annual Reviews in Control*, vol. 50, pp. 49 – 71, 2020.

[6] A. Albu-Schäffer, D. Lakatos, and S. Stramigioli, "Strict nonlinear normal modes of systems characterized by scalar functions on riemannian manifolds," *IEEE Robotics and Automation Letters*, vol. 6, no. 2, pp. 1910–1917, 2021.

[7] D. Lakatos, W. Friedl, and A. Albu-Schäffer, "Eigenmodes of nonlinear dynamics: Definition, existence, and embodiment into legged robots with elastic elements," *IEEE Robotics and Automation Letters*, vol. 2, no. 2, pp. 1062–1069, 2017.

[8] D. Lakatos, K. Ploeger, F. Loeffl, D. Seidel, F. Schmidt, T. Gumpert, F. John, T. Bertram, and A. Albu-Schäffer, "Dynamic locomotion gaits of a compliantly actuated quadruped with slip-like articulated legs embodied in the mechanical design," *IEEE Robotics and Automation Letters*, vol. 3, no. 4, pp. 3908–3915, 2018.

Statement:

I hereby declare that I have prepared this thesis independently and without unauthorized outside assistance, that I have not used any sources or aids other than those indicated, and that I have marked as such any passages taken verbatim or in substance from the sources used.

Erklärung:

Hiermit erkläre ich, dass ich die vorliegende Arbeit selbstständig und ohne unerlaubte fremde Hilfe angefertigt, keine anderen als die angegebenen Quellen und Hilfsmittel benutzt und die den benutzten Quellen wörtlich oder inhaltlich entnommenen Stellen als solche kenntlich gemacht habe.

Paderborn, 28.10.2022

Abstract

One research focus at the Robotics and Mechatronics Center of the German Aerospace Center in Oberpfaffenhofen is the improvement of robotic locomotion capabilities. Therefore, natural role models are analyzed. As an inspiration, mammalian locomotion is analyzed, which is unmatched in its energy efficiency and adaptility due to the opitmal integration of control strategies and intrinsic body dynamics. In an attempt to recreate this integration in robotic hardware, the compliant quadruped Bert has been developed and built as a test platform. As a contribution towards this goal, this thesis investigates the excitation of nonlinear intrinsic motions of one individual leg of the robot Bert. Springs in the joints of the leg enable dynamic motions. As first approach to model the individual leg in Matlab for the controller design process, an elastic double pendulum is set up. This is followed by the consideration of different modelling methods such as the Pfaffian constraints method and the active joints method. These methods lead to a leg model. For the analysis of the intrinsic dynamics, the concept of nonlinear normal modes is used which was recently explored and published by the German Aerospace Center. After the nonlinear normal modes for the leg are computed, the influence of parameter variation on the shapes of manifold and generators is evaluated. Subsequently, a nonlinear normal mode is found that is a prominate candidate to excite an energy efficient hopping motion in the oneleg of Bert. To initialize and stabilize the modal oscillation, a position mode controller is evolved from an existing torque mode controller. After the control framework is set up, tests are performed in the 3D physics simulation software Gazebo with a digital twin of the Bert leg. The experiments showed that some modifications will be needed for the implementation of the developed position controller to work on the real hardware of the Bert leg. Nevertheless, the simulation experiments also showed that the controller is capable to stabilize modal oscillations with little control effort in an idealized system proving the developed control strategy to be highly energy efficient. As a result, this thesis takes another step towards the use of intrinsic system dynamics in the field of robotics based on natural role models.

Zusammenfassung

Die Verbesserung der Fortbewegungsfähigkeiten von Robotern ist ein zentrales Forschungsthema am Institut für Robotik und Mechatronik, Teil des Deutschen Zentrums für Luft- und Raumfahrt in Oberpfaffenhofen. Dazu werden Vorbilder aus der Natur analysiert. Ziel ist es, die hohe Energieeffizienz der Lokomotion von Säugetieren, die aus der optimalen Nutzung der intrinsischen Dynamik des Körpers resultiert, auf den Bereich der Robotik zu übertragen. Um sowohl die Auslegung der intrinsischen Dynamik als auch entsprechende Regelungsstrategien für deren Anregung zu erforschen, wurde der Roboter Bert gebaut. Um dieses weitreichende Ziel zu erreichen, fokussiert sich diese Arbeit auf die Untersuchung eines einzelnen Beins des Roboters Bert. Dieses Bein besteht aus zwei Gelenken, die jeweils von einem Motor angetrieben werden, die über eine Feder mit dem Link verbunden sind. Die Federn in den Gelenken des Beins ermöglichen dynamische Bewegungen. Um das Bert Bein für die Entwicklung einer Regelungsstrategie in Matlab zu modellieren, wird zunächst ein elastisches Doppelpendel aufgesetzt. Es folgt die Betrachtung verschiedener Modellierungsmethoden wie die Pfaffian constraints Methode und die Methode der aktiven Gelenke. Diese Methoden führen zu einem Beinmodell. Für die Analyse der Eigendynamik wird das Konzept der nichtlinearen Normalmoden verwendet, das kürzlich vom Deutschen Zentrum für Luft- und Raumfahrt erforscht und veröffentlicht wurde. Nachdem die nichtlinearen Normalmoden für das Bein identifiziert wurden, wird der Einfluss von Parametervariationen auf die Formen von Mannigfaltigkeit und Generatoren bewertet. Anschließend wird eine nichtlineare Normalmode gefunden, die eine springende Bewegung für das Bein ermöglicht, wenn eine entsprechende modale Oszillation durchgeführt wird. Zur Initialisierung und Stabilisierung der modalen Oszillation wird ein Positionsmodenregler aus einem bestehenden Drehmomentregler entwickelt. Nachdem die Regelungsumgebung aufgebaut ist, werden Tests in der 3D Physiksimulationssoftware Gazebo mit einem digitalen Zwilling des Bert Beins durchgeführt. Auch wenn in diesen Versuchen deutlich wird, dass eine Anpassung des Reglers für die Übertragung auf echte Hardware nötig ist, zeigt die Simulation, dass der entwickelte Regler modale Oszillationen mit einer hohen Energieeffizienz für ein Bein des Roboters Bert stabilisieren kann. Die in dieser Arbeit erarbeiteten Ergebnisse sind somit ein wichtiger weiterer Schritt, um letztendlich die intrinsische Dynamik robotischer Systeme mit entsprechenden Regelungsstrategien auszunutzen, um letztendlich auch Robotern die Lokomotionsfähigkeiten natürlicher Vorbilder zu ermöglichen.

Benchmarking and Validation for Nonlinear Mode Analysis

Contents

Appendix

List of abbreviations

1D, 2D, 3D, ...	1 dimensional, 2 dimensional, 3 dimensional, ...
CTH	Constant target heading
DLR	German Aerospace Center
DoF	Degrees of freedom
e.g.	for example
i.e.	that means
LWR	Light weight robot
PDW	Passive dynamic walker
SEA	Serial elastic actuator

List of symbols

Name	Description	Unit
B	Coordinate System of the Bert leg model	–
DoF	Degrees of freedom	–
E	Total energy	J
I	Coordinate System of the inverted pendulum	–
J_{joints}	Number of joints	–
L	Lagrange equation	–
N_{links}	Number of links	–
P	Coordinate System of the elastic double pendulum	–
S	Coordinate System of the slider crank	–
T	Kinetic energy	J
V	Potential energy	J
α_D	Manifold stabilizer gain	–
δ	Dfference	–
γ_I	Energy controller integrator gain	–
γ_P	Energy controller gain	–
γ	Nonlinear normal mode	–
λ	Relative magnitude of the forces of Pfaffian constraints	–
$\mathfrak{M}_{pc}$	Manifold point cloud representation	–
$\mathfrak{M}$	Manifold	–
$\mathfrak{R}$	Generator	–
ω	Eigenfrequency	Hz
$\overline{E}$	Desired energy	J
τ_1	External input torque in joint one	Nm
τ_2	External input torque in joint two	Nm
φ_1	Angle corresponding to joint one	rad
φ_2	Angle corresponding to joint two	rad
φ_3	Angle corresponding to joint three	rad
$\underline{A}$	Pfaffian constraints base vector	–
$\underline{C}$	Coriolis and Centrifugal matrix	–
$\underline{F}$	External forces vector	–
$\underline{M}$	Mass matrix	–
$\underline{N}$	Potential and kinematic forces vector	–
$\underline{V}_{Grav}$	Gravitational potential	–
$\underline{\dot{x}}$	Velocity space state vector	rads^{-1}

Name	Description	Unit
$\underline{\tau}_E$	Energy torque vector	Nm
$\underline{\tau}_M$	Manifold torque vector	Nm
$\underline{\tau}$	Torque vector	Nm
$\underline{g}$	Gravity vector	–
$\underline{k}_{eq}$	Vector of spring equilibria	m
$\underline{x}$	Configuration space state vector	rad
d_1	Damping constant joint one	$\mathrm{kgm^2s^{-1}}$
d_2	Damping constant joint two	$\mathrm{kgm^2s^{-1}}$
$f_{freedom}$	Number of freedoms provided, e.g. by a joint	–
g	Gravity acceleration	$\mathrm{ms^{-2}}$
i	Counting variable	–
k_1	Stiffness of spring one	$\mathrm{kgs^{-2}}$
k_2	Stiffness of spring two	$\mathrm{kgs^{-2}}$
$k_{1,eq}$	Spring equilibrium one	rad
$k_{2,eq}$	Spring equilibrium two	rad
k	Counting variable	–
l_1	Lenght of link one	m
l_2	Lenght of link two	m
l_3	Lenght of link three	m
$l_{c,1}$	Position of mass one along link one	m
$l_{c,2}$	Position of mass two along link two	m
m_1	Mass one, closest to the base	kg
m_2	Mass two, counted from the base	kg
m_3	Mass three, counted from the base	kg
m_{plane}	Number of freedoms provdided by the chosen plane	–
n	System dimension	–
p_{eq}	Example equilibrium point/number	–
p	Example point/number	–
s	Position of the slider mass	–
t	Time	s

1 Introduction

Although seemingly easy for mammals, locomotion still poses a challenge for robotic systems. Different methods have already been established that enable robots to overcome difficult terrain. However, the robustness and energy efficiency of mammalian locomotion is still unmatchend. It is therefore suggestible to take biology as an inspiration to improve the locomotion skills of robotic systems.

Following this idea, the robot Bert has been developed at the German Aerospace Center (DLR). Bert is a four-legged robot, so-called quadruped, that was built as a test platform to investigate mechanical and control aspects of naturally arising gaits for robotic systems. The eight degrees of freedom (DoF) version of this robot is shown in Figure 1-1. In this version, each of the four legs of Bert has two links connected by two actuated joints, denoted as hip and knee, repectively. Each joint is driven through a serial elastic actuator (SEA), i.e. the motors are connected to the links via a mechanical spring. This enables the system to store energy, similar to the functioning of muscles in biology. To facilitate a rapid-prototyping-concept, Bert was developed as a low-cost system to enable continuously improvement and replacement of components in the research progresses.

Figure 1-1: *The robot Bert in the version called Greybert. The quadruped was developed at the DLR as a low-cost rapid prototyping platform for research on the transfer of natural locomotion to the field of robotics.*

The mechanics of Bert were developed in a way that defined intrinsic oscillations arise. It is the goal of this thesis to exploit these intrinsic motions for locomotion by stabilizing them through corrsponding control algorithms. To give an introduction on this work, the following sections outline the problem statement and objectives for this thesis and as well give an overview on the approach and structure.

1.1 Problem statement

As with most real systems, Bert's mechanics are highly nonlinear. Nevertheless intrinsic periodic motion patterns can be numerically found and mathematically expressed. These so-called nonlinear normal modes, are highly dependent on the systems configuration e.g. regarding the mass distribution or the spring stiffnesses. Moreover, modes are influenced by dissipation. Considering the robot Bert specifically, the calculations of the modes increases in complexity because of the parallel kinematics.

Suitable control strategies to sufficiently suppert the modes in their oscillation and moreover, exploit them for locomotion, are still in development. Recently, a controller has been developed that could support modes of a virtually compliant Lightweight Robot (LWR) through torque control. In the next step, this control startegy should be applied to a truely compliant robotic system with mechanical springs, i.e. Bert. Furthermore, it is of interest to extend the developed strategy to be also functioning in a position control mode.

1.2 Objectives

For the extension of the previously developed control strategy to stabilize nonlinear normal modes, it is the goal to setup a mathematical model of one leg of the robot Bert which should then be analyzed with respect to its nonlinear modes. Based on this, the torque controller should be adapted to a position controller and the existence of the nonlinear modes and the efficiency of the controller will be evaluated in a multi-body simulation. This states a novel contribution and will be the main focus of this masterthesis.

The first model of the Bert leg will be implemented in Matlab. With this model, it will be possible to find and analyze the nonlinear normal modes. Afterwards, the influence of parameters on the shape of the modes should be evaluated. The objective is to identify adjustable parameters that shape the modes, enabling oscillations leading to translational motions that could lateron be exploited for a hopping locomotion of the leg.

Next, the previously developed control strategy has to be adjusted for the Bert leg kinematics and converted to a position controller to support the found nonlinear modes in their oscillation. The controller is evaluated under different conditions e.g. with and without dissipation effects.

1.3 Structure

To solve the predescribed problems and achive the objectives, the thesis follows a scientific approach and structure. For the overall placement in the scientific context, related work is presented first. Here, work is presented showing the energy efficiency of natural

locomotion. Furthermore existing work on using intrinsic system dynamics for locomotion is researched and presented. To handle the problems addressed in this thesis, crucial mathematical and physical fundamentals for achieving the objectives are explained afterwards.

After the groundwork, the thesis starts with the presentation of the modelling approach. By using an elastic double pendulum as a well researched first example, the overall analysis method for the nonlinear modes is validated. Afterwards, the modelling of the Bert leg is approached by introducing two different methods: Pfaffian constraints method and active joints method. This leads to a model of an inverted triple pendulum. Based on this model, the nonlinear modes can be found and analyzed. Different influences such as set spring equilibria are evaluated next. This results in a suitable mode being chosen, designated as a set of target values for the leg to execute oscillating modal oscillations.

The second main part of the thesis adapts the beforementioned control strategy for the Bert leg model. This is done by first validating the given torque control approach with the leg model. Afterwards, the control approach is advanced to meet the reality circumstances such as position controlled joints. After the advanced control strategy is validated with the matlab model, it is further tested with a digital twin of the Bert leg in Gazebo. The test in Gazebo validates the whole approach from the modelling of the Bert leg, to the evaluation of the nonlinear modes and finally to an energy efficient control strategy for one leg of the robot Bert.

This work was developed and supervised at the DLR in cooperation with the Paderborn University. The task for this work was worked out by the supervisors. In regular meetings, the current work progress was controlled by the supervisors and assistance was provided if necessary.

2 Related work

In the following chapter, the topic of this thesis is placed in the existing scientific context of robotic locomotion. The background to the development of the basic idea of using biologically inspired systems and modes for the locomotion of robots is illuminated. Basic literature is presented on which the work on the robot Bert at the DLR and the exploration of modes for locomotion are based.

Accordingly, this chapters first Section 2.1 starts with the presentation of previous scientific work. These deal with the locomotion of animals, including their energy efficiency during locomotion. Subsequently, Section 2.2 leads into the technical area. Here it is described how the work on locomotion models for robots based on nature, among other things, has developed on the basis of the preceding biological research. The focus is on problems that have arisen and from which lessons can still be learned today. After the first steps of physical simulations are described, the concept of so called passive dynamic walker is introduced as a base for the overall use of intrinsic dynamics. Starting from Section 2.3, the focus is sharpened in Section 2.4 and placed on concepts for quadrupeds. Different approaches are considered, which are based, among other things, on the results of biological research. Finally, the last Section 2.5 introduces the quadruped Bert, which is the base of this thesis. Here the system is described, connections to existing work are made and the objectives of the test platform are discussed, from which partial objectives are dealt with in this thesis.

2.1 Biological locomotion background

As early as 1981, research was conducted into the energy efficiency of animals in terms of their locomotion. In [HT81] it was researched to what extent horses use different gaits to realize various movement speeds. A correlation to energy consumption was also established and the result is presented in Figure 2-1. Here, for one of the test horses, the choice of its gaits, as well as its energy consumption over its movement speed are illustrated. The energy consumption is measured as oxygen consumed. At the bottom the histogram shows the area where the horse was free to choose its gait, resulting in three different speeds. In the other areas, the horse walked on a treadmill and thus could not freely choose its speed.

From the results presented above, there is a clearly recognizable correlation between the naturally selected gait, the speed and the energy consumption. Explicitly, a horse apparently chooses the optimal combination of speed and gait in terms of energy with a free choice of speed, since this is exactly where the minima of the evaluation points are lo-

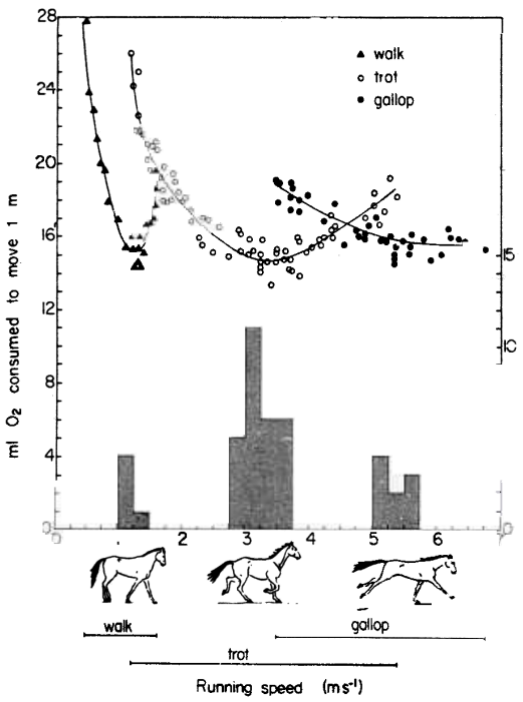

Figure 2-1: *The figure shows the result of a study that looked at the relationship between different gaits and the resulting energy consumption of horses. It was found that there is a strong correlation between the choosage of gaits and the movement speed. The trajectories at the top clearly show that one reason for the gait change is energy efficiency as the energy decreases after changing from one to another gait [HT81, p. 240].*

cated. An additional result is that the choice of a non-optimal gait has a multiple higher energy consumption. This can be seen from the fact that, for example, the energy consumption with the gait trot in the range of less than 2 ms^{-1} is partly more than 10 mL oxygen above the consumption of the gait walking at the same speed.

Building on [HT81], Taylor explained in a further going research [Tay85] with a shift to the mechanical perspective, that the muscle-tendon complexes of animal legs could be regarded as springs. During the experiments in this research, it was found that spring systems are indeed a good modelling for the muscles and tendons of an animal leg. They behave similarly to springs in that they expand and contract oscillatorily during locomotion. The investigations also once again revealed that there is a clear correlation between the use of different gaits and the maximum muscle tension. When a certain maximum muscle tension is reached, the gait is changed, which immediately reduces the tension.

Going beyond this literature and beyond only one tye of animal, in [Sha90] pigs are used for a differernt research. In this work it was explored, which muscle groups are most likely to be modelled by springs. Recommendations are also given for the parameterisation in terms of length and tension of these springs and the length mass correlations.

In Addition to the consideration of the locomotion of animals, legs of humans also serve as a research base for natural locomotion. [GH10] focused on the muscles of the human leg in order to research on a natural control of locomotion. Mainly recurrent muscle reflexes were investigated. In the study it was noted that there is no continuous input by the muscles permanently. In contrast muscle reflexes occur repeatedly to stimulate the movement. Apparently it appears to be the case that the inherent locomotion is to be strengthened and maintained by muscle reflex-like energy inputs at the joints and not initially generated by the muscles nor kept up by a permanent muscle input.

With the large research on horses by Taylor in [HT81] and [Tay85] and with the additional exploration of pigs in [Sha90], this section has presented biological observations related to animal locomotion. [GH10] pointed out, with focus on the human leg, how inherent dynamics are used and actuated in nature. The main open question at this point is: How to enable natural locomotion observations within the robotics area. This will be discussed in the follwoing section.

2.2 Physical simulations based on biological models

Since the motivation of this work is on the exploitation and practical use of the biological relationships described in the previous section, this section introduces the locomotion of mechanical robotic systems based on natural models. The first simulations of multi-legged robots already existed in 1990 [McK90]. At that time, from a literature point of view, a complete simulation of locomotion based on physical calculations could be set up for the first time with a hexapod simulation which imitates a six-legged insect. The insect is shown in Figure 2-2.

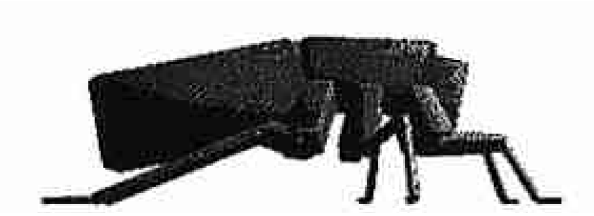

Figure 2-2: *The first physical simulation model of an insect on a biological basis. Natural locomotion was researched for the first time using this example [McK90, p. 50].*

This simulation enabled the exploration of the biological correlations described in the previous section in an engineering context. By using a complete dynamics model, a gait controller and by using dynamic motor programmes, a working simulation could be created. Furthermore [McK90] describes problems and possible solutions for some common problems in the modelling of locomotion modells. One example is the modelling of the ground with the sticky foot model [McK90, p. 64] which is still relevant until today.

In later years, building biologically inspired robots continues to be of great interest, as shown, by the work on the robot BISAM (Biologically Inspired Walking Machine) [LAH02]. The goal still lies in *"taking advantage of the principles observed in natural locomotion"* [LAH02, p. 1]. Due to the availability of physical robotic models as a whole simulation from this time on, the method of virtual prototyping is arising and is also used in the BISAM project. This method corresponds to building the robot first in a simulation, validating the simulation and afterwards realising experiments in reality. Furthermore the basic approach chosen for the robot BISAM was the consideration of a single leg as the starting point for the development of the entire locomotion machine with several legs. Figure 2-3 shows this approach from a biological-mechanical point of view. It is a representation of a leg with upper and lower part whereby it is superimposed by a simplified mechanical representation with joints and rods. Last, there are two attachment points of the muscle. This muscle could be modelled as a spring, stretching and shortening to create the movement of the lower leg.

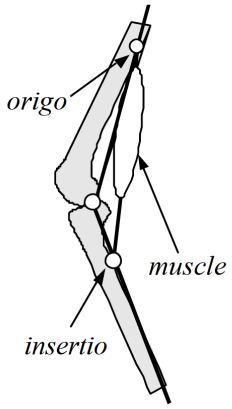

Figure 2-3: *Simplified representation of a single skeletal leg, which is a basis for modelling a single leg of the robot BISAM. Here, "insertio" describes the muscle insertion and "origo" the muscle origin. The white circles represent revolute joints. The grey parts are the representation of the skeletal leg [LAH02, p. 4].*

Building upon the simulation of a single leg, in [LAH02] there was an attempt to build an overall simulation. In this work, bringing together simulation and reality was not successful. Just as in [McK90], the modelling of the ground effect was again difficult in the implementation. Determining the contact forces using a spatial spring damper model that takes into account stick-slip effects was now proposed as a solution in [LAH02]. These first physical simulations are the starting point of the ongoing developement of locomotion models based on inherent dynamics. One outcome of this developement is presented in the following section.

2.3 Passive dynamic walker models

A developement of physical simulation models are passive dynamic walker (PDW). These models and robots are supposed to move independently in oscillatory motions after applying an initial energy. By exploiting the inherent system dynamics, locomotion is realized. Without control or regulation, or without the input of further energy into the system, the case of passive dynamic walkers is assumed to be conservative. Otherwise, damping and frictional effects would cause the system to stall over time or the system would deviate from the locomotive oscillation. One possibility for experiments with such systems is to exploit gravity, which was done in [WSH04]. Here, a simple bipedal system with a point-mass upper body was simulatively set up to run down an incline without initial energy input. The system is shown in Figure 2-4, where the upper filled black circle represents the upper body. The system stands on an incline to move without external influences additional to gravity. In this work, several relevant points were proved: First, a spring was placed in the hip area, which allowed stable walking and whose stiffness had a direct influence on the step frequency. When the stiffness of the spring was increased, an increase in stride frequency was observed. In addition, it was investigated how an upper body could be kinematically incorporated into the model so that stability would improve. Figure 2-4 shows as well how the upper body angle is kinematically constrained with respect to the center between the legs. By keeping it in this position at all times, the stability of walking could be improved overal as well as compared to a PDW without upper body.

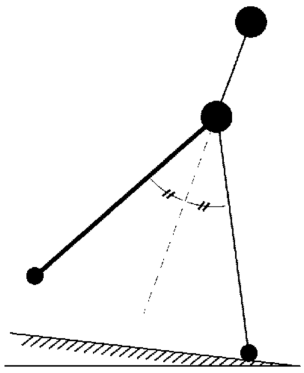

Figure 2-4: *A biped passive dynamic walker example with the kinematic restriction of the upper body to the center between the two legs to improve stability. The PDW stands and walks on an incline. Motion is enabled by gravity. Other forces are not applied [WSH04, p. 682].*

Taking the idea of PDWs further, the research [TZFS04] shows that PDWs can also be actuated, equipped with control strategies and experimentally validated on a real setup. The successful approach taken here is not to disturb the passive gait of the legs as a whole and not to actuate the hip joints directly. Instead, motors were attached to the ankles,

which only move the feet. This leaves the question open to what extent it is possible to stimulate passive gaits or inherent system dynamics directly at the hip joints.

The main point stated in this section is the successful exloration and usage of inherent system dynamics of robots with the use case of PDWs. Getting further, using inherent system dynamics with bipeds can also be extended to quadrupeds which is outlined in the next sections, approaching the focus of this work.

2.4 Locomotion concepts for quadrupeds

This section presents the biologically inspired locomotion of quadruped robots. This is done by presenting different approaches for locomotion concepts and connecting the results of the researches in Section 2.1.

An important research for passive dynamic walking of quadrupeds is [GR14]. The early biological observations of horses as given in [HT81] are addressed. The proposed quadruped realizes energy-optimal locomotion using an optimal control approach. The resulting gaits are vividly illustrated in video form in [GR15]. As a result of the work stands that by the chosen approach indeed the different gaits of horses were recovered also in the simplified quadruped using an optimal control approach. The outcome is illustrated in Figure 2-5. All gaits in the quadruped are within the shaded area, which in turn represents the gaits of the horses. The gaits in this case are represented by measuring and ablating the foot movements onto the axes.

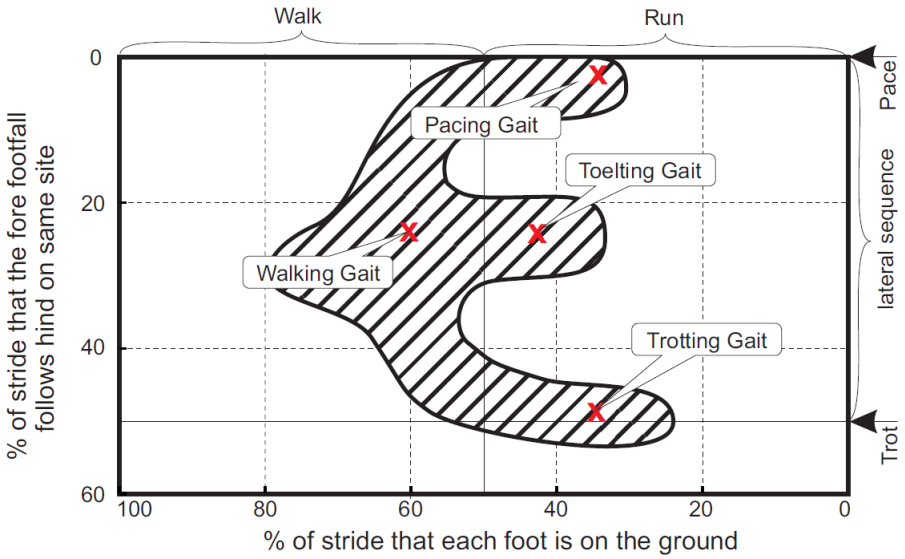

Figure 2-5: *This figure connects the already presented work [HT81] to the research in [GR14]. Here with the represented hatched area the gaits of horses that were found are represented. These gaits were also found in the simplified quadruped, marked as red crosses [GR14, p. 4880].*

Replicating the gaits of horses with a passive dynamic quadruped simulatively, [GR14] proved that it is possible to set up robots that have the same energy optimal gaits as horses. Furthermore, in relation to this work, the following quote conclusion of this research work is crucial:

"In an abstract sense, different gaits can be interpreted as different modes of elastic oscillations that propel the legged system forward. [...] The results presented in this paper are, however, only the tip of the iceberg"[GR14, p. 4880].

This statement raises the question on how to establish locomotion in a quadruped utilizing its system inherent modes. Thus, the literature presented up to this point only forms the foundation of utilization of elastic robots based on natural phenomena. It is of great interest for this work on how to connect biological observations, inherent system dynamics and the so called "modes" that have been mentioned in [GR14].

The results from [GR14] were further developed in [XYR16]. Here, the optimal control approach for finding the optimal gaits was continued and tested on a more realistic model. This model is shown in Figure 2-6. The simple model in [GR14] consist only of an upper body with mass and massless legs. The legs are modelled by a spring each. The leg parts have their own masses, four additional springs were added to the top, damping was added and the torques and velocities have realistic values.

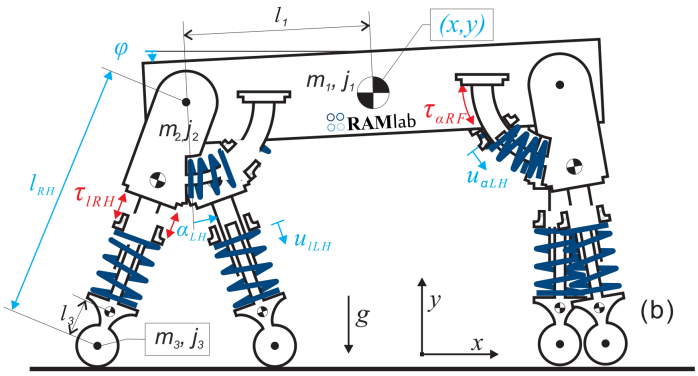

Figure 2-6: *The figure shows the four-legged PDW which has been extended compared to [GR14]. Now the PDW for example has additional springs and legs with masses. This is a good visual example of a realistic quadruped PDW [XYR16, p. 1142].*

An interesting outcome of this model was the reliably representation of ground contact and resulting friction. In addition, some assumptions were also validated using the more realistic model: The energy expenditure is significantly lower under the use of gaits than without the use of gaits. Here, the expenditure was calculated using the cost of transport, which measures the energy expenditure in relation to the distance traveled. Also it has

been again found that a clear connection between the speed and the gait, which is optimal for this locomotion speed,exists.

As a last point of this section, it should be mentioned that there are other possibilities to move a quadruped PDW in a stable way, apart from the approach of optimal control. In a recent work in [LTA20], a PDW was developed, which moves through by entrainment effects. However, instead of placing the excitation in the feet, the excitation was implemented by a moving mass on the upper body. The mass moved by excitation using an electric motor creating entrainment effects on the system, causing it to move. The legs and the upper body have mass in this model.

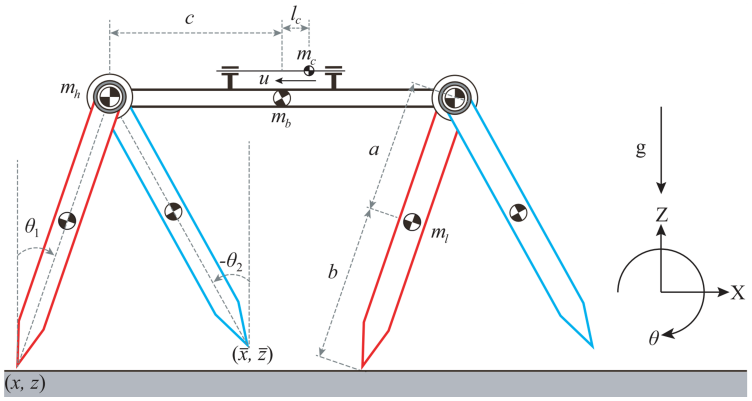

Figure 2-7: *The PDW shown here is taken from [LTA20, p. 4305] and demonstrates an alternative method of implementing system inherent locomotion by exploiting entrainment effects. These effects are generated by the mass movably attached to the top of the superstructure, which in turn can be set into oscillating motion by an actuator.*

One advantage of this setup is that an underactuated system could be moved very efficiently by only one actuator without the input of direct torques. Furthermore, similar to the approach in [TZFS04], the goal here is as well to not disturb the gait by direct joint actuation.

In summary, this section described the development of research into quadruped passive dynamic walkers. It got clear that there are multiple approaches possible to excite passive dynamic walkers and control their motion with the goal of realising an energy optimal gait.

2.5 Quadruped test platform Bert

The previous sections showed results in several areas of inherent dynamics. Observations in the area of biological locomotion were evaluated and physical simulations of naturally inspired robots and passive dynamic bipeds were set up. Lastly the research in the area

of quadrupeds is presented in the previous sections. Now the connection to this work is introduced.

The foundation of this work is the research on the quadruped Bert. Bert is a test platform developed at the DLR which already has multiple variants in terms of its locomotional capacities. The basic information is presented at the webpage of the DLR [DLR22].

The basic structure of the test platform is as follows: Bert has four legs, each leg consisting of an upper and lower leg. There are revolute joints between the upper leg and the body, as well as between the upper and lower leg. Series elastic actuators (SEA) are connected to each joint via belt drives, whereby the independent rotation of the upper and lower leg is realised. The built-in springs guarantee the system's ability to oscillate. The springs are installed between the motor shafts and the belt drives. Depending on the motor position, the rest position of the springs can be adjusted. Rotation of the upper and lower leg deflects the springs independently of each other due to the built-in belt drive set up. Figure 1-1 in the introduction already showed a variant of Bert. In addition, in Figure 2-8 below, a newer version of Bert is shown, which has an important change: At the top of each leg there is an additional joint, which allows internal and external rotation of the legs.

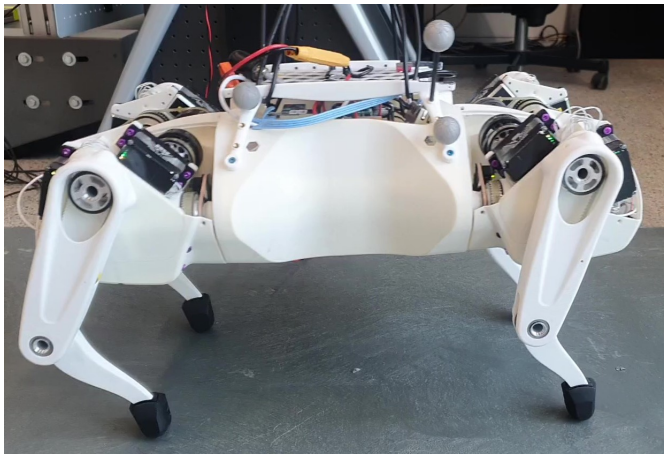

Figure 2-8: *Variant of the quadruped test platform Bert which was developed by the DLR. This variant as well has, in addition to the revolute joints between upper and lower leg and upper leg and body, revolute hip joints allowing internal and external rotation.*

Overall, a cost-effective rapid prototyping test platform was created at DLR in this way. The goal here is the transfer of locomotion patterns from nature to robot systems, which was already addressed in the previous sections with other robots.

In relation to the previously presented work, the following should be highlighted for the Bert robot: The research on different gaits for different speeds aims directly at validating that this fundamentally improves energy efficiency during locomotion. This is based on the presented results of research on horses and their gaits. Furthermore, the use of springs

in Bert's legs follows from the research on leg muscles. This realises dynamic walking and running similar to the locomotion of natural models. In addition, the available means of physical simulations, which were also presented in the previous sections, make the method of virtual and rapid prototyping possible. Before concepts are implemented, they are first tested extensively by simulation, whereby the intrinsic system dynamics are analyzed in detail. Since simulative dissipative effects are neglected, simulations similar to those for the PDWs presented can also be realised. Thus, the possibilities of the robot's locomotion can already be tested without the variable of actuation. In contrast to the presented work, Bert is not controlled by an optimal control approach and not indirectly by entrainment effects. Instead, the intrinsic system dynamics are analyzed in detail in advance and then a novelly control method should be designed that supports the dynamics. The exact theoretical fundamentals for this will be described in the following chapter.

It is subject to this thesis to lay the groundwork to develop such a control approach. To reduce the complexity for this first control implementation, the work will focus on one leg of Bert only. Since the test platform is symmetric, this approach can easily be extended in following work. For the purpose to carry out experiments on one leg of Bert, a test stand has already been set up, which is shown in Figure 2-9. This consists of a single leg attached to a long boom. The result is a floating base with constrained rotation and hopping ability in the xy-plane.

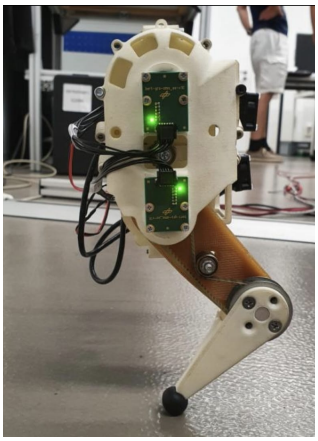

Figure 2-9: *Test rig for experiments on one leg of the robot Bert. This has the advantage that the whole locomotion problem is broken down to a simpler case where only one leg is taken into account with the goal that the leg is hopping forward. The leg is attached to a boom which keeps its orientation and guides the direction.*

The parameters associated with the test bench are shown in the following Table 2-1. The masses of the upper and lower leg, the masses of the boom and the total robot, as well as the spring stiffnesses of the two installed springs are listed. Also an estimation of the damping in the rotational joints and both lengths of the legs are given.

Table 2-1: *Standard parametrization of the robot Bert with a focus on the one leg test rig. This leg is based on the eight DoF robot without a hip joint. The parametrization is the goal to be implemented by the simulations in this work. Related work with paramters can be found in [SGSA22] and [LPL+18].*

Description	Value	Unit
Upper leg mass	0.05	kg
Upper leg length	0.08	m
Lower leg mass	0.107	kg
Lower leg length	0.08	m
Mass of the body o the one leg test rig	0.367	kg
Total mass of the one leg test rig	0.524	kg
Upper spring constant	2.93	kgs^{-2}
Lower spring constant	2.94	kgs^{-2}

The test bench shown here has already been used to test a modelling of the Bert leg in [CDGA22], whereby a simplified variant was used here in which the leg was modelled as a single spring standing at an angle on the ground with a mass attached to its upper end. Also, in the work [LPL+18], different gaits of the Bert leg have already been investigated, with a focus on the slip-effect already mentioned in the previous sections. The motors used with Bert have also been analyzed and characterised in the work [SGSA22]. Last,in [DLBA] already tried a simplified control strategy on the one leg test rig with some challenging problems such as friction.

Compared to the previous work, this thesis focuses on the adaption of a controller strategy for the use with one leg of Bert. The aim is to develop a position control approach based on the inherent system dynamics of one leg.

To sum up, in this chapter the biological research on animal locomotion has been put into a context with the development of systems locomoting by exploiting system inherent dynamics resulting in the test platform Bert. Thereby, first in Section 2.1 the biological background research was presented. An advantage of using different gaits in terms of energy efficiency could be derived as well as nature based modelling possibilities. Then, the engineering context was introduced in Section 2.2 with the introduction of the first developed biological simulation models. Subsequently, PDWs and bipeds used for research on locomotion based on intrinsic dynamics were described in 2.3. After this introduction the concepts of quadrupeds was outlined with a focus on the usage of the previous biological research in 2.4. The final part of the Chapter 2.5 introduces the quadruped Bert which was developed at the DLR and is a test platform for research on the transfer of natural locomotion patterns. By presenting this related work, the research basis of this thesis is set to analysing the inherent system dynamics of the robot Bert with the aim to utilize

the analysis for biologically inspired energy efficient locomotion. Next, in the following chapter, the theoretical-mathematical foundations necessary for the realisation of the goal, the dynamics analysis and utilisation, are presented and the novel methods for the description of the system dynamics are introduced.

3 Fundamentals

In the previous chapter, related work to robotic locomotion was presented including the connection of biological observations to the engineering context. Additonal, the quadrupedal robot, which serves as a test platform for novel control strategy development. Subject of this chapter are the fundamental theories that are needed for the extension of existing control theory that will be the focus of this thesis. Furthermore, the considered kinematics and dynamic models that are implemented for this thesis are presented as well as the position control approach that should be implemented to extend previous control approaches.

To begin, in Section 3.1 concepts to describe constrained dynamic systems are presented. Additionally, an introduction to parallel kinematics is given. Since the modelling of dynamics after describing the kinematics with the Lagrange method is a well known standard, it will not be detailed in this thesis. In Section 3.2, the mode theory is explained, where the differences, but also the similarities between linear and nonlinear modes are explained. Subsequently, the control strategy for stabilizing systems to their modes is introduced in Section 3.3. Finally, in Section 3.4 strategies are listed to get from an arbitrary joint configuratioin on the mode trajectories.

3.1 Constrained and parallel kinematics

In robotics, there are many use cases for modelling serial kinematics. These include standard industrial robots such as the vertical articulated robot, which makes up the majority of industrially used robots [PD19]. Such robot has serial kinematics with multiple joints arranged in sequence. The counterpart to serial kinematics is parallel kinematics. While in serial kinematics the individual axes are arranged one after the other, the axes of motion are arranged differently in parallel kinematic robots. Here, all motion axes act directly on the platform, which carries the tool in the case of industrial robots [WB05]. Stating the difference, in serial kinematics, the tool is placed at the end of an open chain or sequence of links and joints. In parallel kinematics, the tool is instead connected to multiple links resulting in parallel motion of the links during a process.

Considering the work on the robot Bert, we can define subtasks with serial kinematics as well as those with parallel kinematics. First, a single leg of the robot can be considered serially as a sequence of rotary joints. However, with respect to the test rig presented in Section 2.5 where one leg is attached to a suspension, it is necessary to go beyond purely serial kinematics, since DoF are negated by the suspension. Thus, kinematic constraints are necessary. This will be explained further in Subsection 3.1.1. Looking at a 2D

representation of the entire robot Bert, parallel kinematics can be identified with two legs standing on the ground. In this case, the pose of the body is directly dependent on the axes of motion of both of the two legs, which corresponds to the above described structure of parallel kinematics. The approach in describing parallel kinematics will be introduced in Subsection 3.1.2.

3.1.1 Constrained serial kinematics

The first step in dealing with modeling the constrained kinematics of a system is often to determine the DoF of the system. The procedure for this is described and explained in [LP17]. It is explained how the total number of DoF of a system can be described as a function of the number of elements on the links and joints. Here Grüblers Formula

$$\text{DoF} = m_{plane}(N_{links} - J_{joints}) + \sum_{i=1}^{J_{joints}} f_{\text{freedom},i} \tag{3-1}$$

can be applied. Here, m_{plane} is either three or six for the planar or spatial space, respectively. N_{links} is the number of links and J_{joints} is the number of joints. Last $i = [1, ..., J_{joints}]$ with $f_{\text{freedom},i}$ being the DoF provided by joint i. Grübler's formula can be used for both serial and parallel kinematics, with and adjusted formula and the floor being added as another link for parallel kinematics.

By calculating the DoF for a dynamic system, the number of variables that are needed to describe the system is determined. This number is equal to the number of DoF and are often referred to as active variables with the corresponding joints being called active joints [MLS94]. By this method a constrained system can be described by a minimal number of variables.

However, there are reasons to continue describing the system in an unconstrained manner. By describing a dynamic system as a whole without constraints and then inserting constraints after modeling, the comparison between the constrained and unconstrained system can be easily made. Sometimes it is also of interest to describe rotational motion in Cartesian space requiring more variables and constraints to be defined.

To constrain an unconstrained system in its motions, according to [MLS94] Pfaffian constraints can be used. By the method of Pfaffian constraints, the possible trajectories that the system can have are restricted with respect to its velocity. This is realized by the introduction of so-called constraint forces.

For the mathematical explanation of these constraints, as given in [MLS94], the equations of motion

$$\underline{M}(\underline{x})\ddot{\underline{x}} + \underline{C}(\underline{x}, \dot{\underline{x}})\dot{\underline{x}} + \underline{N}(\underline{x}, \dot{\underline{x}}) + \underline{A}^T(\underline{x})\lambda = \underline{F} \tag{3-2}$$

are given in standard Lagrangian robotic notation extended by the term $\underline{A}^T(\underline{x})\lambda$, which introduces the constraint forces. Here $\underline{x}$ represents the system's configuration space vector with $\dot{\underline{x}}$ and $\ddot{\underline{x}}$ denoting the first and second time derivative of it. $\underline{M}(\underline{x})$ denotes the mass matrix and $\underline{C}(\underline{x}, \dot{\underline{x}})\dot{\underline{x}}$ denotes the Coriolis and centrifugal forces. Furthermore, the vector $\underline{N}(\underline{x}, \dot{\underline{x}})$ sums up potential forces as well as possible dissipative effects of the system. The vector $\underline{F}$ denotes external system input forces. In detail $\underline{A}^T(\underline{x})$ is a non-normalized basis for the constraint forces and λ gives the relative magnitudes of the forces of constraint [MLS94].

With the notation in (3-2) a constrained dynamic system can be described. An important part of the constraining is the calculation of $\underline{A}(\underline{x})$ and λ which is given in [MLS94]. After defining the constraint itself, it is differentiated which leads to the form

$$\underline{A}(\underline{x})\dot{\underline{x}} = 0.$$

After obtaining $\underline{A}(\underline{x})$, λ can be calcualted by

$$\lambda = \left(\underline{A}(\underline{x})\underline{M}(\underline{x})^{-1}\underline{A}^T(\underline{x})\right)\left(\underline{A}(\underline{x})\underline{M}(\underline{x})^{-1}\left(\underline{F} - \underline{C}(\underline{x}, \dot{\underline{x}})\dot{\underline{x}} - \underline{N}(\underline{x}, \dot{\underline{x}})\right) + \dot{\underline{A}}(\underline{x})\dot{\underline{x}}\right). \tag{3-3}$$

Inserting $\underline{A}^T(\underline{x})$ and λ into (3-2) leads to the full description of the dynamics of a constrained system.

In this subsection it was shown which possibilities exist to describe a system with constrained kinematics. The active joints method and Pfaffian constraints method will be used in the following of this thesis to model one leg of the robot Bert.

3.1.2 Parallel kinematics by loop closure equations

The description of systems with parallel kinematics has similarities with the constraining of serial systems mentioned above. Basically, the description is based on the assumption that the loop closure equations are set up which are also constraint equations.

Following [LP17], these equations describe the closing of the kinematic chain. For the example of an industrial robot, it results that the platform guiding the tool always remains horizontal to the ground. Thus, with k being the amount of loop closure equations and n being the system's uncosntrained dimension of the configuration space, a total of $k \leq n$ equations can be found, which reduce the dimension to $n - k$. The loop closure equations

can then be used to proceed according to the method of Paffian constraints described in the previous subsection.

Another example that has similarities with the 2D robot Bert is the four bar linkage also presented in [LP17]. This parallel mechanism is shown in Figure 3-1 and consists of three links. It is called four bar linkage because in a parallel mechanism the ground is also counted as a bar.

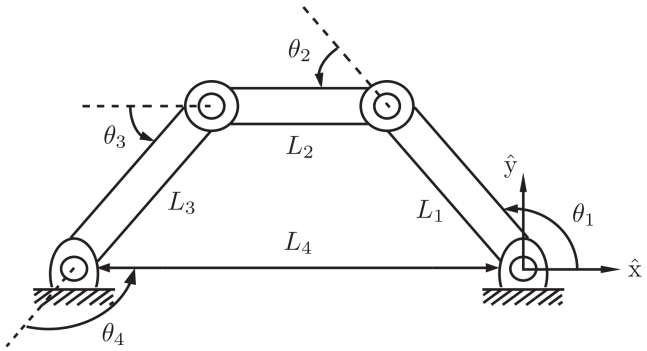

Figure 3-1: *Four bar linkage as an example parallel system which is given in [LP17, p. 29]. This system has similarities with the robot Bert and can easily be extended to describe the kinematics of the 2D Bert seen from one side.*

To describe the kinematics of this system, in [LP17] the loop closure equations are given as

$$\begin{aligned} L_1\cos(\theta_1) + L_2\cos(\theta_1+\theta_2) + ... + L_4\cos(\theta_1+...+\theta_4) &= 0, \\ L_1\sin(\theta_1) + L_2\sin(\theta_1+\theta_2) + ... + L_4\sin(\theta_1+...+\theta_4) &= 0, \\ \theta_1+\theta_2+\theta_3+\theta_4-2\pi &= 0. \end{aligned}$$

This basic example can be used as a template for the loop closure equations of the robot Bert when considering it in a planar 2D configuration. It needs to be extended to be a six bar linkage because one leg of Bert consists of two bars.

For the complete robot Bert, it would thus be possible to find a complete dynamics description by inserting the kinematic constraints with loop closure equations. It would be conceivable to set up the loop closure equations for the 2D case seen from the side in a first step and then to consider the 3D whole robot. In summary, this section outlined an approach to describe the kinematic relationships for one leg of the robot Bert, as well as for the entire robot, and to obtain the complete dynamics equations.

3.2 Linear and nonlinear normal mode theory of elastic multi-body systems

In the modelling, analysis and control of technical systems, a decision must always be made between approaching elastic multi-body systems dynamics by linearization or taking the entire nonlinear systems behaviour into account. In this context, almost all systems relevant for applications today are nonlinear, i.e. the quadruped Bert. It is the interest of this thesis to extent on the approach to use these intrinsic nonlinear dynamics of Bert for the purpose of locomotion and create a energy efficient way to control it.

Therefore, in the following two subsections, the linear and nonlinear mode theories are presented. Since linear modes are well known, they will be shortly introduced in Subsection 3.2.1. The new nonlinear mode theory is discussed afterwards in Subsection 3.2.2. This theory is based on the latest findings of research by the DLR. Overall the following two subsections are intended to provide an overview to the understanding of modes without going into too much deatil about the mathematical basics regarding the proof of existence or their calculation. Rather, the application of the mode concept is the focus of this work.

3.2.1 Linear mode theory and difficulties with nonlinear system analysis

Linear modes form the basis on which the theory of nonlinear modes discussed in this thesis is built. For this reason, the principle of linear modes is only used as an introduction to the theory of nonlinear modes with emphasis on the difficulties and differences betweeen linear or linearized systems and nonlinear systems.

According to [Fli09], linear modes are special solutions of dynamics equations from which a certain frequency, generally denoted by ω, results. Oscillations of a dynamic system with ω are called normal modes, where a system always has exactly as many normal modes as DoFs. Osciallations on a linear mode only oscillate in a subspace of the configuration space. For linear modes this subspace is particularly simply forming a hyperplane. For the excitation of such linear normal modes, if a conservative linear elastic multi-body system is deflected to a certain point outside of its rest position and released afterwards, it will oscillate on its normal mode with the frequency ω.

Considering any linear system given in state space representation, the normal modes for this system can be easily found by the approach of eigenvectors and eigenvalues determined for the dynamics matrix.

As described in [Fli09], the individual partial solutions can be superimposed for linear multi-body systems. This superposition principle is only valid for linear systems and does not hold for nonlinear systems [Kha00, p. 3]. This implies one of the most difficult

problems in the study of nonlinear systems and their behaviour. Nonlinear multi-body systems cannot be broken down into *n* partial systems. It might be possible to break them down into more than *n* partial solution.

Generally speaking, various properties that are simple for system analysis of linear systems are lost for a nonlinear system. Moreover, trajectories of the phase plot are not always elliptical at a larger distances from the rest position [Kha00].

As stated in [Kha00], a nonlinear system can be linearized and enabling the calculation of eigenvalues afterwards. However, there are two problems with linearisations in terms of their mapping of the overall system dynamics:

"First, since linearization is an approximation in the neighborhood of an operating point, it can only predict the "local" behavior of the nonlinear system in the vicinity of that point. [...] Second, the dynamics of a nonlinear system are much richer than the dynamics of a linear system"[Kha00, p. 3].

This statement motivates this work to consider the nonlinear system directly rather than using the common method of linearization. Additionally, according to [Kha00], there are also phenomena in the field of nonlinear systems that cannot be described by linear models. These include chaotic trajectories and a finite escape time. Furthermore, nonlinear systems can go to infinity in finite time and can have so-called *"multiple modes of behaviour"[Kha00, p. 4].* In addition, limit cycles (closed trajectories) can form and a nonlinear multi-body system can have multiple equilibria. The latter means that a single nonlinear system has several different behavioral modes, which need to be delimited from the linear normal modes. These behavioral modes are also This is a central point of this thesis and will be introduced theoretically in the following subsection with the goal to identify the behavioral modes which perform modal oscialltions that can be called nonlinear normal modes.

In this subsection linear modes were outlined and some elementary useful properties of linear systems and nonlinear systems in comparison were addressed. Additionally it was shown why it is necessary to move away from linear and linearized systems in order to comprehensively represent nonlinear system dynamics.

3.2.2 Nonlinear normal modes theory

As already mentioned, nonlinear systems exhibit a variety of phenomena that complicate analysis and control. The most commonly used solution for analysis of nonlinear systems has been to linearize them causing the above mentioned disadvantages. For this reason, a

great deal of research effort is devoted to improving the analysis and usability of nonlinear system dynamics and modes.

One of the first works which tries to apply the concept of normal modes to the nonlinear case is [LFA17]. A method is introduced by which parameters can be chosen for multi-body systems to shape the normal modes of the system. The example system here is the complex pantograph leg of the robot Bert. This model ist three-segmented and has the advantage of keeping the foot parallel to the thigh. Ultimately, this work demonstrated that 1D oscillatory modes for such a leg could be found with success. It was shown here that by suitable parameter design, constant modal vectors result, enabling constant system oscillations along the vectors.

The relatively practical approach from [LFA17] has shown that an normal mode concept can also exist for nonlinear systems like a leg. [DLBA19] is a follow up work which shows research on this approach on a nonconservative nonlinear 2D planar mass-spring-damper system. It is presented that by modal characterization, the exact description of the two normal modes existing for the system is possible. The work [DA21] presented an approach combining control theory with nonlinear modal analysis and nonlinear modes. This paper emphasizes the general concept for which the analysis of nonlinear modes can be exploited: Instead of forcing a system to perform a certain motion by control, the intrinsically preferred motion of the system is to be found and supported through adequate control.

Emerging from this previous work, in [AD20] the idea to comprehensively establish the overall theoretical concept of nonlinear modes while using it to generate robust oscillations through a better understanding of robotic dynamics is presented. In [AD20], the aforementioned work is summarized and a generalization for multibody systems is made, resulting in a concept that can also be used for control engineering applications. Even though the mathematical discussion of the concept of nonlinear modes is not the focus of this thesis, the terms and definitions from the previously mentioned work will be used later on. Therefore in the following they will be introduced.

Predominantly in [AD20] three central terms, which are important for this master thesis, are used. First, the notion of nonlinear normal modes, further denoted by γ, can be precisely defined. Thereby it is determined that a nonlinear mode is basically a extended Rosenberg mode. A Rosenberg mode is defined in [Ros60]. Two conditions of Rosenberg's definition of modes are maintained within the definition of modes by [AD20] developed by the DLR. Namely, only those evolutions of a nonlinear system are nonlinear modes which are periodic and line shaped in configuration space. The condition of Rosenberg that a mode passes through the equilibrium no longer holds. This excludes all other oscillations occurring at different energy levels as well as vanishing. This con-

nects the concept of modes of linearized systems, which are also valid in the region of the equilibrium, with the concept of nonlinear modes.

Building on this, the next central notion introduced is the generator, denoted by $\mathfrak{R}$ which is the starting point for movement along the mode. A generator is defined as:

"[...] a collection of evolutions of increasing energy starting from a local minimum"[AD20, p. 61].

A less mathematical definition of a generator would be that it is a certain collection of points on modal oscillations. At these points, the velocities of the system are zero. From these points, when set as the initial condition of the system, the system oscillates on the mode associated with the generator at a particular energy level. Finally, building on the nonlinear normal mode γ and the generator $\mathfrak{R}$, the notion of the eigenmanifold, further denoted by $\mathfrak{M}$, is introduced. It is defined as:

"[...] a manifold having a generator, and at the same time collecting trajectories verifying the two conditions [periodicity, line-shaped]"[AD20, p. 61].

Thus it can be summarized that an eigenmanifold is a manifold which contains the generators and the modes, i.e. all trajectories designated as such, of a dynamic system. Each normal mode has one generator from which oscillations of different amplitudes, depending on the energy level of the system, result. To visualize the presented ideas of generators $\mathfrak{R}$ and and $\mathfrak{M}$, Figure 3-2 shows a suitable illustration. This figure shows $\mathfrak{M}$ as a collection of periodic closed orbit trajectories resulting in the visualized inverted bell shape. Furthermore, $\mathfrak{R}$ collects all point on $\mathfrak{M}$ with zero velocity. From every point $(p, 0)$ on $\mathfrak{R}$ a modal oscillation $(\gamma_{(p,0)}, \gamma'_{(p,0)})$ on $\mathfrak{M}$ results.

After this definition of nonlinear normal modes was set up, research was done to concretize and test the theoretical concept of nonlinear modes. For example [ALS21] and [SA22] give a narrower definition of nonlinear normal modes: strict nonlinear normal modes.

To sum up, in this section, linear modes were first introduced in general.Then, in the second subsection, the transition to the new theory of nonlinear modes was made. The developement of the concept was described and the main work [AD20] that gives the definitions for the nonlinear normal modes was presented. Thus, this subsection established the needed theoretical basis to exploit the nonlinear mode theory for the design of a suitable control strategy to keep a systems oscillating on its nonlinear normal mode The extension and verification of this concept is the main goal of this thesis. For this purpose,

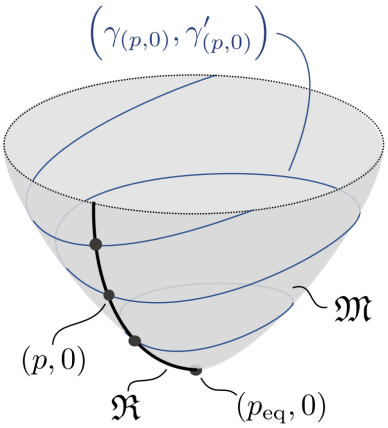

Figure 3-2: *An illustration of the generator* $\mathfrak{R}$ *and manifold* $\mathfrak{M}$ *concept where to each point* $(p,0)$ *a different trajectory* $(\gamma_{(p,0)}, \gamma'_{(p,0)})$*, denoting a nonlinear normal mode* γ*, is corresponding.* $(p_{eq},0)$ *denotes the equilibrium point.*

an already developed control concept is taken up in the following Section 3.3 and is later applied to one leg of the robot Bert.

3.3 Control approach for the stabilization of nonlinear modes

From the point of view of control engineering, the previously introduced nonlinear normal modes could be regarded as set trajectories for trajectory tracking. In order to be able to realize modal oscillations during operation of a real system, a controller is necessary which can bring and keep the system to and on a desired mode. In particular, a closed-loop feedback control for the compensation of damping and friction effects on a real system has to be applied.

In the recent work [DCGA21], impulsive control actions were proposed to change the normal mode of a nonlinear conservative mechanical system with two normal modes during operation. However, this control approach focuses on impulsive actions mainly and does not take nonconservative systems into account. For this reason in this master thesis a different control approach is used which is subsequently introduced.

The developed control startegy of [BSAD22] calculated the desired torque $\underline{\tau}$ to be commanded to the robot. This work was developed at DLR and deals with a serial robot, the KUKA iiwa. This robot has seven DoF and therefore seven nonlinear normal modes. These were calculated for this work in order to excite them using the derived novel controller. In this paper, six of the seven normal modes have already been successfully excited.

The developed control strategy provides the required control input $\underline{\tau}$ as an output. It consists of the sum two parts: A manifold stabilizer $\underline{\tau}_M$ and a energy controller denoted by $\underline{\tau}_E$. Combined $\underline{\tau}_M$ and $\underline{\tau}_E$ lead to the total torque $\underline{\tau}$.

To derive the Manifold Stabilizer, first the nearest point of the eigenmanifold $\mathfrak{M}$ to the current state needs to be found by

$$\left(\underline{X}, \dot{\underline{X}}\right) = \underset{(\tilde{\underline{x}}, \dot{\tilde{\underline{x}}}) \in \mathfrak{M}}{\operatorname{argmin}} \left\| \begin{bmatrix} \underline{x} \\ \dot{\underline{x}} \end{bmatrix} - \begin{bmatrix} \tilde{\underline{x}} \\ \dot{\tilde{\underline{x}}} \end{bmatrix} \right\|^2, \tag{3-4}$$

where $\tilde{\underline{x}}$ and $\dot{\tilde{\underline{x}}}$ are basically the configuration space vector and its derivative on the eigenmanifold. $\underline{x}$ and $\dot{\underline{x}}$ are the configuration space vector of the system and its derivative. The resulting $\underline{X}$ and $\dot{\underline{X}}$ are the nearest points found on the eigenmanifold.

The search for the nearest point of the eigenmanifold is illustrated in Figure 3-3. Here, on the left side, the manifold $\mathfrak{M}$ is shown in grey. Furthermore, the discrete point cloud representation of the eigenmanifold $\mathfrak{M}_{\text{pc}}$ is denoted by blue point on $\mathfrak{M}$. The goal is to find the point $\left(X, \dot{X}\right)$ of the discrete eigenmanifold which has the smallest distance d to the current state $(x, \dot{x})$ of the systme. The search itself is executed with a kd-tree which is shown on the right side of the figure. By using the kd-tree method, calculation speed can be increased such that the controller can run in realtime. For this purpose, the point cloud is generated beforehand, enabling a search algorithm to split the point cloud into sections step by step. The computational time is largely reduced since the whole point cloud does not need to be searched and it is split up iteratively instead.

With this approach it is possible to find the closest point of the eigenmanifold in realtime. After the point is found, it used to calculate the needed torque $\underline{\tau}_M$ by the manifold stabilzer to reach the nearest point on the manifold.

By multiplying the distance with the mass matrix $\underline{M}(\underline{x})$ and an optimal selectable gain α_D, $\underline{\tau}_M$ follows as

$$\underline{\tau}_M \left(\underline{x}, \dot{\underline{x}}; \mathfrak{M}_{pc}\right) = \alpha_D \underline{M}(\underline{x}) \left(\dot{\underline{x}} - \dot{\underline{X}}\right), \tag{3-5}$$

It should also be emphasized here that the manifold stabilizer uses only the velocity $\dot{\underline{X}}$. This is based on empirical values from [BSAD22]. Though it has not yet been researched why exactly stabilizing the eigenmanifold only based on the velocity differences works better than additionally adding the angle differences.

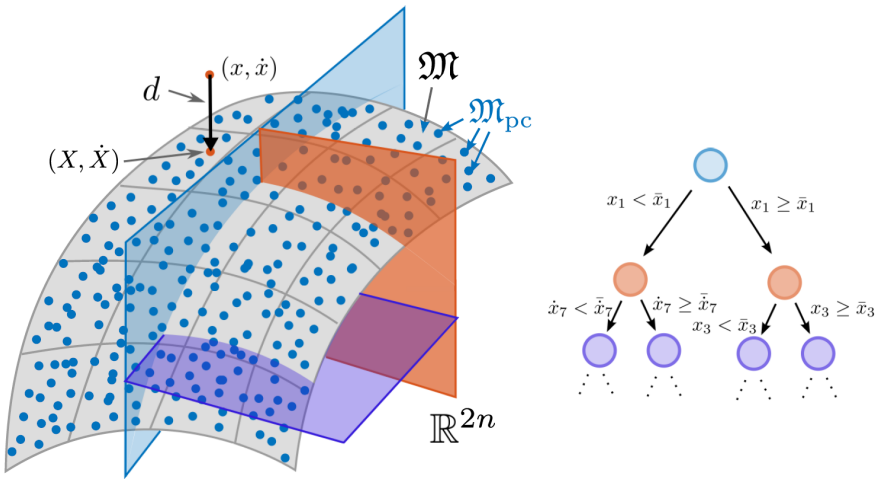

Figure 3-3: *Illustration of the search for the nearest point of the discrete point cloud eigenmanifold $\mathfrak{M}_{\mathrm{pc}}$ to the current state $(x, \dot{x})$ of the system on the left side. The goal is to find the point of the manifold with the shortest distance d by using the kd-tree method shown on the right side. This method seperates the point cloud in half in every further step which results in increased computational speed [BSAD22, p. 3].*

In the next step, the energy controller $\underline{\tau}_E$ is calculated by taking the difference to a desired energy into account. The equation for calculating $\underline{\tau}_E$ is given by

$$\underline{\tau}_E\left(\underline{x}, \underline{\dot{x}}; \overline{E}\right) = \gamma_P \underline{M}(\underline{x})\left(\overline{E} - E\left(\underline{x}, \underline{\dot{x}}\right)\right)\underline{\dot{x}} + \gamma_I \underline{M}(\underline{x})\left(\int\left(\overline{E} - E\left(\underline{x}, \underline{\dot{x}}\right)\right)\delta t\right)\underline{\dot{x}}, \tag{3-6}$$

where $\overline{E}$ is the desired total system energy, or the desired energy level which needs to be defined beforehand. γ_P and γ_I are gains for the energy difference and the integrated energy difference.

By summing up $\underline{\tau}_E$ and $\underline{\tau}_M$,

$$\underline{\tau}\left(\underline{x}, \underline{\dot{x}}\right) = \underline{\tau}_E\left(\underline{x}, \underline{\dot{x}}; \overline{E}\right) + \underline{\tau}_M\left(\underline{x}, \underline{\dot{x}}; \mathfrak{M}_{pc}\right), \tag{3-7}$$

results. Both parts of $\underline{\tau}$ depend on the current state, but only the energy controller depends on the desired energy level $\overline{E}$ and only the manifold stabilizer depends on the discrete point cloud manifold $\mathfrak{M}_{pc}$. By obtaining the total $\underline{\tau}$, a feedback control is applied to keep the trajectory of a nonlinear system on its eigenmanifold.

As a summary, this section introduced a previously derived control strategy to keep a robot on its nonliear mode. The motivation and the procedure were explained on the one hand and the mathematical implementation was presented on the other hand. So far, this controller has been tested on the LWR with simulated elastic joints. It is the goal of

this thesis to apply the derived controller on a truely compliant system, namely the robot Bert.

3.4 Interception control

Previously, a concept for nonlinear normal modes was introduced and and a control strategy with the goal to keep a system on its nonlinear normal mode was defined. The control strategy presented focuses primarily on maintaining or achieving a desired energy level and is ideally used in the vicinity of the manifold or on an normal mode of the system in question. What has been less closely considered is how to move the systems trajectory from any initial value in the range of the state space to the normal mode with a predictable and controlled motion. It is the question of this section on how to setup a control that can be used if the systems trajectory is far away from the manifold. The approach chosen to answer this question in this thesis is called interception control.

In the engineering field, there are already many approaches for tangenting an ideal line. The goal is always not to hit the ideal line orthogonally, but to approach it asymptotically in the direction of motion. In the context of this work, the mentioned ideal line represents the nonlinear normal mode on which the system would be located with the current energy level.

A use case can be found in the field of vehicles and their driver assistance systems. Here, the task of changing lanes is considered. A driver or the assistance system has the task to reach the target lane asymptotically. Otherwise very jerky direction changes would result. There is a broad research base on this area from both a technical and a human behavioral point of view.

The question of how humans generally want to intercept a moving target has already been discussed in several studies such as [ZW17]. Furthermore, different models have been created. In [Faj13] an affordance-based model is set up for this purpose, which includes various influencing factors that affect humans in the interception process. This incorporates the widely used bearing angle model and increases the complexity with respect to human factors. In order to draw a benefit for this work, in the following the focus is put on the simpler bearing angle model, which also forms the basis of the study presented in the following.

In [ZSR19], research was conducted on how people generally steer a vehicle. This paper presented different strategies for interception of a moving target. The study showed that one strategy best represents human behavior. This strategy is called Constant Target Heading and is illustrated in Figure 3-4. Here the situation is shown from a bird's eye view. An actor (gray body with white circle as head) has the goal to hit a target (gray

cylinder) moving from left to right. Different angles were distinguished in the study. In the image, β represents the target-heading angle. The arrow in front of the actor is the velocity direction of the actor. Thus, it is clear that in the CTH strategy the driver always aims with the angle β in front of the target in its direction of motion. Here $\dot{\beta} = 0$, the offset of aiming in front of the target, remains constant. Furthermore, φ describes the direction angle of the actor and ψ the bearing angle of the moving target.

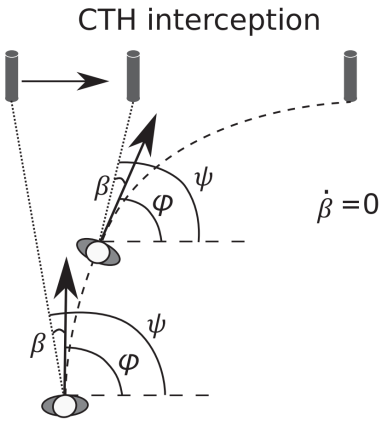

Figure 3-4: *Illustration of the Constant Target Heading (CTH) strategy. The basic idea of this strategy is that the actor is always heading in front of the moving target in its moving direction with a fixed angle β [ZSR19, p. 2].*

Intercepting a moving target by aiming at a fixed distance in front of its current position in its direction of motion seems to be a valid strategy. For this reason, the strategy CTH is used in this work to reach the target, in context the normal mode. This will lead to an asymptotically approach to the normal mode equally to the dashed line shown in the Figure above.

Now that a strategy has been selected based on observations from humans, it is embedded in the engineering context. The focus here is on how implementation can take place from a control engineering point of view. If staying with assistance systems of cars and the tasks of lane changing, there are some relevant approaches in this field. For example, [NGGP08] deals with overtaking maneuvers and accompanying lane changes and proposes fuzzy control as a solution approach. [RTLZ00] is another work dealing with autonomous driving vehicles and control strategies for them. The main focus is on the longitudinal and lateral control of the vehicle motion. For this thesis especially the consideration of the lane change is relevant.

The basic approach for this task proposed in [RTLZ00] is the split of the task into different subtasks and states. This is shown in Figure 3-5. This split is done to model a fitting lane change trajectory dependent on the current state of the change. The vehicle travel direction is from left to right and the lane change is done from the top lane to the bottom

lane in this example. Based on this classification of states, the target trajectory can be

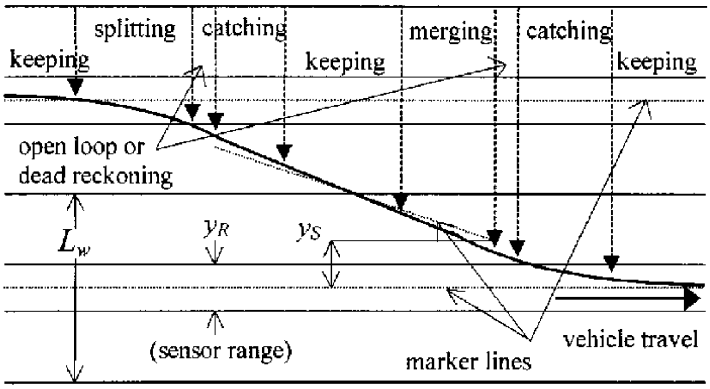

Figure 3-5: *Different states of the lane change task as proposed in [RTLZ00, p. 700]. The trajectory is build up by a polynomial of third order and, as intended by the context, asymptotically approaches the*

modeled depending on the current position of the vehicle. In [RTLZ00] it is suggested to use a third degree polynomial, which results in the equation

$$y_d(x) = a_3x^3 + a_2x^2 + a_1x + a_0$$

with $y_d(x)$ being the vehicles lateral track dependent on its longitudinal position x. It is proposed to model the polynom as given by

$$\begin{aligned}
a_0 &= y_d(0),\\
a_1 &= \dot{y}_d(0),\\
a_2 &= -\frac{2(y_d(x_f) - y_d(0))}{x_f^3} + \frac{\dot{y}_d(x_f) + \dot{y}_d(0)}{x_f^2},\\
a_3 &= \frac{3(y_d(x_f) - y_d(0))}{x_f^2} - \frac{\dot{y}_d(x_f) + 2\dot{y}_d(0)}{x_f},
\end{aligned}$$

with the parameters being dependent on the current state of the lane change. Here, x_f denotes the length of the trajectory. To choose the other parameters, a discrete parametrization is proposed which is dependent on the current state of lane change. These parameters are given in Table 3-1. Here t_a denotes the initial time with $y(t_a)$ and θ_a denoting the initial lateral position and the initial yaw angle of the vehicle from the initial lane direction. y_s is the lateral distance to the lane that is to be intercepted and θ_c is the yaw angel to the new lane. ψ is an angle that can be implemented depending on the systems noise level. With this approach, it is possible to plan an ideal trajectory that ensures a lane change from one lane to a new lane with asymptotic convergence to the new lane. In the context of the application of this thesis, this can ensure that the desired normal mode is reached

Table 3-1: *Parametrization and trajectory planning for the states of a lane change as given in [RTLZ00, p. 701]. The corresponding states are shown in Figure 3-5.*

State	$y_d(0)$	$\dot{y}_d(0)$	$y_d(x_f)$	$\dot{y}_d(x_f)$
Splitting	0	0	$-y_s$	$\theta_c + \psi$
Merging	0	0	y_s	$-\theta_c - \psi$
Catching	$y(t_a)$	θ_a	0	0

without overshooting or generating jerky behavior. For the implementation of the control itself, a standard trajectory-following control or a state control with target trajectory will be used.

In summary this chapter presented the fundamental theory focusing on mathematical and pyhsical approaches needed for the work presented in this thesis. It started of with the introduction of constrained and parallel kinematics in Section 3.1 defining the concepts of Pfaffian constraints and loop closure equations. Then, the theory of normal modes of linear and nonlinear dynamic systems was presented in Section 3.2 with an emphasis on the newly developed concept of nonlinear normal modes. The last two Sections 3.3 and 3.4 showed the control approaches. Following these theoretical fundamentals, dynamics simulations will be set up in the following chapter with the use of kinematic constraints and furthermore the concept of nonlinear normal modes will be validated with these systems.

4 Identification and analysis of nonlinear normal modes through dynamics simulations

After the related work and the basics of robotic locomotion as well as the mathematical-physical fundamentals for this work have been explained in the previous chapters, here the dynamics simulations setup within this thesis are presented. The presented models increase in complexity working towards the dynamics model of one leg of the robot Bert, on which the previously explained controller to stabilize nonlinear modes should be implemented. Finally, results regarding the usability of nonlinear normal modes for locomotion are shown.

The chapter starts with the modelling of an elastic double pendulum in Section 4.1. In the next step, Pfaffian constraints are introduced in Section 4.2 as a method to model a constrained system. Following the introduction of the Pfaffian constraints, the active joint method is shown next in Section 4.3. Last, the nonlinear normal modes of the setup models are found numerically and investigated with respect to varying parameters in Section 4.4.

Based on previous research on nonlinear modes of mechanical systems, the tool nnormal modes was developed at the DLR. This tool is capable of finding the generators and corresponding nonlinear modes of systems based on dynamics equations or -urdf models. The dynamics equations have to be in standard notation given by

$$\underline{M}(\underline{x})\ddot{\underline{x}} + \underline{C}(\underline{x}, \dot{\underline{x}})\dot{\underline{x}} + \underline{g}(\underline{x}) = 0$$

with minimum descriptive coordinates $\underline{x}$. For the calculation, the mass matrix $M(\underline{x})$, the coriolis and centrifugal matrix $\underline{C}(\underline{x}, \dot{\underline{x}})$, as well as the vector $\underline{g}(\underline{x})$ containing gravitational force and spring forces are needed. In addition, the potential $\underline{V}_{Grav}(\underline{x})$, the potential arising from gravity, must be calculated and passed to the tool. Based on the given DoFs of the system, nnormal modes can obtain the generators and corresponding modes for a predifined energy range. This work aims at further exploration of the nonlinear normal modes obtained with this tool. For this reason, the calculation is not considered here and the generators and normal modes are always taken as given after the appropriate modeling of the system.

4.1 Elastic double pendulum

As a first approach, this work models a scientifically well researched and well known system and uses it for gaining first experiences with nonlinear modes. This system is

the double pendulum, which in the inverted case is already a commonly used model for articulated robotic legs, such as the Bert leg.

The basic double pendulum, which is used in this work, was modeled according to [Del11]. This model was extended through the additions of spring rest positions k_{eq}, as well as the possibility to independently define the mass positions. This was done to meet the application case in a better way. Furthermore, the angles are defined in the physical way, dependent on the vertical axis. This results in the spring rest positions k_{eq} being defined the same way as the joint angles. These definitions of the angles hold for the whole thesis and all simulations that are set up.

The pendulum is shown in Figure 4-1. The coordinate system P is located in the revolute joint of the base. The gravitational force acts in negative y_P direction. The pendulum consists of two masses m_1 and m_2, in this case, mounted to the ends of the massless links. The positions of the masses can be changed along the link lengths l_1 and l_2 via the parameters $l_{c,1}$ and $l_{c,2}$ while for the double pendulum, $l_1 = l_{c,1}$ and $l_2 = l_{c,2}$ is chosen, i.e. the mass is located at the end of each link. Both revolute joints are provided with torsion springs with the spring stiffnesses k_1 and k_2. The upper torsion spring is attached to the base and the lower spring is attached between the two links. Both joints have a direct input of an input torque given by τ_1 and τ_2. In addition, possible counter torques due to damping with parameters d_1 and d_2 are introduced.

As a first step for the analysis of this system, the number of DoF is calculated with Grüblers Formula which was introduced in 3.1.1. Taking the provided formula (3-1), two DoF are the result for the elastic double pendulum. This is the first step needed to model a dynamic system because according to the Lagrange formalism, as many coordinates as DoF are needed. Furthermore this is the first requisit needed for the nnormal modes tool.

In the next step, the associated differential equations are briefly discussed. The angles are defined dependent on the vertical axis, also denoted by the y_P-axis. Since the double pendulum represents an established system, the derivation of the differential equations will be abbreviated here and will be completed with the representation of the resulting energies

$$\begin{aligned} T &= \frac{1}{2}m_1(\dot{x}_{P,1}^2 + \dot{y}_{P,1}^2) + \frac{1}{2}m_2(\dot{x}_{P,2}^2 + \dot{y}_{P,2}^2), \\ V &= \frac{1}{2}k_1(\varphi_1 - k_{1,eq})^2 + \frac{1}{2}k_2(\varphi_2 - \varphi_1 - k_{2,eq})^2 + m_1 g y_{P,1} + m_2 g y_{P,2}, \end{aligned} \tag{4-1}$$

where T is the kinetic energy and V is the potential energy. $x_{P,i}$ and $y_{P,i}$ are the Cartesian coordinates representing the position of mass i in the given Cartesian coordinate system

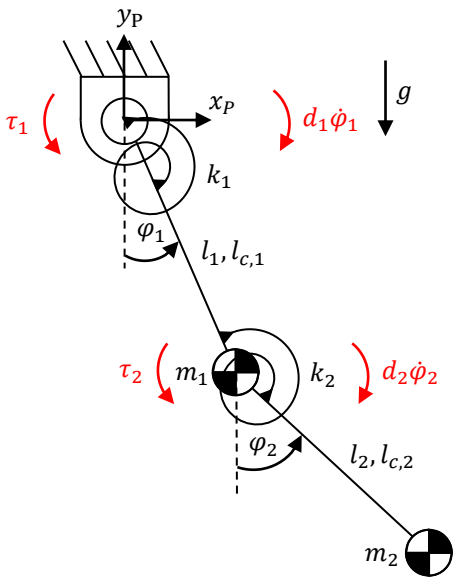

Figure 4-1: *The elastic double pendulum used in this thesis consists of 2 links, 2 masses and two rotational springs. The actuation is realised through torques at the joints. The pendulum is used as a modelling approach for this thesis.*

P. Inserting the angular representations of the Cartesian coordinates into the energies, acoording to the Lagrange formalism, the differential equations thus result in

$$\frac{\delta L}{\delta \dot{\varphi}_1}\delta t - \frac{\delta L}{\delta \varphi_1} + d_1\dot{\varphi}_1 = \tau_1,$$
$$\frac{\delta L}{\delta \dot{\varphi}_2}\delta t - \frac{\delta L}{\delta \varphi_2} + d_2\dot{\varphi}_2 = \tau_2,$$

with

$$L = T - V.$$

The external torque inputs τ_1 and τ_2 and the linear damping terms with the damping constants d_1 and d_2 are introduced as well. An example of the conversion from the Cartesian coordinates to the angular representation is shown in (4-5). The pendulum simulation is intended to be a basic simulation and is accordingly parameterized with default values, which are shown in Table 4-1. Even though damping parameters are given here, most of the thesis is considering the conservative system. The first simulations are done with the conservative system and the calculations with the nnormal modes tool are done with external forces and the damping chosen as zero.

Table 4-1: *Standard parametrization of the double pendulum simulation. Note that the damping is not always used and mostly the conservative system is used for analysis and evaluation.*

Description	Name	Value	Unit
Gravity constant	g	9.81	ms^{-2}
Upper mass	m_1	1	kg
Upper mass position along the first link	$l_{c,1}$	1	m
Upper link length	l_1	1	m
Upper spring constant	k_1	10	kgs^{-2}
Upper spring equilibrium position	$k_{1,eq}$	$\frac{\pi}{2}$	rad
Upper damping coefficient	d_1	0.1	kgm^2s^{-1}
Lower mass	m_2	1	kg
Lower mass position along the second link	$l_{c,2}$	1	m
Lower link length	l_2	1	m
Lower spring constant	k_2	10	kgs^{-2}
Lower spring equilibrium position	$k_{2,eq}$	$\frac{\pi}{2}$	rad
Lower damping coefficient	d_2	0.1	kgm^2s^{-1}

As described in the previous chapter, there are big differences between linear and nonlinear systems. To underline the differences between linear and nonlinear systems, some of the already mentioned nonlinear properties are describe with the phase plot of the elastic double pendulum shown in Figure 4-2. The way of presentation chosen here will be further used in the course of the work. The color of the trajectory changes with time. The color legend showing the simulation time is placed on the right. The initial position of the pendulum (black marker) with initial velocities equal to zero, was chosen randomly here. Furthermore the damping is set to zero resulting in a conservative system.

The nonlinear behavior of the pendulum is apparent from this figure. It does exhibit a complex behavior, indicating nonlinearity. Most importantly, the phase plot also does not form an ellipse, which would be a clear sign of a linear system.

According to the definition of nonlinear normal modes given in the last chapter, this is not a nonlinear normal mode of the system due to the lack of a line shape, which would be surprising due to the random initial condition. Now, to get the nonlinear normal modes of the system and to analyze them, the DLR tool nnormal modes is used. The standard parameterization of the double pendulum shown in Table 4-1 is used. The result is always discrete, both eigenmanifold $\mathfrak{M}$ and generator $\mathfrak{R}$ are pointclouds or arrays and no continuous functions.

After the computation, it is expected that the conservative double pendulum can be given an arbitrary point of $\mathfrak{R}$ as initial value and will oscillate on the associated eigenmanifold

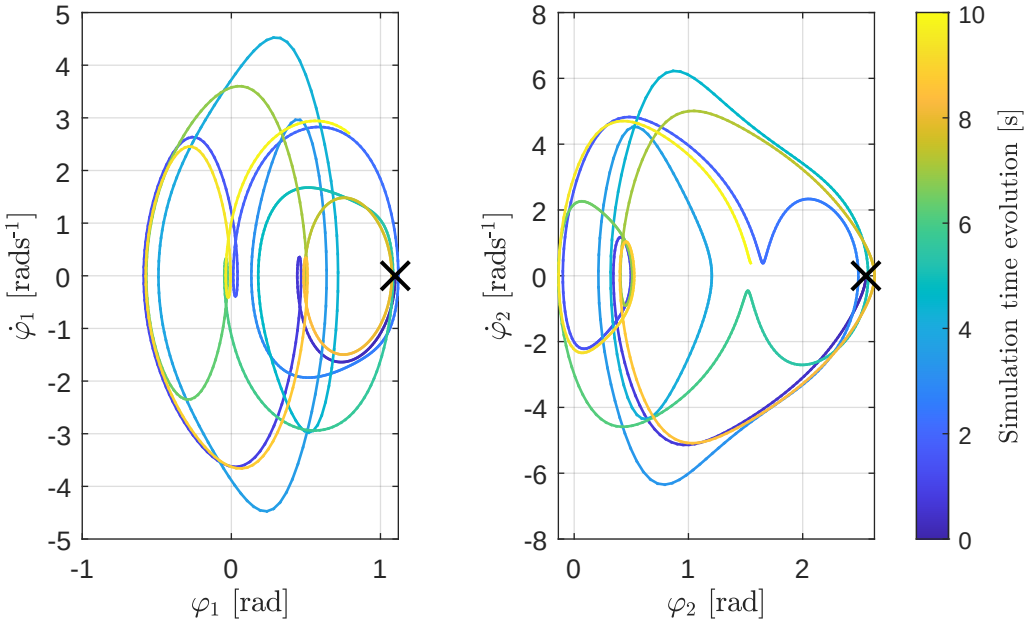

Figure 4-2: *Phase plot of the double pendulum that shows its nonlinear nature. The pendulum angles are shown on the horizontal axis, the corresponding velocity is shown on the vertical axis. The colorful trajectory illustrates the time evolution by changing its color over time. The black marker highlights the initial condition.*

$\mathfrak{M}$. This is validated in simulation and the result is shown in Figure 4-3. Two simulations were performed for this plot. For the upper two plots, the initial condition of the pendulum was chosen according to the first of two possible generators, corresponding to the two DoF of the double pendulum. For the lower two plots, a point of the other generator was chosen. In red the normal mode is shown on which the system should oscillate, respectively. For each computed energy level, there are two points of the generator (blue) as the start and end points of the modal oscillation and one modal oscillation (red). The black marker again represents the chosen starting point and the color gradients of the trajectories provide information about the time course. When combining the upper two and lower two plots it would results in a 4D manifold

The result of the simulation of the double pendulum is clear: The modes calculated by the nnormal modes tool are valid for the designed double pendulum. The pendulum remains on the mode as desired after the start on the generator, it does not leave the mode and performs modal oscillations on the eigenmanifold. This leads to the result that the Matlab framework built in this thesis, provides the correct inputs for the nnormal modes tool and is capable of providing, together with the nnormal modes tool, sufficient outcomes for the analysis of nonlinear normal modes.

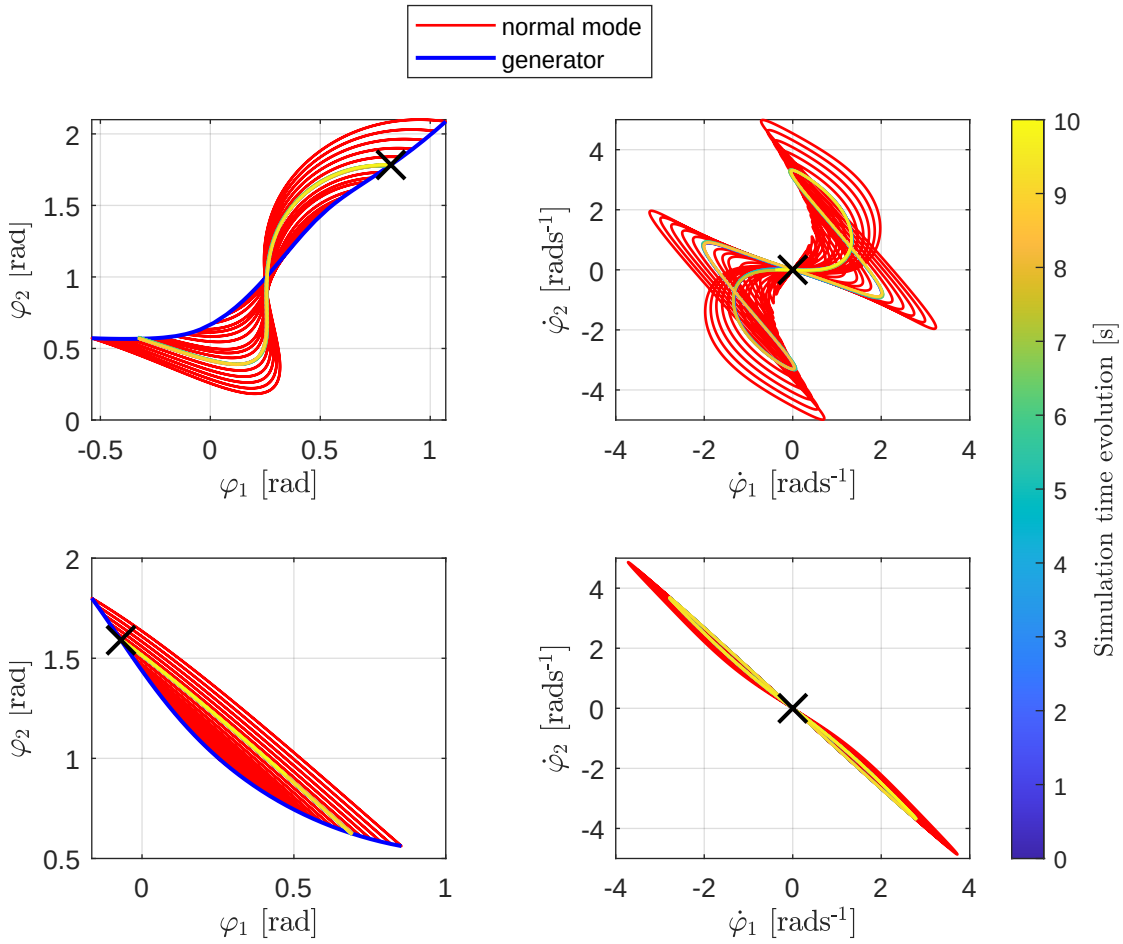

Figure 4-3: *Two simulations have been performed: The top two plots show the result for generator and mode one, the bottom two show the result for generator and mode two. The black marker highlights the initial condition. For the conservative pendulum, the trajectory actually runs perfectly on the modes, validating the system with these modes.*

In addition, in Figure 4-2, there is a phase plot shown for the simulation on the first mode from Figure 4-3. It can be observed that the system is not chaotic anymore and oscillates regularly.

In this trial the pendulum performs periodic recurring oscillations and the trajectory is closed leading to the result that the nonlinear normal modes where sucessfully found for this system.

To sum up, this section introduced the approach to model a well known system with similarities to the one leg of Bert. Is was the aim to set up a framework in the software Matlab for modelling a dynamic system, calculating its eigenmanifolds and generators afterwards and validating the results visually. Also it was shown in the plots that the nonlinear normal modes behave as expected and defined in the previous chapter and that

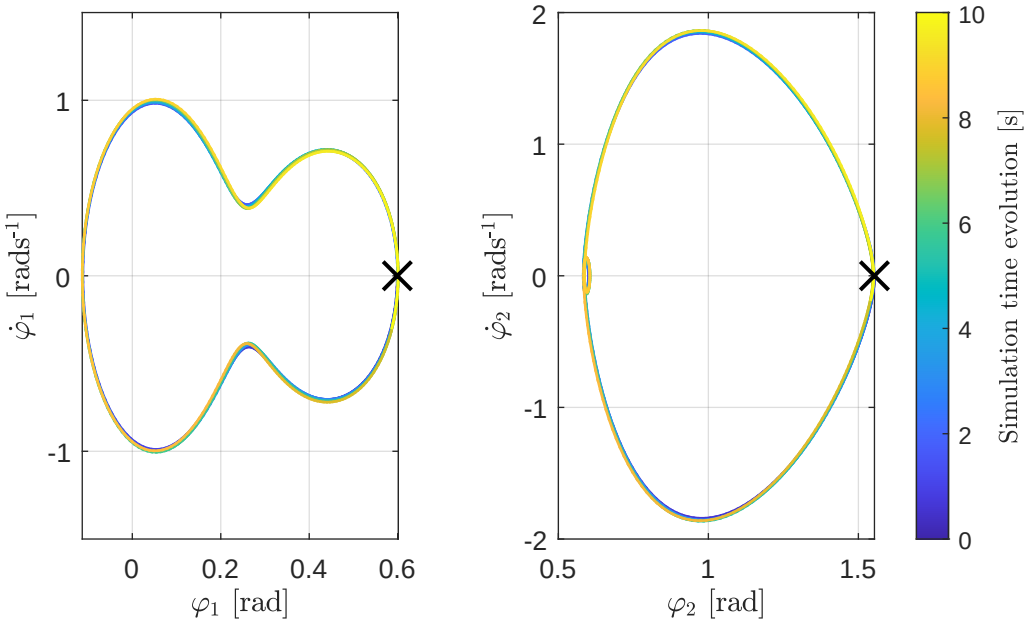

Figure 4-4: *Phase plot of the double pendulum that shows how well the pendulum oscillates periodically as it is on its normal mode. The pendulum angles are shown on the horizontal axis, the corresponding velocity is shown on the vertical axis. The colorful trajectory illustrates the time evolution by changing its color over time. The black marker highlights the initial condition.*

the nonlinear properties could be found in the phase plots accordingly. Now, the step is to approach a suitable model of the Bert leg.

4.2 Application of Paffian constraints - Inverted Pendulum

After the sucessful simulations with the elastic double pendulum in the previous section, the aim is now to approach a model for the one leg test rig. As shown previously in Section 2.5 in Figure 2-9, the test rig consists of an upper and lower leg link as well as a part of the body. Seeing this from the perspective of modelling dynamics, an inverted tripple pendulum results, when the foot is fixed at the ground. The double pendulum is extended by another revolute joint and another mass at the end. This top link stays upright at all the time because it is constrained upright in the Bert leg test rig through the attachment to a boom. The test rig will be modeled in a two dimensional plane with a planar triple pendulum, without introducing three dimensional parallel kinematics with the boom. Therefore, the first idea in this thesis is to constrain the motion of the pendulum by introducing constraint forces with the method of Pfaffian constraints. First an example is presented which also provides possible results for ongoing work with the robot Bert.

Afterwards a constrained pendulum simulation is set up to obtain a suitable model that represents the test rig dynamics.

4.2.1 Introductory example simulation of a planar pendulum

To constrain the triple pendulum to meet the dynamics of the test rig, the method of Pfaffian constraints is chosen. This method is described in [MLS94]. There, a planar simple pendulum example was proposed to show the usability of an approach with Pfaffian constraints. The pendulum is shown in Figure 4-5. The idea is to model a single mass in a Cartesian space and constrain its dynamics to meet the dynamics of a pendulum. Therefore the Cartesian coordinate system with axes x_E and y_E is placed in the revolute joint. Additionally gravity pointing in negative y_E-direction is introduced as well as the parameters l_1 and m_1 denoting the length of the link and the mass which is placed at the end of the link.

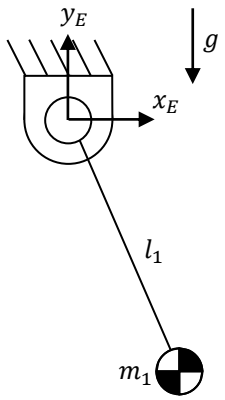

Figure 4-5: *The planar simple pendulum in Cartesian space as a useful example on how constraints can be used to describe the dynamics of a system [MLS94, p. 270].*

The dynamics equations are described in [MLS94] as well as a suitable constraint. The mass is supposed to stay on the circular trajectory around the revolute joint by the constraint

$$x_E^2 + y_E^2 = l^2.$$

Given the method of Pfaffian constraints, already described in 3.1.1, the constraint is first derived leading to $\underline{A}(q) = \begin{bmatrix} x_E & y_E \end{bmatrix}$ and then inserted into the extended dynamics equations form (3-2) together with λ being calculated by (3-3). This leads to the whole dynamics expression as

$$\begin{bmatrix} m_1 & 0 \\ 0 & m_1 \end{bmatrix} \begin{bmatrix} \ddot{x}_E \\ \ddot{y}_E \end{bmatrix} + \begin{bmatrix} 0 \\ m_1 g \end{bmatrix} - \frac{1}{l_1^2} \begin{bmatrix} x_E \\ y_E \end{bmatrix} \left(m_1 g y_E + m_1 \left(\dot{x}_E^2 + \dot{y}_E^2 \right) \right) = 0 \tag{4-2}$$

It has to be noted that the constraint was inserted into λ before the insertion to the whole dynamics.

This approach has two advantages in terms of dynamics modelling: First, it is possible to describe the dynamics of a system with a number of variables unequal to the DoF. With the dynamics equation in (4-2), the, with respect to Grüblers formula in (3-1), one degree of freedom pendulum, can be described with two Cartesian variables x_E and y_E. This is linked to the second advantage: It is possible to describe the position of a mass in Cartesian space and e.g. get the translational movement of the mass directly in x_E-direction, which is also shown in Figure 4-6. In the left plot, the x_E-direction movement is shown with the current positon of the mass marked in dark blue just as in the right plot. The right plot shows the pendulum with the link in black and the constraint in dashed red. For this simulation, parameters from Table 4-1 were chosen.

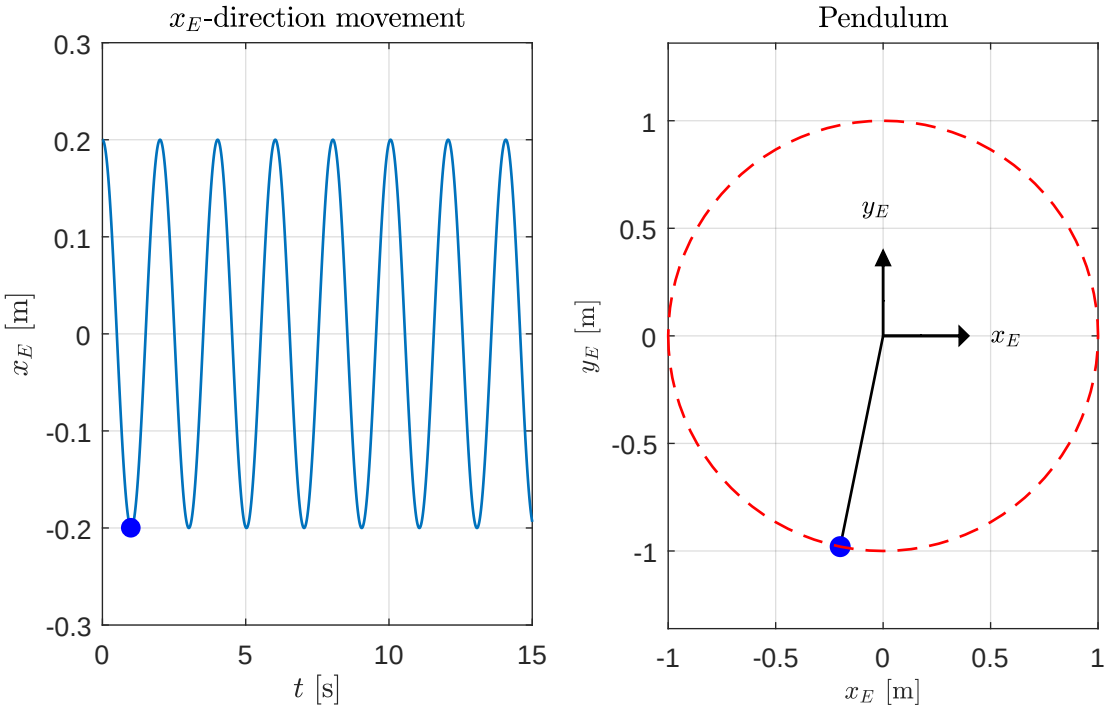

Figure 4-6: *The movement of the planar simple pendulum described in x-direction in Cartesian space.*

The main goal of using Pfaffian constraints with the triple pendulum was, to meet the dynamics of the test rig. Therefore, after the sucessful simulation of the simple planar pendulum, the inverted triple pendulum simulation is set up with a suitable Pfaffian constraint.

4.2.2 Modelling of an inverted pendulum with Paffian constraints

The next step to model the dynamics of the one leg test rig is to set up a inverted triple pendulum with constraints. The goal is that the triple pendulums top link, representing the body of the oneleg test rig, is constrained in its rotation axes. The pendulum is shown in Figure 4-7. It has three links with lengths l_1, l_2 and l_3. Furthermore, the masses m_1, m_2 and m_3 are defined with their positions, seen from the respectively previous joint, l_{c1}, l_{c2} and $l_{c3} = l_3$. The coordinate system I is placed in the base revolute joint. The gravitational force g is pointing downwards in negative y_I-direction. The pendulum has 2 springs k_1 and k_2 at the upper two revolute joints analogue to the implementation in the Bert leg. The pendulum can be described with the angles φ_1, φ_2 and φ_3 denoting the movement of the three revolute joints, all describing the position relative to the orthogonal of the ground.

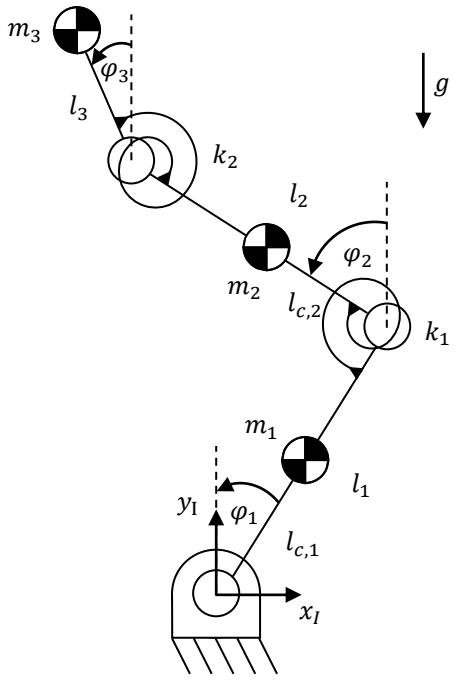

Figure 4-7: *Structure of the inverted triple pendulum with the goal to constrain angle φ_3 in a way that link three is always vertical. The springs ensure the upright position of the inverted pendulum.*

As a first step, the DoF are calcuated with the formula (3-1). This results in three DoF validating the choice of the three angles to describe the pendulums movement. The energies of the inverted pendulum are similar to the energies of the double pendulum in (4-1)

with the addition of the third mass and a different definition of the springs. This leads to

$$T = \frac{1}{2}m_1(\dot{x}_{I,1}^2 + \dot{y}_{I,1}^2) + \frac{1}{2}m_2(\dot{x}_{I,2}^2 + \dot{y}_{I,2}^2) + \frac{1}{2}m_3(\dot{x}_{I,3}^2 + \dot{y}_{I,3}^2),$$
$$V = \frac{1}{2}k_1(\varphi_2 - \varphi_1 - k_{1,eq})^2 + \frac{1}{2}k_2(\varphi_3 - \varphi_2 - k_{2,eq})^2 + m_1 g y_{I,1} + m_2 g y_{I,2} + m_3 g y_{I,3},$$

with T denoting the kinetic energy and V the potential energy. x_I and y_I denote the positions of the masses in Cartesian space of the coordinate system I. Furthermore, $k_{1,eq}$ and $k_{2,eq}$ are the spring equlibrium positions in rad. Note again that the angles are expressed in physics definition orthogonal to the ground and not in robotics notation dependent on the previous angle, respectively. Therefore, the spring energies are each dependent on both of the joint angles describing the two link positions that the springs are connected to, respectively.

With the Lagrange method and $L = T - V$, the resulting conservative system of equations of motions is then given by

$$\begin{aligned}
\frac{\delta L}{\delta \dot{\varphi}_1}\delta t - \frac{\delta L}{\delta \varphi_1} &= 0, \\
\frac{\delta L}{\delta \dot{\varphi}_2}\delta t - \frac{\delta L}{\delta \varphi_2} &= 0, \\
\frac{\delta L}{\delta \dot{\varphi}_3}\delta t - \frac{\delta L}{\delta \varphi_3} &= 0.
\end{aligned} \tag{4-3}$$

These equations describe the dynamics of an unconstrained elastic triple pendulum. After this fundament is laid, the next step is to introduce a constaint that keeps the system's body, denoted by m_3, upright at all times.

The proposed constraint is

$$\varphi_3 = 0,$$

and the derivation by all three angles leads to the Pfaffian constraint as

$$\underline{A}\begin{bmatrix} 0 \\ 0 \\ \dot{\varphi}_3 \end{bmatrix} = \begin{bmatrix} 0 & 0 & 1 \end{bmatrix}\begin{bmatrix} 0 \\ 0 \\ \dot{\varphi}_3 \end{bmatrix} = 0,$$

resulting in the obtaining of $\underline{A}$. Now, λ has to be calculated by first rearranging the equations of motion in (4-3) to standard Lagrange form and then inserting the resulting matrices into (3-3). This is done computationally in Matlab.

As λ and $\underline{A}$ are calculated and the equations of motion are rearranged, they can be inserted into (3-2) which leads to a third order representation of the constrained inverted triple pendulum.

With this constrained system of equations, simulations were performed validating the approach. The result is shown in Figure 4-8. The left plot shows the time evolution of the three angles of the three joints. The right plots shows the acting constraint forces for all three joints. For this simulation, the pendulum was released from a arbitrary configuration space point including the constraint leading to $\varphi_3 = 0$. If the constraint is not ensured within the initial condition, the simulation breaks.

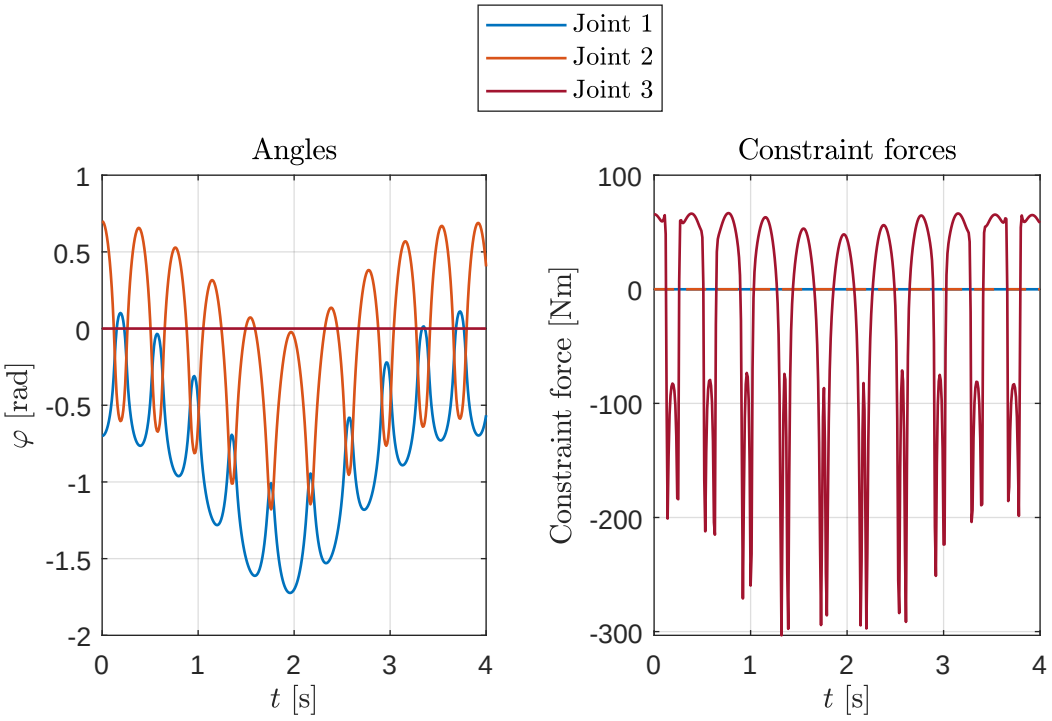

Figure 4-8: *Simulation results of the constrained inverted triple pendulum, validating the calculations and constraint assumptions. The constraint forces only act in joint three assuring the upright position of the third link. Furthermore the joint 3 stays at zero with its angel φ_3 shown in brown.*

By analysing the plots it stands out that the third angle of the third joint stays exactly at zero at all times. This implies that, even though there are modeled dynamics for the third joint, it stays at zero due to the constraint forces shown on the right. The constraint forces only act in the third joint. The evolution of the force trajectory is oscillating with the motion of the other two joints

As desired, the modeled dynamic system indeed behaves similar to the one leg test rig. The conclusion is that the constrained inverted triple pendulum is a good planar model for the test rig. However, there is a problem with the caluclation of the nonlinear normal

modes of this system. The tool nnormal modes is only capable to calculate the normal modes of a system described in minimal coordinates. It is not capable, yet, to give the normal modes for a constrained system as the constrained inverted triple pendulum. Therefore, there is the need for a different approach to calculate the normal modes for this system which follows in the next section. Even though the constraining method with Pfaffian constraints can not be used for now, it has some advantages that could be used in the future if nnormal modes was able to calculate the normal modes for a system not written with minimum coordinates. This method could be used to describe the motion of the robot in Cartesian space. Furthermore, it might be of interest to use this method, if other kinematic constraints appear within the ongoing developement of the robot Bert. Nevertheless, constraining can not yet be used which leads to a different approach in the following section to model the one leg test rig.

4.3 Active joint method - Modelling of the one leg test rig

As the previous section was successful in modelling the test rig but failed with the calculation of the nonlinear normal modes, the goal of this section is to propose an approach for the test rig modelling that is well suited for normal modes calculation. As in the previous section, first an easier example system is considered using the active joints method described in 3.1.1. After the modelling of the example system, the Bert test rig is modelled accordingly where the constraint of the body being upright could be seen as a loss of one degree of freedom. This assumption is validated by a comparison with the modeling approach of the previous section with Pfaffian constraints.

4.3.1 Introductory example simulation of a slider crank

When considering multibody and multijoint systems that are attached to the ground at more than one point, the active joint method can be used to fully describe the systems dynamics. Due to the kinematics and constraints introduced by the joints and attachments to the ground, it is possible to describe a system only with the movement of a subset of joints being used.

To describe this idea visually and as an approach, a slider crank mechanism is considered. This mechanism is proposed in [LP17, p. 18] and has a closed chain kinematic. The system is shown in Figure 4-9. In this case, mass m_3 is located on a linear guide with fixed stops on the right and left, and a spring with constant k_1 at one side ensuring elastic movement. Furthermore two links with lengths l_1 and l_2 are connected to the mass m_3, which have the mass m_1 and m_2. The positions of the masses are l_{c1} and $l_{c,2}$. The kinematic chain is closed by the base revolute joint with the state as the angle φ_1. The coordinate system S is located at this joint. Another angle φ_2 is defined at the top describing the

motion of the revolute joint at the top. Furthermore, variable s, which is the positon of the mass m_3 on the prismatic joint, is introduced.

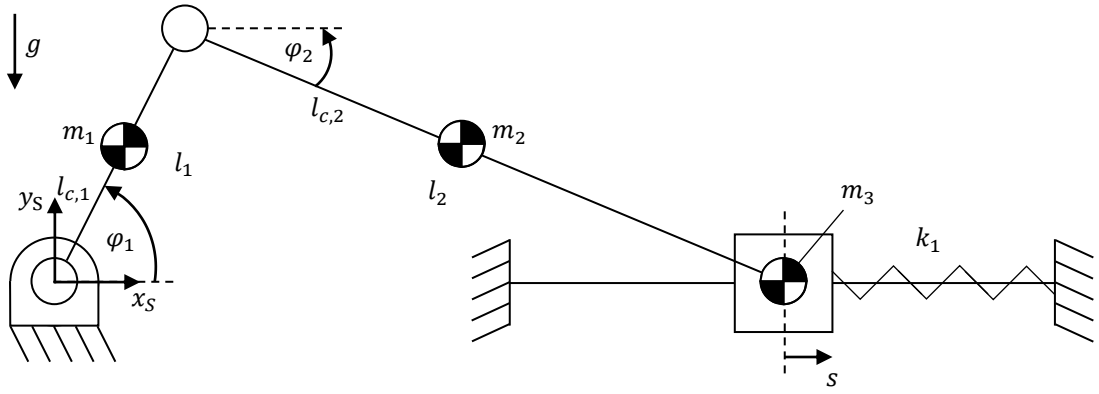

Figure 4-9: *The slider crank, whose simulation serves to illustrate the active joint method. Furthermore it represents system with a closed chain. The system was proposed in [LP17, p. 18].*

Again it is important to carefully calculate the DoF for this system with Grüblers formula (3-1). There are two ways of dealing with it, either taking the ground into account as a link or not taking it into account but taking the prismatic joint as two joints, each providing one degree of freedom. The result for this system is one degree of freedom. The active joint method now proposes to model the dyamics according with one active variable. The kinematics dependencies are then fully described only with this one variable.

For the slider crank, the chosen variable is φ_1. To denote φ_2 in depending of φ_1 and to denote the mass positions only with respect to φ_1 as the only time dependent variable, a kinematic relation is proposed as

$$\varphi_2 = \frac{l_2 \varphi_1}{l_1}, \tag{4-4}$$

resulting from

$$\frac{l_1}{\varphi_1} = \frac{l_2}{\varphi_2}.$$

The equations result from the constraint that the end of link two where mass m_3 is located needs to stay at $y_S = 0$. Therefore, the relations of link lengths one and two and angles one and two need to be equal.

The next step is again to define the energies of the system. In this case the needed mass positions are first defined with both angles φ_1 and φ_2. Afterwards, (4-4) is inserted resulting in

$$T = \frac{1}{2}m_1(\dot{x}_{S,1}^2 + \dot{y}_{S,1}^2) + \frac{1}{2}m_2(\dot{x}_{S,2}^2 + \dot{y}_{S,2}^2) + \frac{1}{2}m_3(\dot{x}_{S,3}^2 + \dot{y}_{S,3}^2),$$
$$V = \frac{1}{2}k_1(s - k_{1,eq})^2 + m_1 g y_{S,1} + m_2 g y_{S,2} + m_3 g y_{S,3},$$

with x_S and y_S denoting the Cartesian mass positions dependent on angle φ_1 and $k_{1,eq}$ denoting the spring equilibrium. The variable s is defined as

$$s = l_1 \cos(\varphi_1) + l_2 \cos(\varphi_2) \quad = l_1 \cos(\varphi_1) + l_2 \cos\left(\frac{l_2 \varphi_1}{l_1}\right).$$

As it can be seen, s can be substituted by a term that is only dependent on φ_1, the active joint variable.

Taking the Lagrange method the equation $L = T - V$, the resulting ordinary differential equation is then given by

$$\frac{\delta L}{\delta \dot{\varphi}_1}\delta t - \frac{\delta L}{\delta \varphi_1} = 0,$$

resulting in a system of order one fully describing the whole dynamics of the slider crank. To verify the correctness of the relation, simulations have been carried out which are detailed in A1-1.

Comparing the constraining with Pfaffian constraints and the active joints method, the difference is clear: While with Pfaffian constraints, the state vector contains all introduced variables, e.g. all angles, with the active joints method, the other variables need to be calculated as a second step via the used kinematic relations. But as the system has one degree of freedom, the minimum number of variables to describe it is also one. By taking the active joint method, this criterion for the nnormal modes tool is satisfied which makes this method suitable for the use in the modelling of the one leg test rig. Therefore, in the next part, the one leg test rig is modelled with the active joint method.

4.3.2 Modelling of the one leg test rig with the active joint method

After the modelling of the test rig was successful with the Pfaffian constraints, but it could not be used with nnormal modes, the approach chosen now is the active joint method. The goal is to rethink the kinematics of the system leading to a description method with

minimum coordinates and the capability of correct actuation as predefined by the test rig.

Considering the Bert leg test tig in three dimensional space, there is a closed chain resulting through the attachment to the boom. This leads to the idea that the third upper joint of the triple pendulum is not providing any freedom and is instead constrained to zero degrees. Following this, inserting three joints and three links into Grüblers formula (3-1) and adding that only two of the joints provide one degree of freedom each, the formula returns two DoF. Following the active joint method, there should be two active variables chosen describing the movement of two of the joints leading to the minimum coordinate representation of the system.

The corresponding system is illustrated in Figure 4-10. Here, the coordinate system B is again placed in the base revolute joint and the gravity g is pointing in negative y_B-direction. The links and joints are described above in Figure 4-7. But there are also differences: One big difference is the decoupling of the springs. For the robot Bert, spring one with stiffness k_1 is only dependent on the angle φ_1 with the other end attached to the body or to the ground in the case of the one leg test rig. The same holds for the second spring with k_2 whereas this spring is only dependent on angle φ_2. Additionally the constraint of the angle φ_3 is already illustrated in the structure with the desired value of zero. Furthermore, damping with coefficients d_1 and d_2 as well as actuating input torques τ_1 and τ_2 are introduced at the joints two and three.

For the modelling of this system, it is important to keep the structure of the real test rig in mind. As the base joint describes the foot, it is not actuated. The angles φ_1 and φ_2 at joints one and two can also each be found at the respectively next joints, with the zero angles being defined downwards. This leads to the following dynamics modelling.

First, the mass positions are defined for the obtaining of the energies as

$$\begin{aligned}
&x_{B,1} = l_{c,1}\sin(\varphi_1),\ y_{B,1} = l_{c,1}\cos(\varphi_1),\\
&x_{B,2} = l_1\sin(\varphi_1) - l_{c,2}\sin(\varphi_2),\ y_{B,2} = l_1\cos(\varphi_1) + l_{c,2}\cos(\varphi_2),\\
&x_{B,3} = l_1\sin(\varphi_1) - l_2\sin(\varphi_2) - l_3\sin(\varphi_3),\ y_{B,3} = l_1\cos(\varphi_1) + l_2\cos(\varphi_2) + l_3\cos(\varphi_3),
\end{aligned} \tag{4-5}$$

with the corresponding time derivatives calculated with Matlab respectively. Now, as the active joint method provides to use as many variables as DoF, the two angles φ_1 and φ_2 are chosen for the description as with these angles, the actuation as well as the spring

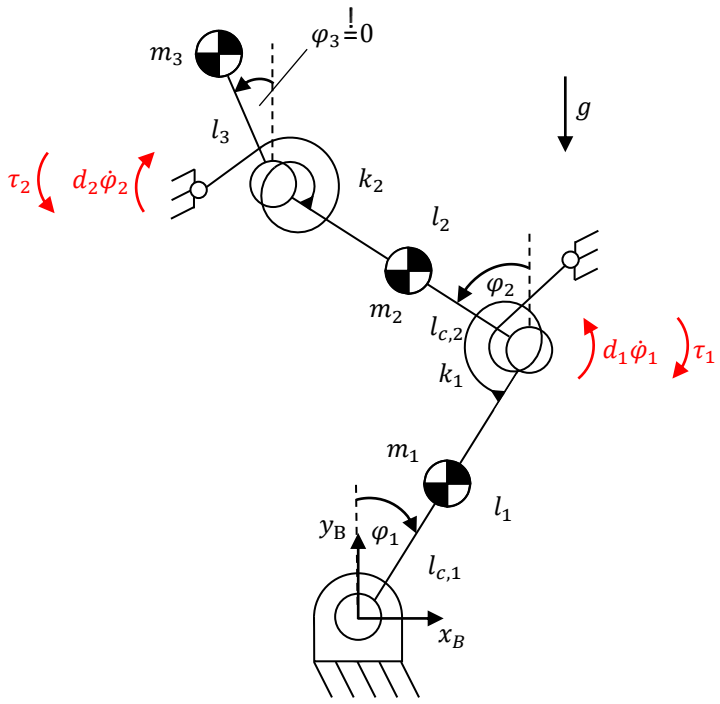

Figure 4-10: *This figure shows the planar structure of the final modelling of the one leg test rig. Special focus is placed on the springs which are decoupled. That means they are just dependent on one angle or only dependent on the orientation of one of the leg parts. The angles are chosen according to the test rigs strcuture exciting exactly these angles via motors.*

forces can be described easily. As the requirement is $\varphi_3 = 0$, this is inserted into the mass position definition, adjusting the third row of (4-5) to

$$x_{B,3} = l_1 \sin(\varphi_1) - l_2 \sin(\varphi_2) - l_3 \sin(0) = l_1 \sin(\varphi_1) - l_2 \sin(\varphi_2),$$
$$y_{B,3} = l_1 \cos(\varphi_1) + l_2 \cos(\varphi_2) + l_3 \cos(0) = l_1 \cos(\varphi_1) + l_2 \cos(\varphi_2) + l_3.$$

Now the three mass positions are only dependent on the two angles φ_1 and φ_2. With this description of the system with two variables is as desired, the next step is again to define the energies. Here, again a special focus has to be placed on the spring definitions as the spring movement is only dependent on either one of the angles. The kinetic energy T and the potential energy V are yet defined as

$$T = \frac{1}{2} m_1 (\dot{x}_{B,1}^2 + \dot{y}_{B,1}^2) + \frac{1}{2} m_2 (\dot{x}_{B,2}^2 + \dot{y}_{B,2}^2) + \frac{1}{2} m_3 (\dot{x}_{B,3}^2 + \dot{y}_{B,3}^2),$$
$$V = \frac{1}{2} k_1 (\varphi_1 - k_{1,eq})^2 + \frac{1}{2} k_2 (\varphi_2 - k_{2,eq})^2 + m_1 g y_{B,1} + m_2 g y_{B,2} + m_3 g y_{B,3},$$

with $k_{1,eq}$ and $k_{2,eq}$ denoting the spring equilibrium positions in rad. Taking a step, the resulting dynamics system is of second order and can be described as

$$\frac{\delta L}{\delta \dot{\varphi}_1}\delta t - \frac{\delta L}{\delta \varphi_1} + d_1\dot{\varphi}_1 = \tau_1,$$
$$\frac{\delta L}{\delta \dot{\varphi}_2}\delta t - \frac{\delta L}{\delta \varphi_2} + d_2\dot{\varphi}_2 = \tau_2,$$

again with $L = T - V$, respectively. Furthermore the actuation τ is included as well as damping with the coefficients d.

The advantage of this model of the one leg test rig is, that it is written in minimum coordinates respectively. This enables the calculation of the normal modes with the tool nnormal modes.

As the nonlinear normal modes can be calculated now, the model is first parametrized with the parameters of the test rig. The paramters are shown in Table 4-2. Main differences in comparison to the standard parameters used with the double pendulum are the leighter weight, the shorter link lengths and at the same time the greater spring stiffness. The assumption is that this will result in higher frequencies that might require a high sampling rate for simulations and for the test rig real time facilities.

Table 4-2: *Parametrization of the one leg test rig of the robot Bert. Note that the damping is not always used and mostly the conservative system is used for analysis and evaluation.*

Description	Name	Value	Unit
Gravity constant	g	9.81	ms^{-2}
First mass	m_1	0.05	kg
First mass position along first link	$l_{c,1}$	0.0384	m
First link length	l_1	0.08	m
First spring constant	k_1	2.94	kgs^{-2}
First spring equilibrium position	$k_{1,eq}$	0.5	rad
First damping coefficient	d_1	0.3	kgm^2s^{-1}
Second mass	m_2	0.107	kg
Second mass position along second link	$l_{c,2}$	0.0338	m
Second link length	l_2	0.08	m
Second spring constant	k_2	2.93	kgs^{-2}
Second spring equilibrium position	$k_{2,eq}$	0.5	rad
Second damping coefficient	d_2	0.3	kgm^2s^{-1}
Third mass	m_3	0.367	kg
Third link length	l_3	0.05	m

The next step is to calculate the normal modes with the nnormal modes tool. As the default value for the maximum energy of mode calculation is 10 J, the value is lowered

and set to 3 J because of the already high frequencies expected at lower energy levels due to the stiff springs and small masses. The resulting two normal modes are shown in Figure 4-11. Here, the trajectory is again plotted with changing color over time showing that the trajectory is on the desired mode at all times. The upper two plots show the first normal mode, the lower two show the second normal mode. It requires two plots for each mode because the normal mode is of dimension four.

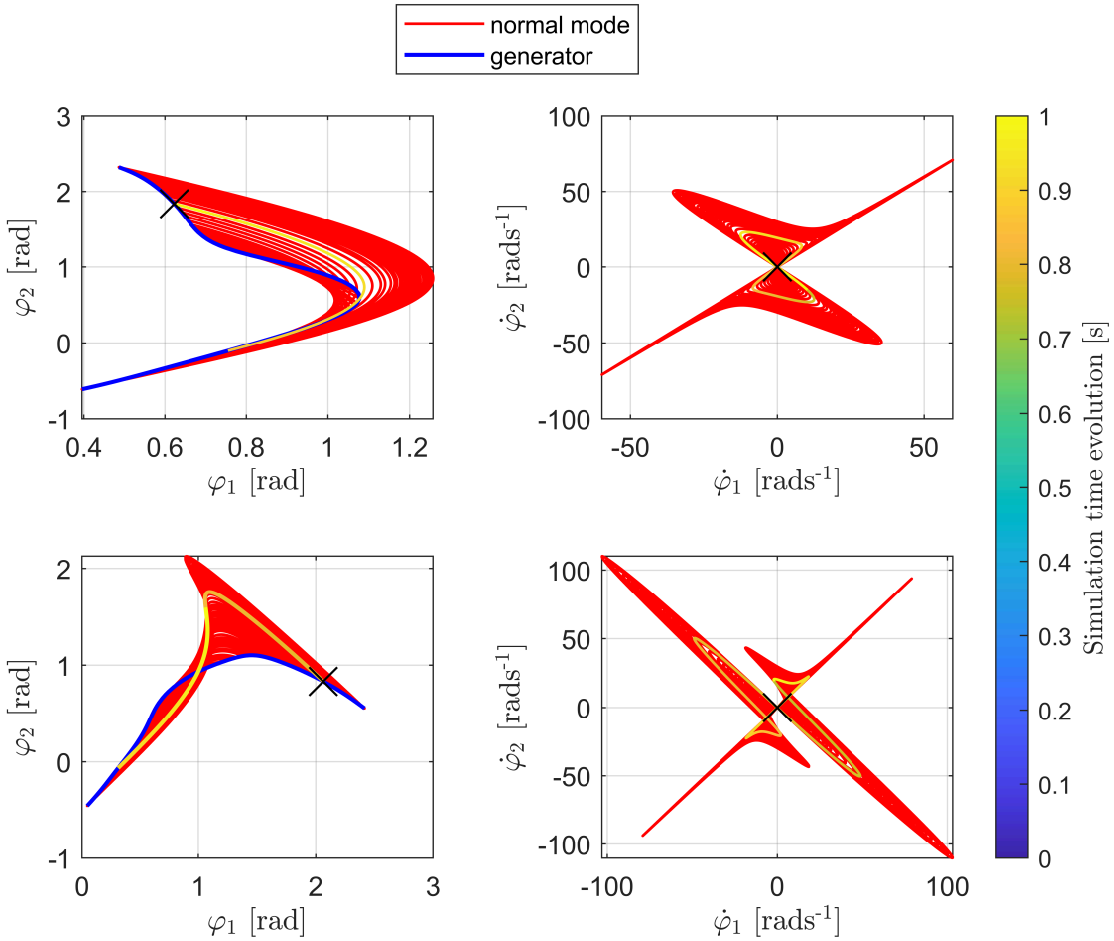

Figure 4-11: *This is the results calculated by the nnormal modes tool for the modeled Bert leg with the active joint method. Two simulations have been performed: The top two plots show the results for generator and mode one, the bottom two plots show the results for generator and mode two. The black marker highlights the initial condition. For the conservative system, the trajectory runs perfectly on the modes, validating the system with these modes.*

The goal with the calculation on the normal modes is the analysis of the shapes and trajectories and evaluate possibilities to use them for locomotion. This validation of the locomotion potential is described in the next section.

Also, to analyze the modal oscillation of the Bert leg with realistic parameters, analysing the time evolution is important as well. In the following Figure 4-12, the trajectories of the angles and the energies are plotted. By reviewing the time evolution of the angles, the frequency can be estimated. In this case the frequency of the oscillation is 4 Hz. Furthermore the composition of the total energy can be analyzed. As the energy level corresponds to the optimal normal mode that the system should oscillate on, knowing and analysing the energy levels for the system is crucial, e.g. to provide desired energy levels for the control of an normal mode oscillation. As the passed maximum energy level that should be calculated by nnormal modes was 3 J, it is clear that the system will be on that energy level close to the end of the generator.

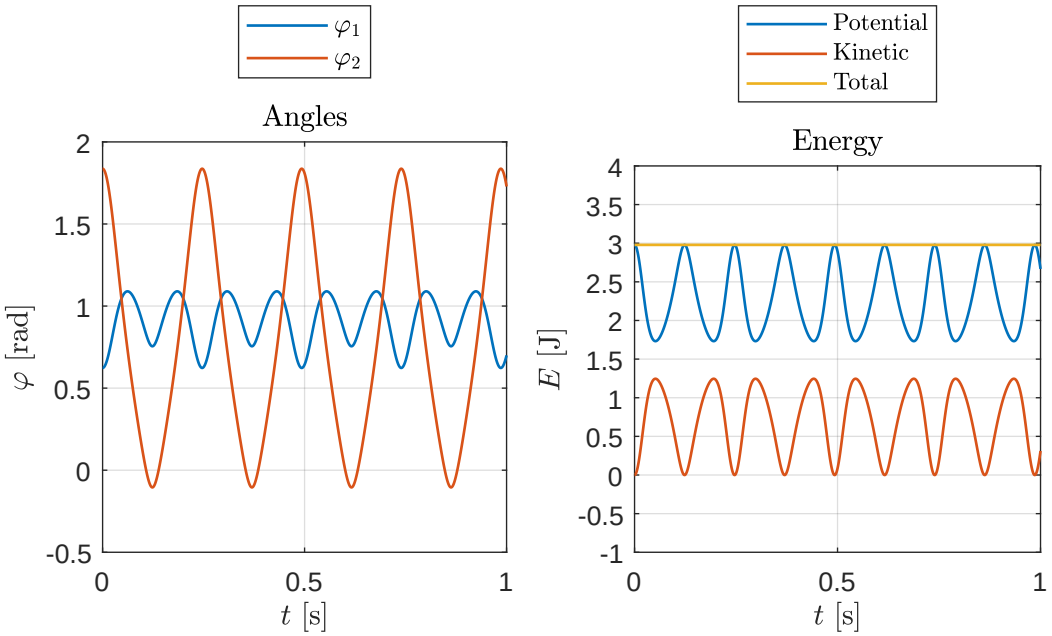

Figure 4-12: *This is the time evolution of the angles and the energies of the modeled bert leg when it is on its normal mode, shown in the upper two plots in Figure 4-11. The time evolution provides more information about frequencies and energies than just the normal mode plot.*

To sum up, with the approach of the active joints method, it was possible to obtain a dynamic system that reproduces the behaviour of the real test rig well in terms of the upright body position. Moreover, with this method the calculation of the normal modes was successful and has been validated in this section. To take a step closer to the usecase of the robot, the next section aims to present different analysis of the nonlinear normal modes of the Bert leg model. This is among other things done by switching parameters and evaluating the impact on the normal mode shape.

4.4 Validation of nonlinear normal modes regarding parameter influences and usability

After the simulation of the Bert leg itself has been validated and successfully setup, the next goal is an analysis of the nonlinear normal modes in terms of the desired use case. Therefore, different simulation experiements are proposed introducing damping and varyig parameters to change the shape of the normal mode.

4.4.1 Damping influence on the modal oscillation

As so far, the simulations of the set up systems had not been under the influence of damping and thus been conservatively evaluated. To evaluate how damping changes the behaviour of the system in terms of the modal oscillations on its normal mode, simulations with damping were run and a result is shown in Figure 4-13. The figure shows the two trajectories of the angeles over the time on the top left side. The righthand top side plot illustrates the distance from the manifold calculated as the eucledian norm of the deviation of all four states to the manifold. The bottom plot shows the normal mode with the two angles on the two axes. Furthermore, the generator is displayed and the simulation course is yet again colored over time. The simulation was done with damping coefficients chosen to 0.001 kgm^2s^{-1} leading to a smooth transition to the equilibrium. The other parameters are chosen according to Table 4-2.

As it can be seen in the upper left plot, the oscillation of the angles are decreasing over time due to the loss of energy induced by the damping. As the distance plot on the right upper side shows, there is a distance immediately increasing after the release from the generator peaking at 0.1 s. After the peak it can be said that the deviation of the state from the manifold is decreasing. This could be caused by the state approaching the equilibrium thus resulting in an approach to the manifold as the equilibrium is part of the manifold. The bottom plot underlines the two observations of the upper plots. It shows by the colored time course that the angles are approaching the equilibrium. It also shows the deviation from the normal mode illustrated in red, as e.g. the time course is overshooting in the area of the inital condition.

As a result of these observations, not only is a controller needed to input the energy that is lost by dissipation, but it also needs to ensure that the oscillations stay on the manifold. The non conservative system does not fully stay on the manifold by itself when released from a point of the generator. This is one of the reasons why a control strategy is proposed and implemented in the following chapter.

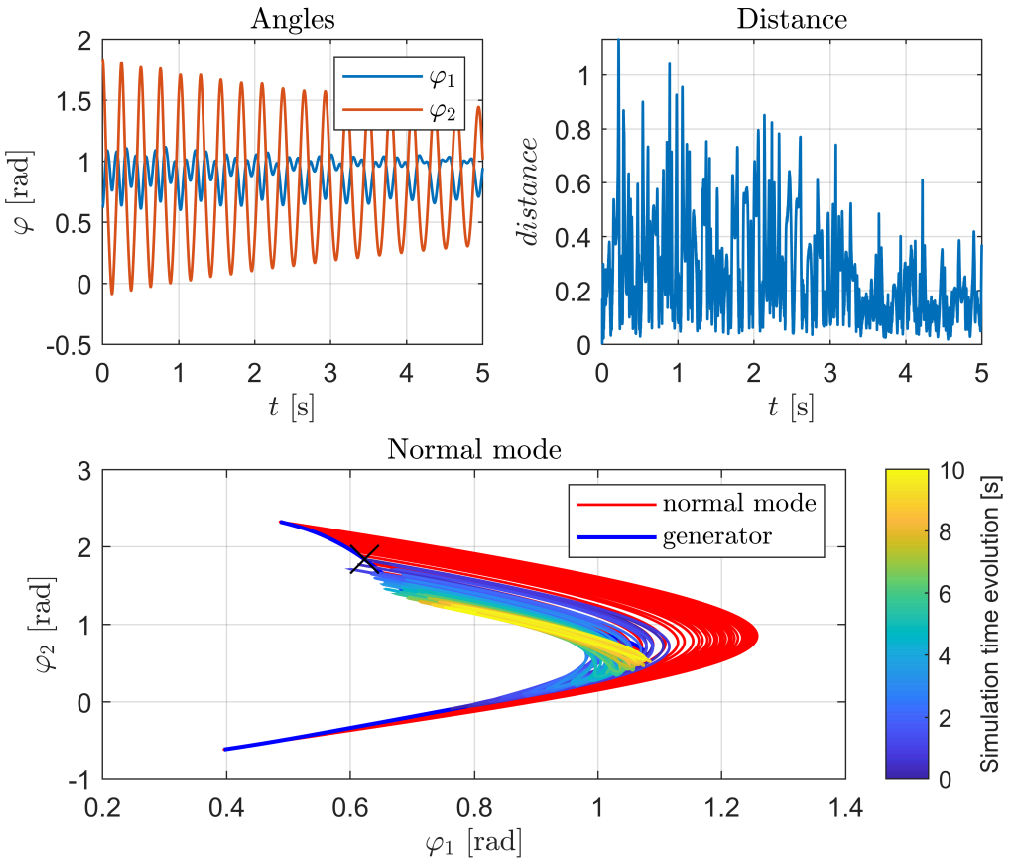

Figure 4-13: *Simulation of the model for the one leg of the robot Bert influenced by damping. This shows the how the system react to damping while executing modal oscillations. The distance is the euclidean norm of the deviation of the state to the manifold.*

4.4.2 Generator dependency on the springs equilibria

By analysing the emerging manifolds and generators in a detailed way when varying parameters, a better understanding of the systems behaviour and possible modal oscillations is gained. In this context, especially the spring equilibria are adjustable for the Bert leg since the position of the SEA links are corresponding to the spring equilibria positions. Therefore, the spring equilibria can be changed dynamically at the real test rig. The detailed implementation of the test rig setup with motors is discussed in the following chapter regarding the control. Overall, it is of interest to investigate on the resulting modal oscillations when varying the spring equilibria positions.

To get an overview on the influence of this parameter, a five by five grid is set up and multiple generators are calculated for every equilibrium chosen. The outcome of this approach is shown in Figure 4-14. Here, the mentioned grid was set up for spring equilibrium positions in a range from $-\frac{\pi}{2}$ rad to $\frac{\pi}{2}$ rad with an increment of $\frac{\pi}{4}$ rad. The legend

denotes $\underline{k}_{eq} = \begin{bmatrix} k_{1,eq} & k_{2,eq} \end{bmatrix}$, respectively with each entry. The upper plot shows the generators for manifold one, the lower plot shows the generators for manifold two. The axes show the two angles φ_1 and φ_2 that are used to describe the Bert leg dynamics. The dots that have the same color as the line that they are placed on, denote the equilibria of the systems equlibria. It is worth mentioning here that the systems overall equilibria are not equalling the spring equilibria due to gravity.

To present a visual illustration of the resulting poses of the Bert leg, Figure 4-15 shows nine equilibrium poses of the leg corresponding to the inner nine equilibrium points of the used grid in Figure 4-14. The colors are matching to this figure as well. The center of each of the nine images with the poses, matches the equilibium position regarding the axes again denoting φ_1 and φ_2.

Getting to the analysis of the generator plots with the corresponding poses, the symmetrical structure of the Bert leg is clearly visible. The poses have symmetry axes in terms of these with positive and negative sign and same absolute values of k_{eq}. Furthermore, by looking at Figure 4-14, there are some switches in the shape of the generators. For the spring equilibria $k_{eq} = \begin{bmatrix} -\frac{\pi}{2} & -\frac{\pi}{2} \end{bmatrix}$ rad and $k_{eq} = \begin{bmatrix} \frac{\pi}{2} & \frac{\pi}{2} \end{bmatrix}$ rad, there is a sudden change in the orientation of the resulting generator. It can be said that the two generators in the lower plot suddenly change their orientation by $\frac{\pi}{2}$ rad. Especially the upper plot corresponding to manifold one shows multilple orientation changes of the generator by $\frac{\pi}{4}$ rad. For further research it could be of interest to investigate on the switching in detail and execute experiments in the surrounding of the switching point. Another interesting detail in terms of the symmetry could be a change of movement direction executed by simply switching the generator and manifold that are used by choosing a different set of spring equilibria.

To sum up, the two plots shown in this section are a first approach to intensify the research on the behaviour of nonlinear normal modes and their generators in terms of their paramters. The change of the generators shape appears to be steady in some intervals during the variation of k_{eq}. Though, it stands out that there are sudden switches in the orientation of the generators, rotating the generator by $\frac{\pi}{4}$ rad and even by $\frac{\pi}{2}$ rad. This needs to be further investigated and can be an advantage for intentional switches of the systems behaviour. Although these sudden switches can also be a risk when a reliable system behaviour is desired.

4.4.3 Influence of the springs equilibria for the usecase of hopping motion

The goal with the one leg test rig is a hopping motion ideally leading to a translational movement of the whole leg. This is to be achieved with the use of the nonlinear normal modes while this part aims to analyze the mode shapes resulting from the parametrisation of the model with a focus on the desired usecase.

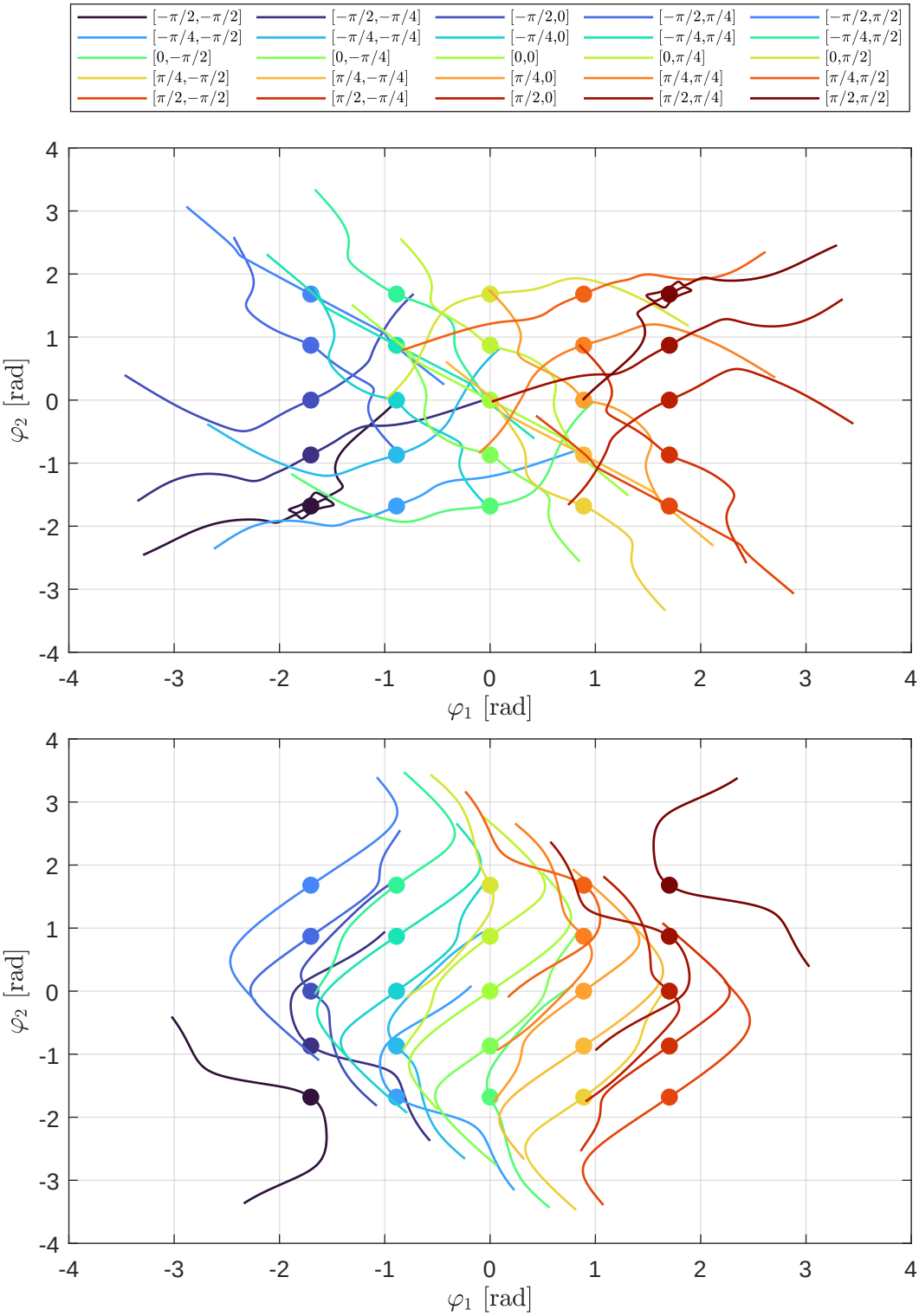

Figure 4-14: *This illustration shows the resulting generators when varying both spring equilibria k_{eq} individually. The legend shows the variation where one legend entry is $k_{eq} = \begin{bmatrix} k_{1,eq} & k_{2,eq} \end{bmatrix}$, denoting the spring equilibria of springs one and two, respectively. A five by five grid of spring equilibria variations with a range from $-\frac{\pi}{2}$ rad to $\frac{\pi}{2}$ rad was used with an increment of $\frac{\pi}{4}$ rad. The upper plot shows the generators for manifold one, the lower plot shows the generators for manifold two.*

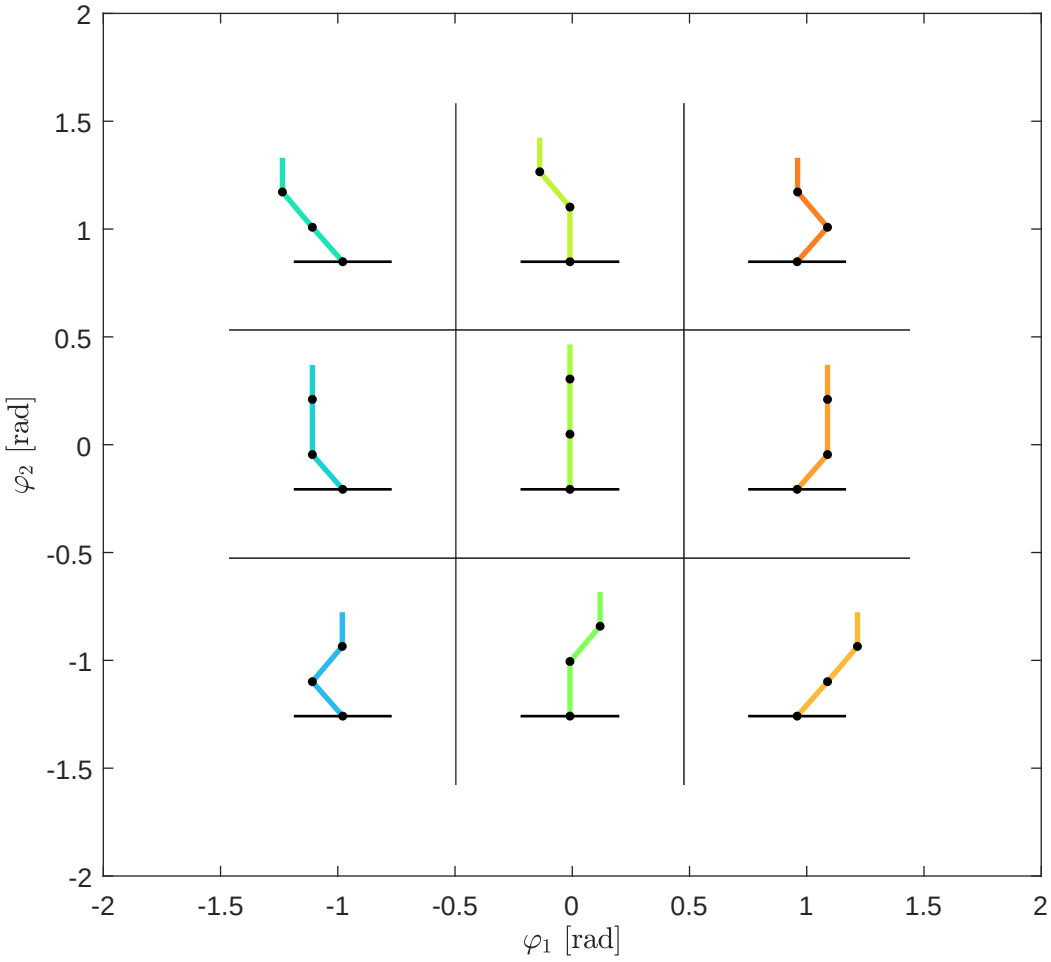

Figure 4-15: *For the plot introduced in Figure 4-14, showing the resulting generators by spring equilibria variation, the corresponding equilibrium poses of the Bert leg are illustrated. The inner three by three grid of generators is shown with the Bert leg giving a refined image of the actual emerging rleg poses.*

Changing the parameters of the leg model will change the shape of the normal modes and therefore the motion of the robot. As the robot is built up taking several factors into account concerning the parametrisation, it is most senseful and usability friendly, as in the previous section, to change the spring equlibria. It is to be analyze which resulting modal oscillations might be useful for locomotion. As an approach for the evaluation, the variation range of the spring equlibria is defined. As seen in the previous section, the spring equilibria have a great impact on the systems overall equilibrium. For the usecase it is not senseful to choose a range greater than 0.5π rad positive and negative since otherwise the limitations of the test rig are reached. Furthermore, in this case, both

spring equilibria are always chosen to be equal. This is reaonable since the leg is desired to execute the hopping motion upright which is ensured by equal spring equilibria.

After these definitions, several calculations of the manifolds were performed in the defined range of the two spring equilibria k_{eq}. The results are shown in Figure 4-16 with Subfigure 4-16a illustrating the outcomes for the first manifold and Subfigure 4-16b illustrating the results for the second manifold. The dark blue lines show the generators. All other colors show different normal modes on different spring equilibria positions k_{eq} and are desired to advance the readability.

As seen in the plots, there are different areas of normal mode shapes resulting from the change of k_{eq}. Especially in Subfigure 4-16a, there are four basic unique shapes generated. The other Subfigure 4-16b shows only one unique shape within the variation. Unique is in this case defined in that way, that if two normal modes are just mirrored due to the symmetric setup of the Bert leg or if two normal modes are just scaled or displaced in comparison to each other, they are seen as one kind of shape.

Thus, 5 different evaluations are performed to evaluate suited normal modes and normal mode configurations for hopping movement. The analysis results of three shapes of manifold one in Subfigure 4-16a are illustrated in **??**. These are not suitable for hopping due to the great changes in angle φ_1 during the modal oscillation resulting in a wavering motion around joint one. Therefore, in the following, two results of the analysis of the different shapes will be discussed. Figure 4-17 illustrates a possible normal mode for the desired motion. The normal mode of the second manifold, which can be seen in the upper plot, has the configuration $k_{eq} = 0.5$ rad. An example modal oscillation on the normal mode is shown in yellow. The goal of estimating the usability is reached by the connection with the three subplots at the bottom. On the modal oscillation, there are three colored markers denoting three states. Two of these are at the generator, respectively and one is interim between the two generator points. Consequently, the corresponding pose sequence of the Bert leg is then shown in the three subplots. This represents a modal oscillation sequence of the Bert leg which would be executed if the two motors were controlled for to a position of $k_{eq} = 0.5$ rad for the spring equilibria.

In comparison to this first figure, the second Figure 4-18 shows another possible modal oscillation. In the upper plot, an normal mode of manifold one, as illustrated in Subfigure 4-16a, is visualised. Again, in yellow there is an example trajectory shown and three markers on it denote three example Bert leg poses. These poses can be analyzed in the subplots and the bottom of the figure.

Overall, looking at the pose sequences of the leg in the shown figures, the desired periodical bending and stretching of the knee which could result in a steady hopping motion can be found. The leg does not lean too much to the front and back while bending the knee, as

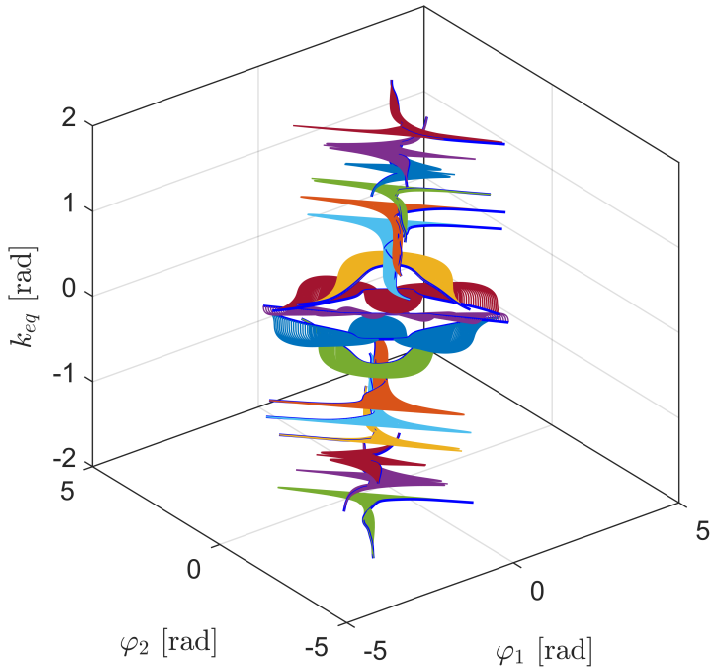

(a) *normal modes of manifold one*

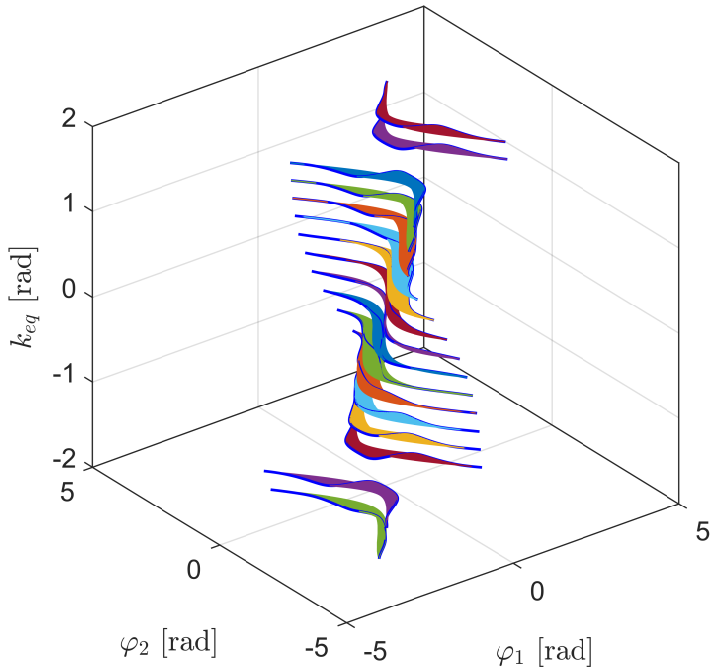

(b) *normal modes of manifold two*

Figure 4-16: *Illustration of the nonlinear normal modes of the Bert leg model each resulting from a different choice of* k_{eq}*. The generators are shown in dark blue and the different colors of the normal modes are chosen for visibility reasons. The range for* k_{eq} *is* 1.6 rad *from negative to positive with an increment of* 0.2 rad.

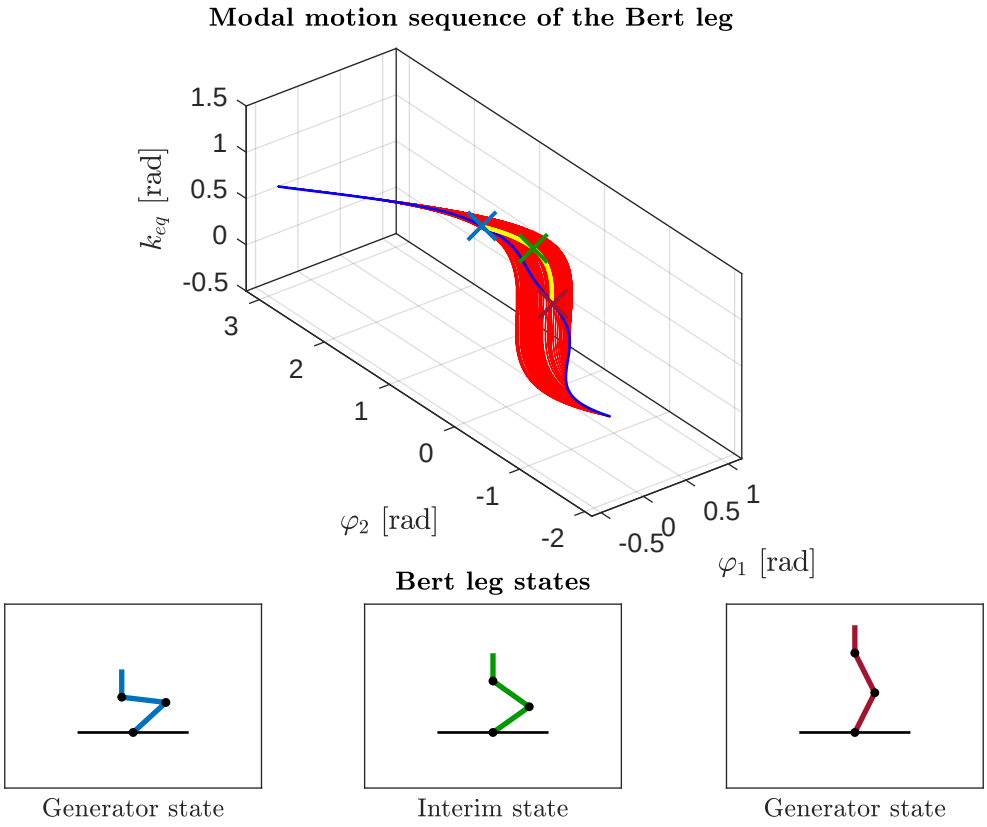

Figure 4-17: *Illustrational motion sequence of the one leg test rig oscillating on the normal mode of manifold two resulting from choosing* $k_{eq} = 0.5$ rad. *The result is a straightening and flexing of the leg which could lead to a translational hopping motion. Characteristic is that the leg is moving back and forth with the angle* φ_1 *during the straightening and flexing with angle* φ_2.

it does while oscillating on the other normal modes shown in the appendix **??**. Therefore, with these two proposed normal modes it should be possible that the leg performs the desired hopping movement.

When comparing the two proposed solutions, one solution has more advantages concerning the desired hopping motion than the other. The reasons stand out when taking the overall shape of the two eigenmods into account as well as the overview Figure 4-16. For the first normal mode shown in Figure 4-17, a broad range of inital conditions on the generator can be chosen and the movement stays approximately the same due to the steady shape. In contrast, the shape of the second normal mode 4-18 changes greatly. It is not possible to choose greater inital conditions than in the proposed example as the leg then executes movement in the ground. This also limits the maximum energy level (corresponding to the distance of the initial consition on the generator to the equilibrium) that can be chosen with this normal mode. Though, if friction is taken into account, a higher chosen energy level could be needed. The last argument against the second pro-

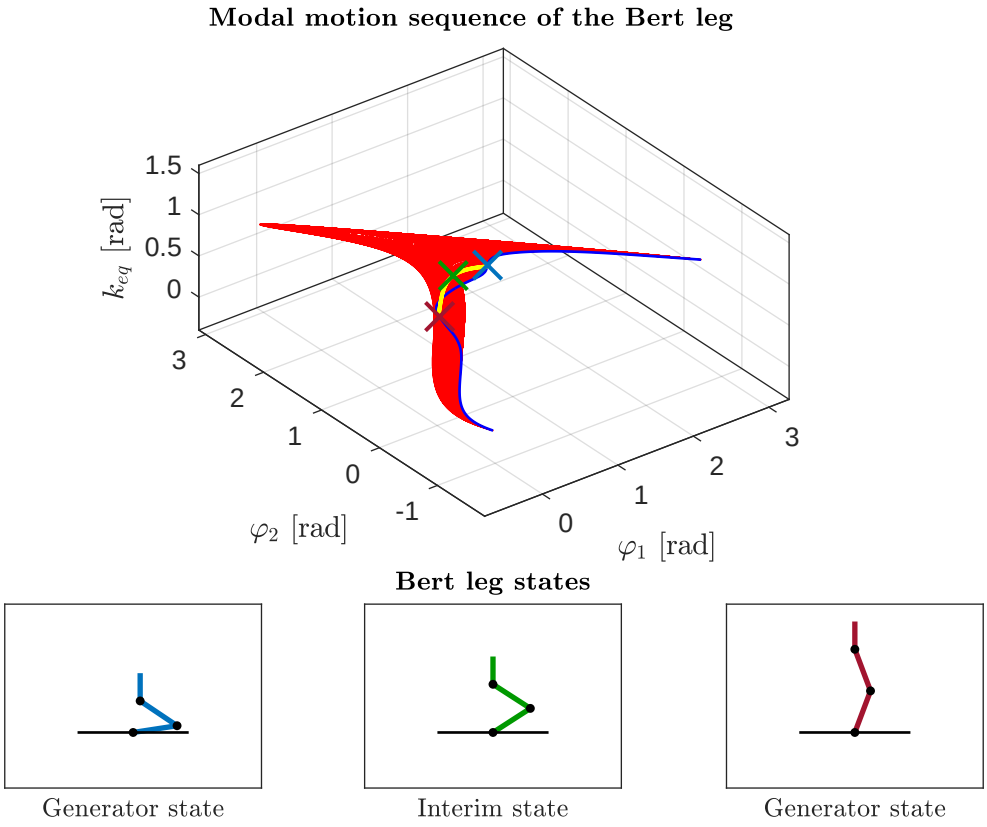

Figure 4-18: *Illustrational motion sequence of the one leg test rig oscillating on the normal mode of manifold one resulting from choosing* $k_{eq} = 0.5$ rad. *The result is a straightening and flexing of the leg which could lead to a translational hopping motion. Characteristic is that the leg's body stays approximately above the the foot during straightening and flexing.*

posed normal mode from Figure 4-18 is the overall evolution of the normal mode shape along the variation of k_{eq}. The triangular shape is lost if k_{eq} is chosen to be less than 0.5 rad resulting in unsuitable shapes as shown in the appendix. In comparison to this, the first normal mode from Figure 4-17 stay with its shape in the range from $k_{eq} = -1.2$ rad to $k_{eq} = 1.2$ rad. This greatly increases the suitability of the first proposed normal mode.

In conclusion, this section presented an approach to find suitable configurations for the Bert leg resulting in a proposed normal mode solution for the desired hopping motion in Figure 4-17. Additionally to this explicit solution, an overall advice can be generated from the data since this normal mode stays its shape for the range from $k_{eq} = -1.2$ rad to $k_{eq} = 1.2$ rad. Thus, for detailed experiments k_{eq} should be chosen withing this range. The goal is now to run tests with this parametrization in the physical 3D software Gazebo for validation and Benchmarking purposes.

To sum up the whole chapter, the whole approach of modelling the Bert leg test rig with different methods was sucessful to this state. A solution for a modal oscillation of the model that seems to be capable of performing hopping motion was found. The results in terms of the choosage of parameters derived from the data can now be used with Gazebo. For this a controller will be implemented in the following chapter to encounter damping and other external effects and to stabilize and change the desired modal oscillation on the fly.

5 Control strategy to stabilize nonlinear modes

After the dynamics simulations have been set up in the previous chapter and the nonlinear normal modes are validated for the usecase, the overall stabilization of modal oscillations has to be achived next. As presented in the last section of the previous chapter, damping disturbs the modal oscillations, shifting the trajectory from the manifold. Furthermore it can be the case, that the system is not on the manifold initially. For both cases, a control is needed, acting against the damping, stabilizing a modal oscillation out of any state and eliminating model uncertainties. The goal is to get the system to stay on its normal mode at a desired energy level under more difficult nonconservative conditions.

In this chapter the first step is the application of the described mode control approach in Section 5.1 for the set up leg model of the robot Bert. Therefore, the controller is first designed with suitable gains using an objective function. Afterwards first results with the proposed torque controller are presented. Then, in Section 5.2, the torque mode controller is advanced and adapted to approach the realities of the Bert leg introducing SEAs. As the adaption is done, the controller is finally used with the digital twin of the Bert leg in Gazebo in Section 5.3. The chapter quits with the last part showing limitations of the control approach.

5.1 Application of the mode controller

The first step to use the proposed control on the Bert leg is to choose the controller gains optimally. This is done with an objective function in the following part. After the gains have been chosen, the control strategy is validated in the second part to validate the usability.

The torque control strategy is illustrated in Figure 5-1 by showing the control loop. The desired values for the control are the 4D manifold values $\underline{X}$, $\dot{\underline{X}}$ and the desired Energy level $\overline{E}$. The values to compare them to at the sum are the current angules and angular velocities of the Bert leg as well as the current total energy. Due to the sum with the negative sign for the current values, the results are $\delta\underline{X}$, $\delta\dot{\underline{X}}$ and δE. The differences are inserted to the control algorithm calculating the needed torques with (3-5) and (3-6) resulting in $\underline{\tau}_M$ and $\underline{\tau}_E$. Inserting $\underline{\tau}_M$ and $\underline{\tau}_E$ into (3-7) finally gives $\underline{\tau}$. $\underline{\tau}$ is applied at the Bert leg which abbreviated shown on the right side of the figure. The torques act directly at the joints.

This is the proposed basic torque control strategy applied to the Bert leg. To use the controller with the Bert leg and to run simulations with it, the gains of the controller have to be chosen which is presented in the following part.

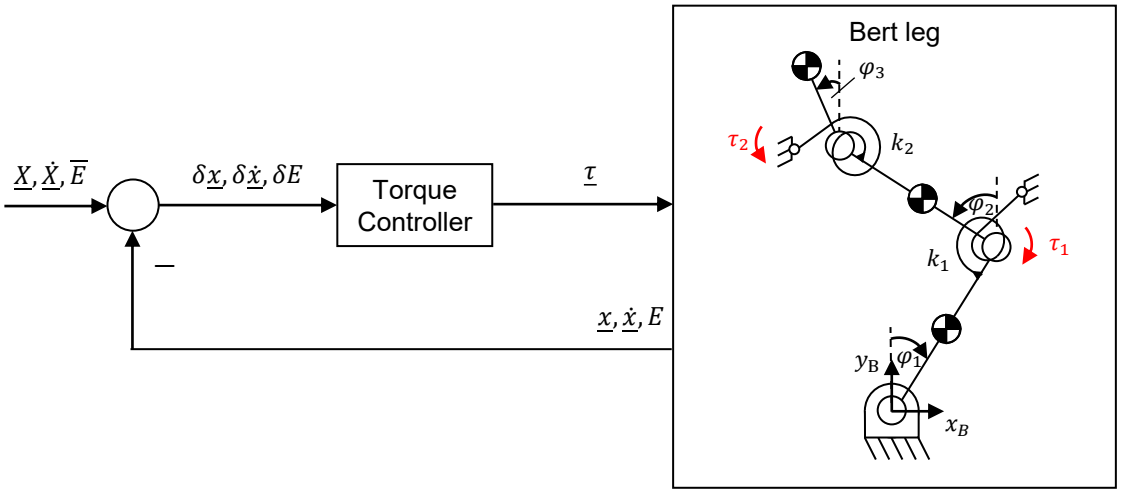

Figure 5-1: *Torque control strategy to stabilize modal oscillations with the Bert leg illustratively shown on the right. The Torque controller works as outlined in Section 3.3.*

5.1.1 Optimal design of the controller with a penalty function

For the design of the controller, the gains need to be estimated. For an estimation of the gains it is a common approach to choose a suitable example situation for a control usecase where the controller has to ensure a given energy level and the modal oscillation. Then an optimization with an objective function using the gains as optimization variables is performed to get a fit of the controller for the common usecase. The proposed objective function takes the resulting difference of the energy trajectory to the desired energy into account as well as the distance of the state trajectory to the manifold. This results in the objective function $J(\underline{R})$ as

$$J(\underline{R}) = \underset{\underline{R}}{\operatorname{argmin}} \sum_{i=0}^{T} \left\| \begin{bmatrix} \dot{\underline{x}}(\underline{R})_i - \dot{\underline{X}}_i \\ E_d - E_i(\underline{R}) \end{bmatrix} \right\|_2 \tag{5-1}$$

with

$$\underline{R} = \begin{bmatrix} \alpha_D & \gamma_P & \gamma_I \end{bmatrix}$$

and with $\dot{X}_i$ being calculated according to (3-4) at every time step i. With the objective function an example situation for a controller task is set up. The lsqnonlin solver is used with the levenberg-marquardt algorithm [Mat22]. The optimization is a first step to get an idea of a potential solution. Though, the finally chosen gains will be estimated according to the optimization results as well as the map of objective function values shown in Figure 5-2. For this figure, a grid of the gains α_D and γ_P is set up. Afterwards, the example

situation is executed for every variation of the gains given by the grid. The result is a 3D map with the gains as the $x-$ and $y-$axis and the objective function value at the $z-$axis. The range of the two gains was choosen in a suitable surrounding of the outcome of the optimization resulting in a range from 0 to 45 for γ_P and 0 to 6 for α_D.

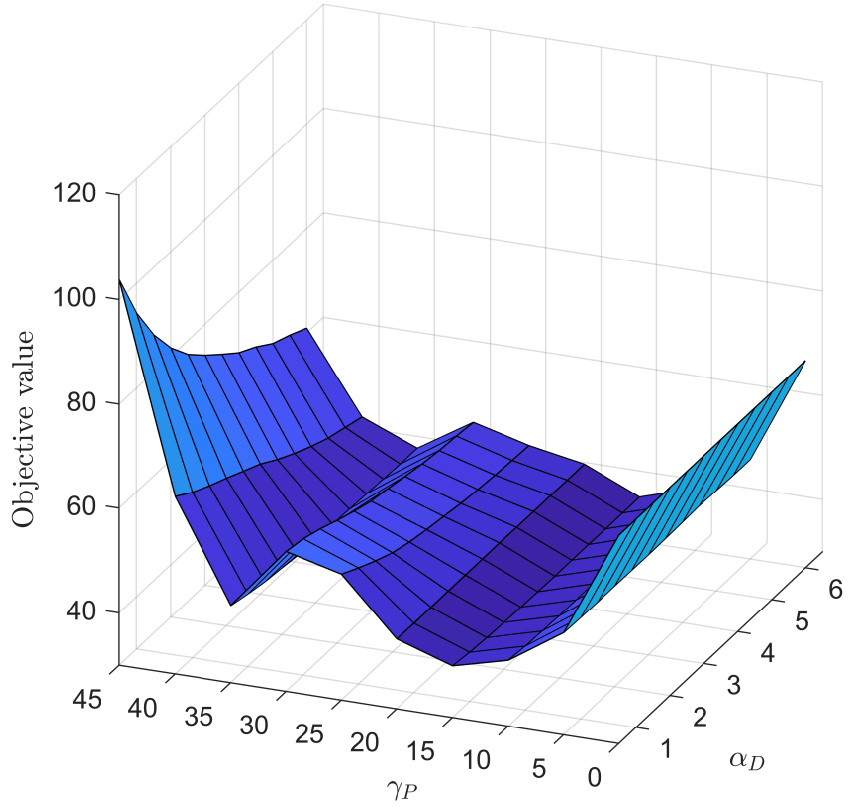

Figure 5-2: *Resulting torque controller gains map with the objective function values on the $z-$axis. An example situation was simulated with the torque controller and the corresponding gains for every point of the map and the objective function value was calculated, respectively.*

The map is presenting an overview on how to choose the controller gains appropriately. The energy controller gain γ_P has a great impact on the outcome as the objective function value raises quickly when the gain is chosen different from the two minimum value areas at approximately 15 and 35. The choosage of the manifold controller gain α_D has less impact on the outcome as the objective function value does not increase or decrease much. By taking the optimization and the shape of the objective function map into account, the gains are chosen to be $\alpha_D = 5$, $\gamma_P = 15$ and $\gamma_I = 8.8 \cdot 10^{-6}$. The integrator gain γ_I for the energy controller emerges from the optimization. α_D is chosen to be five as the objective function reaches a minimum at this point considering the range of α_D. γ_P is chosen to be 15 as the objective function reaches one minimum here. The other minimum at 35 is

not considered because of the rapid increase in the objective function value with a slight increase of γ_P.

5.1.2 Torque controller results

As the controller gains were found in the previous part, the validity of the controller with the chosen gains is tested simulatively. Therefore different simulations where performed where the controller had to ensure a stable modal oscillation as well as the desired energy level. One example is shown in Figure 5-3. In this figure, the time course of the system's total energy is shown in the left plot as well as the desired energy with a green dashed line. This line is also present in the plot on the right side where the normal mode is shown in red as well as the generator in blue. The right plot also shows the time evolution of the simulation. The initial situation is denoted by the black marker.

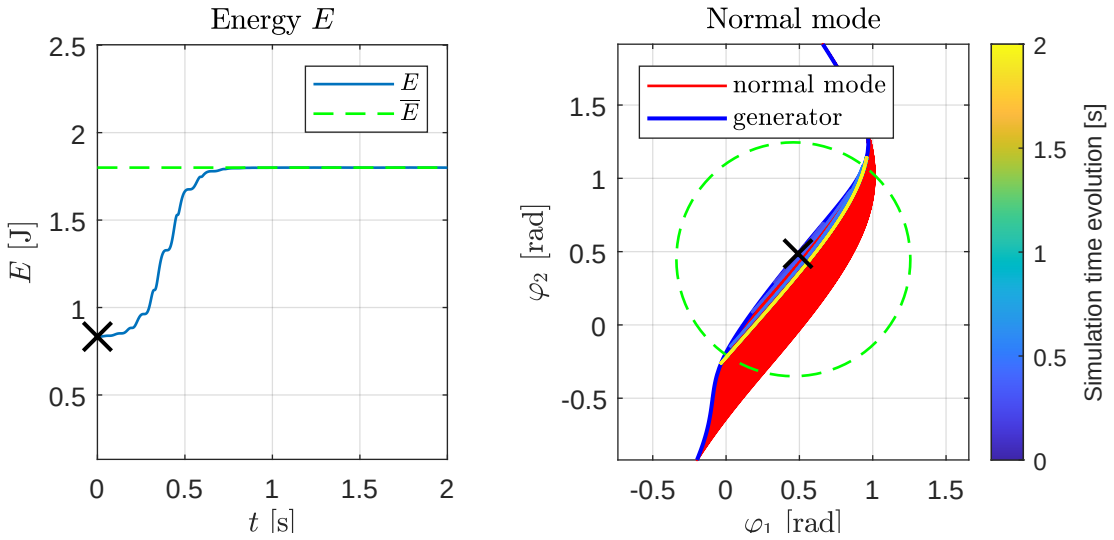

Figure 5-3: *One result of the torque controller validation simulations. The desired energy is set to a higher level than the inital energy. The initial state is located on a generator point. After the release, the torque mode controller shifts the trajectory to the desired energy level while ensuring the modal oscillation at all times.*

As it can be seen in the left plot, the energy reaches the desired energy of 1.8 J within 0.5 s and stays perfectly with it. Furthermore, the right plot shows the same result with the time evolution reaching the circled desired energy at the generators. As the velocity is zero at the generators and the system is conservative, it can be concluded that the energy always stays at 1.8 J during the whole modal oscillation. During the oscillation, when the trajectory is not on the circled desired energy level, the lag of potential energy is compensated by an increase in kinematic energy which is not shown here for readability reasons. The sum of potential and kinetic energy must always result in the desired energy

which can also be concluded by the left plot. Furthermore, the time evolution stays on the mode during the energy increase and does not overshoot the generator at the desired oscillation. This validates that the controller is capable of ensuring modal oscillations as well as a desired energy level.

To conclude, in this section, optimal controller gains were found and used with the proposed torque mode controller. During the validation with example simulations it was shown that the controller works as desired. As the robot Bert is actuated with SEAs, it can not be controlled with torques as inputs. The needed adaption of the mode controller to meet this requirement is presented in the following section.

5.2 Adaption of the mode controller

Now that the torque mode controller has been validated, the next goal is to adapt the mode controller framework to meet the requirements of the one leg test rig. The leg at the test rig, and also all the joints of the whole robot Bert are driven by SEAs. These motors need a desired motor link angle as an input and give the desired link position as the output with a delay. This delay can be described with the motor time constant T. Therefore, the needed adaption is, that the control frameworks output rather needs to be a desired motor link angle than a torque. There is no torque anymore that is directly applied to the joints. The joints are from now on actuated via inputs to the springs on the equilibria side of the spring. By changing the equilibria of the springs with the SEAs, torques can be indirectly applied to the joints as the spring torques change, respectively.

To present a visual overview on the setup, the adapted control framework is presented in Figure 5-4. The framework is extended by a position controller and a motor compared to the torque controller framework in 5-1. Furthermore the inputs of the Bert leg are adjusted to be the angles θ_1 and θ_2 changing the springs equilibria and therefore inducing a change of the torques in the joints, respectively. There is direct joint actuation anymore. The joints are now actuated through the change of the spring torques. The torque controller part and the summation point are the same as in the torque controller framework.

The provide the background on how the position controller and the motors work, the details with equations are presented now. The conversion of the torque controller output $\underline{\tau}$ to the desired motor link angles $\underline{\theta}_d$ is done with the inverse spring stiffness matrix. The desired motor motor link angles without any desired additonal torque equals $\underline{k}_{eq} = \begin{bmatrix} k_{1,eq} & k_{2,eq} \end{bmatrix}^T$, the default spring equilibria of the leg. Also, for these equilibria, the normal modes of the system are calculated. By ensuring the motor motor link angles at the default spring equilibria, a default spring torque is applied to the joints dependent on the current joint angles. This Torque is denoted by $\underline{\tau}_{ds}$. Now, an additional torque $\underline{\tau}_{cs} = \underline{\tau}$, equalling

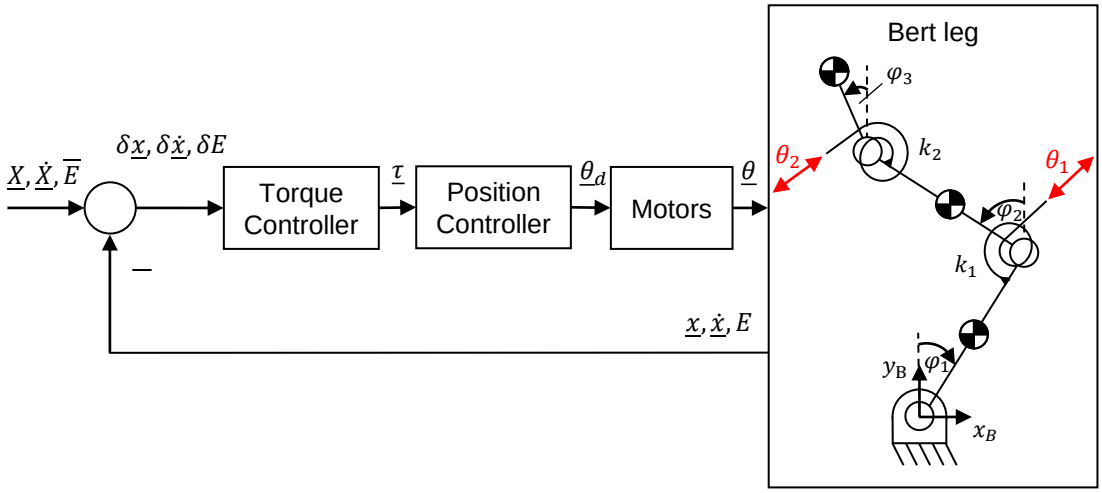

Figure 5-4: *The position mode controller framework which is an adjusted torque mode controller framework. The additions are the position controller, the motors and the adjustment of the leg model now getting the motor link angles $\underline{\theta}$, previously the spring rest positions, as the input.*

the torque calculated by the torque controller part, has to be applied to the joints through the springs. This leads to the equation

$$\underline{\tau}_s = \underline{\tau}_{ds} + \underline{\tau}_{cs}$$

After this definition, the next step is the calculation of the $\underline{\tau}_{cs}$. By first considering $\underline{\tau}_{ds}$ to be

$$\underline{\tau}_{ds} = \underline{K}\,(\underline{\theta} - \underline{x})\,,$$

which is the standard formula to calculate a spring torque. Basically the torque results from the difference between the two attachment points (states $\underline{\theta}$, motor motor link angles and $\underline{x}$, joint angles), multiplied with the stiffness matrix $\underline{K}$ of the system. Taking a step, for the calcualtion of $\underline{\tau}_{cs}$, it follows

$$\underline{\tau}_{cs} = \underline{K}\,(\delta\underline{\theta} - \delta\underline{x})\,, \tag{5-2}$$

with the assumption that an additional motor link angle $\delta\underline{\theta}$ is needed to apply the desired torque. Moreover, $\delta\underline{x}$ is chosen to be zero, as the torque should only be applied through

a change in the motor link angles and not by a change in the systems state. Inserting this into (5-2) and solving for $\delta\underline{\theta}$ and additionally substituting $\underline{\tau}_{cs} = \underline{\tau}$, the result is

$$\delta\underline{\theta} = \underline{K}^{-1}\underline{\tau},$$

with $\delta\underline{\theta}$ being the angles that have to be add up to the default motor link angles $\underline{k}_{eq}$. As the last step, the overall desired motor link angles for a controller torque $\underline{\tau}$ are then given by

$$\underline{\theta}_d = \underline{k}_{eq} + \delta\underline{\theta} \quad = \underline{k}_{eq} + \underline{K}^{-1}\underline{\tau}. \tag{5-3}$$

Through these conversions, the position controller is set up using (5-3) to calculate the desired motor link angles $\underline{\theta}_d$ during the simulation.

To complete the simulation setup and position control framework, a model for the motor dynamics is needed. The SEAs are modeled with a PT2-element resulting in a delay of the setting of the desired motor link angles. Thus, the dynamics of one of the motors can be described as

$$\ddot{\theta} = \left(\frac{1}{T}\right)^2 (\theta_d - \theta) - \left((2\zeta\frac{1}{T}\right)\dot{\theta},$$

with ζ being the damping ratio and T being the motor time constant. ζ is always equal to one as it is assumed that these motors never overshoot. By choosing T, the motors appear to be faster and slower for a smaller and larger time constant.

Overall, the position control approach is now fully described with the implementation of the position controller part and the motor models. As the goal with the position control approach is to adjust the control framework in a way that it meets the reality, it is a natural progression to also evaluate the needed motor speed next. Especially it is of interest to investigate on the biggest allowable T, i.e. the slowest possible motor behaviour. This evaluation is done with the objective function (5-1) with the gains $\underline{R}$ chosen according to the torque controller framework and the optimization variable being T. For the considered example situation, the resulting objective values when varying the motor constant T are plotted in Figure 5-5. T was varied in the range from 0.001 s to 0.1 s.

The result of the motor speed evaluation is explicit: If a motor time constant higher than 0.015 s is chosen, the objective value increases rapidly resulting in poor control outcome. Therefore, for the following simulation steps, a motor constant of 0.01 s is chosen as a compromise between the upper bound of 0.015 s and the sample time of the simulations of mostly 0.001 s. The large decrease to a comparatively higher steady level of the objective value when the motor time constant is higher than 0.035 s is connected to the example

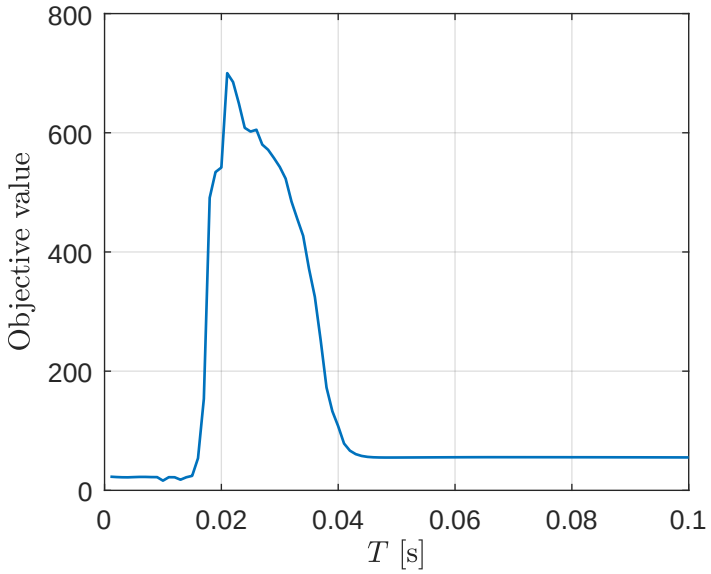

Figure 5-5: *Motor time constant T evaluation with the example situation and the objective function with a variation of the time constant from* 0.001 s *to* 0.1 s *and fixed controller gains as in the torque controller framework.*

simulation duration. If the motor time constant is this high, the motor is not reacting at all during the whole simulation time leading to a good fit on the manifold (as the initial condition is on a generator point) but a poor fit to the desired energy level.

After the definition of the motor time constant T, it is reasonable to run another optimization of the controller gains. Therefore, the objective function (5-1) is used again and another gains map as shown in A3-1 is considered. The result is $\alpha_D = 4$, $\gamma_P = 25$ and $\gamma_I = 8.8 \cdot 10^{-6}$ based on the optimization result and the evaluation of the gains map.

As the position control framework is defined now and the gains as well as the motor time constant are specified, a validation is the next step. Again, some example simulations with different situations are considered for the controller evaluation. One example outcome is shown in Figure 5-6. The resulting time course on the normal mode is shown on the right plot and is similarly perfect to the result with the torque mode controller in Figure 5-3. In the left plot, the trajectory of one motor link angle and the default spring equilibrium are shown.

By analysing the left plot, it can be observed that the motor link angle θ_1 is alwas following the desired angle $\theta_{1,d}$ with an offset. This shows the depedency on a suitable motor speed as the offeset increases with slower motor speed. The default value of the spring equilibrium is reached with some noise at approximately 0.6 s. As the motor angle is approaching this value, the torque equals zero and no additional inputs have to be computed, also validating the energy efficiency of the approach for a conservative system. When the

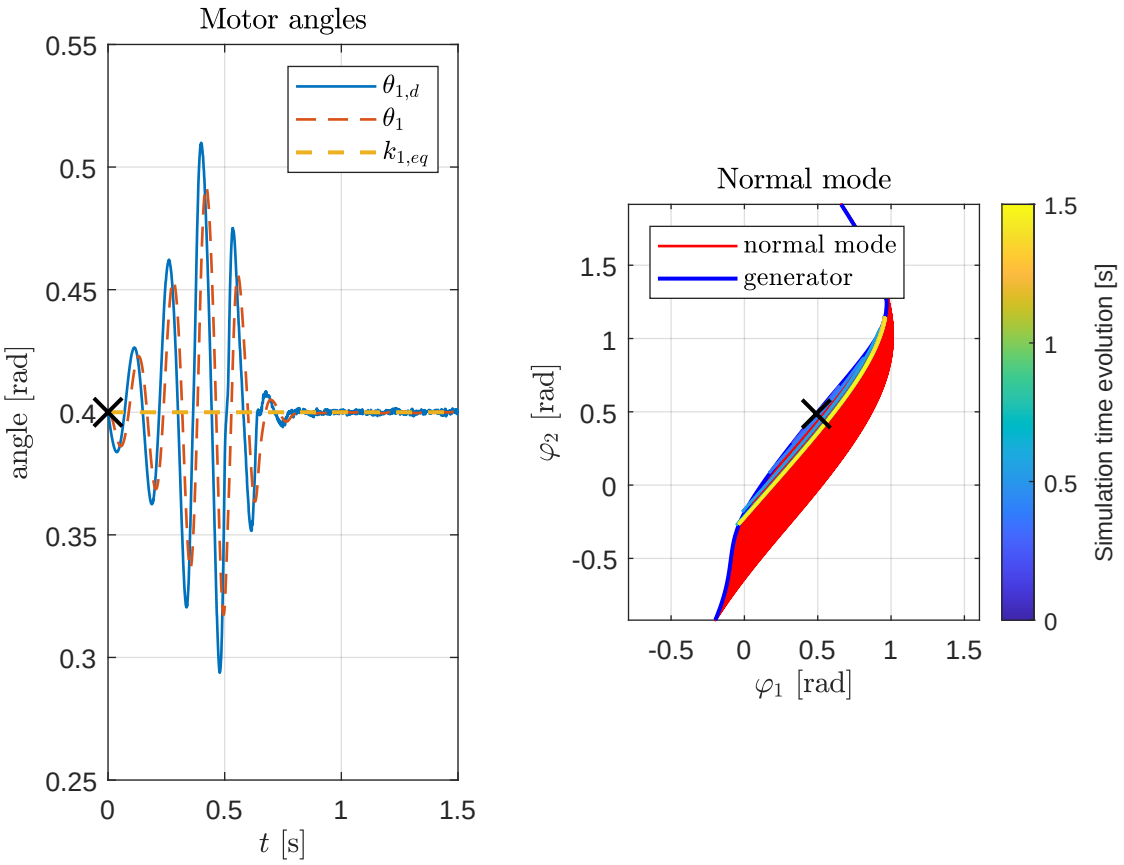

Figure 5-6: *One result of the position mode controller validation simulations. The desired energy is set to a higher level than the inital energy. The initial state is located on a generator point. After the release, the position controller framework shifts the trajectory to the desired energy level while ensuring the modal oscillation at all times. The left plot shows the trajectory of one motor link angle and the default spring equilibrium.*

modal osciallation is established with the desired energy level, no further input is needed which maximizes the energy efficiency.

To sum up, this section presented the sucessfull implementation of the adapted torque mode controller: The position mode controller framework. This framework takes the torque controller into account and extended it with the ability to output desired motor link angeles for the used SEA motors. The position mode control was validated and is, with a fast motor speed, capable of shifting the systems trajectory to a desired energy level on the modal oscillation. As the motor speed has a big influence, this factor needs to be kept in mind. The next step is the validation of the position control framework with a digital twin of the Bert leg in Gazebo. By this, a more detailed model of the Bert leg is tested with the control approach.

5.3 Controller application with a digital twin in Gazebo

The position control framework performed well in the task of stabilizing the modal oscillation for the leg model set up in Matlab. The modelling in matlab includes the main dynamics of the Bert leg. However, the dynamics and effect acting on the leg are much richer in real life. Therefore a digital twin was set up at the DLR in the past. With this digital twin, the computed nonlinear normal modes will be verified in the following section. Furthermore several tests will be done with the position mode controller evaluating the performance. In the end, some limitations of the controller are described and shown.

The Gazebo model is shown in Figure 5-7 seen from two different angles. The foot remains fixed to the ground due to the different dynamics when the leg is in the air. The foot is modelled as a ball joint. The parameters are the same as shown in Table 4-2. The body is illustrated by the white cube. The motors with the springs are modeled as a PD term.

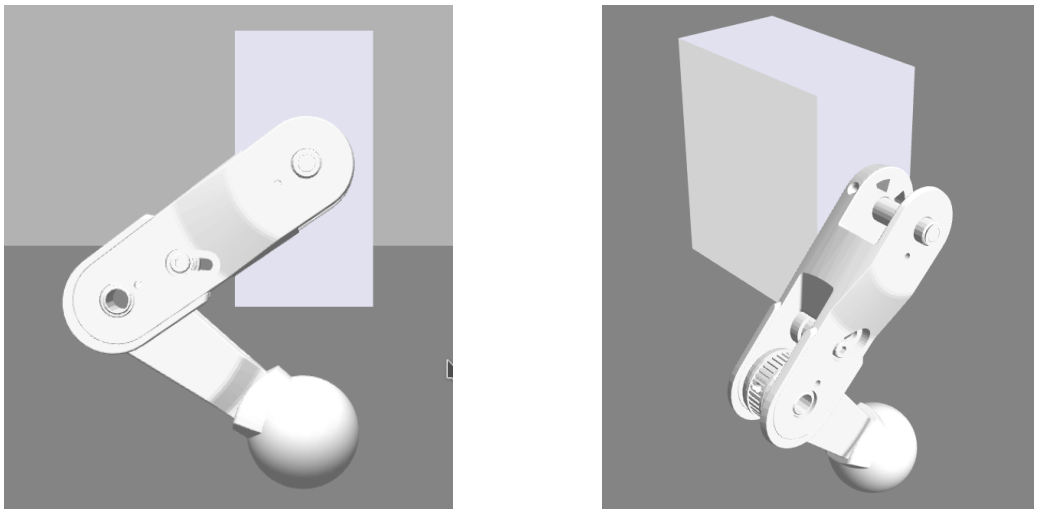

(a) *Portrait view of the leg* (b) *Sideview of the leg*

Figure 5-7: *Images of the physical 3D leg model of Bert in Gazebo presenting a refined idea of the set up.*

As a first step, the fit of the nonlinear normal mode, computed for the mathematical matlab model, needs to be verified with the Gazebo model. This is done by setting a generator point as the initial condition for the Gazebo model and releasing it. The result is shown in Figure 5-8. The plot on the left side shows the standard mode representation used in this work with the 2.3 s simulation trajectory colored time dependent. The Gazebo model is released from the initial condition on the generator denoted by the black marker. Corresponding to the resulting modal oscillation, the oscillation sequence of the leg model is illustrated on the right side of the figure. Here, the upper and lower generator state,

corresponding to the left plot, are shown as well as an interim state inbetween. The damping of the system is chosen to be zero for this test.

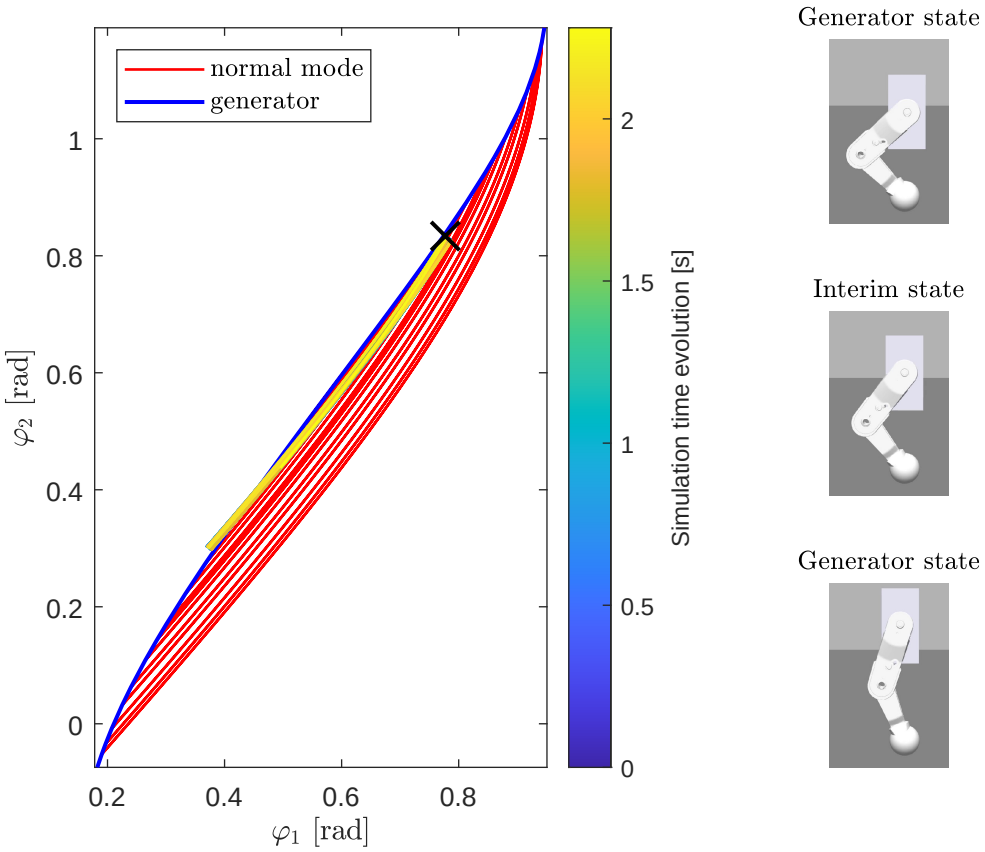

Figure 5-8: *Verification test for the fit of the computed nonlinear normal modes to the Gazebo model. The left plot shows the used normal mode and generator as well as the simulation time course. On the right side, the motion sequence of the leg model is illustrated with three states.*

The result of the test is that the computed nonlinear normal mode fits to the Gazebo model appropriately. Compared to the simulations in Matlab, a decrease fit of the time course on the mode can be observed. Though, the system oscillates along the mode with the possiblity to enhance the modal oscillation by the position mode controller next.

After the nonlinear normal modes are verified for the Gazebo model, the next point of interest is the position mode controller. The Gazebo model gets the desired spring equilibrium angles $\underline{\theta}_d$ as the input from the controller. As a first test for the controller, it is evaluated whether the controller is capable of initializing a modal oscillation for the Gazebo leg model out of the equilibrium position. This test was executed and the resulting trajectories are plotted in Figure 5-9. The top plot shows the release of the model out of the equlibrium as denoted by the black marker. The lower plot shows the trajectory of $\tau_{C,2}$, the overall desired input torque for joint two, as an example.

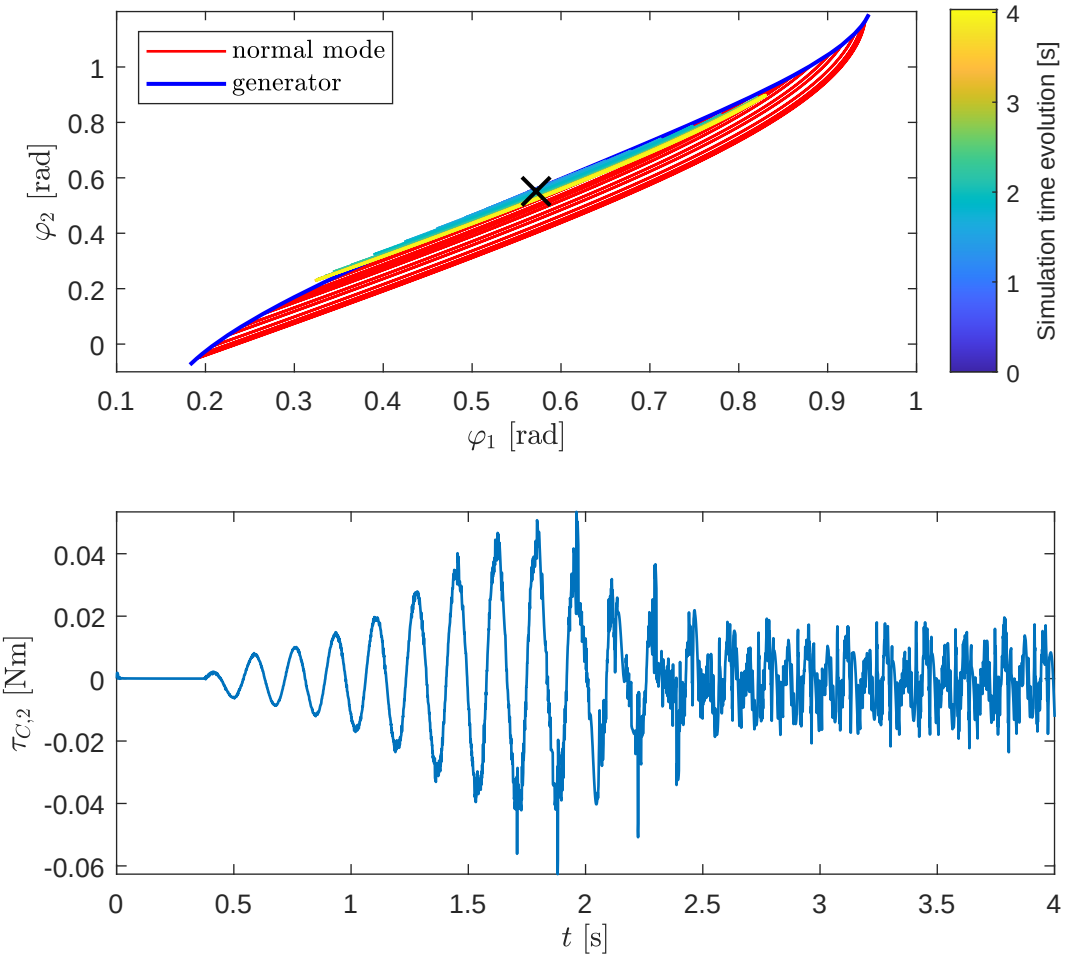

Figure 5-9: *Excitation of the modal oscillation by the position mode controller out of the equlibrium for the conservative system. The lower plot shows the desired torque input $\tau_{C,2}$ to the joint two. The torque is converted to a desired change in the motor angle of the second motor.*

By analyzing the figure above, it can be seen that the controller performs well in increasing the energy level to the desired energy level and keeping track of the nonlinear normal mode at the same time. Furthermore the matching energy seems to be reached at about $2.0-2.5\,\mathrm{s}$ as the controller torque largely decreases in this area. Only maximum controller torques of $0.015\,\mathrm{Nm}$ for the second joint are needed after the energy level is reached. This already is a first implication of the energy optimallity of the approach.

By analyzing the energy time course in more detail, more insights on the control frameworks behaviour during the process can be gained. Therefore another simulation is performed with a change in the desired energy during the simulation. Figure 5-10 shows the trajecories of the angles in the upper plot and the time course of the energy E and the

desired energy $\overline{E}$ in the lower plot. The desired energy is changed from 1 J to 0.8 J at 2 s and back to 2 s at 4.5 s.

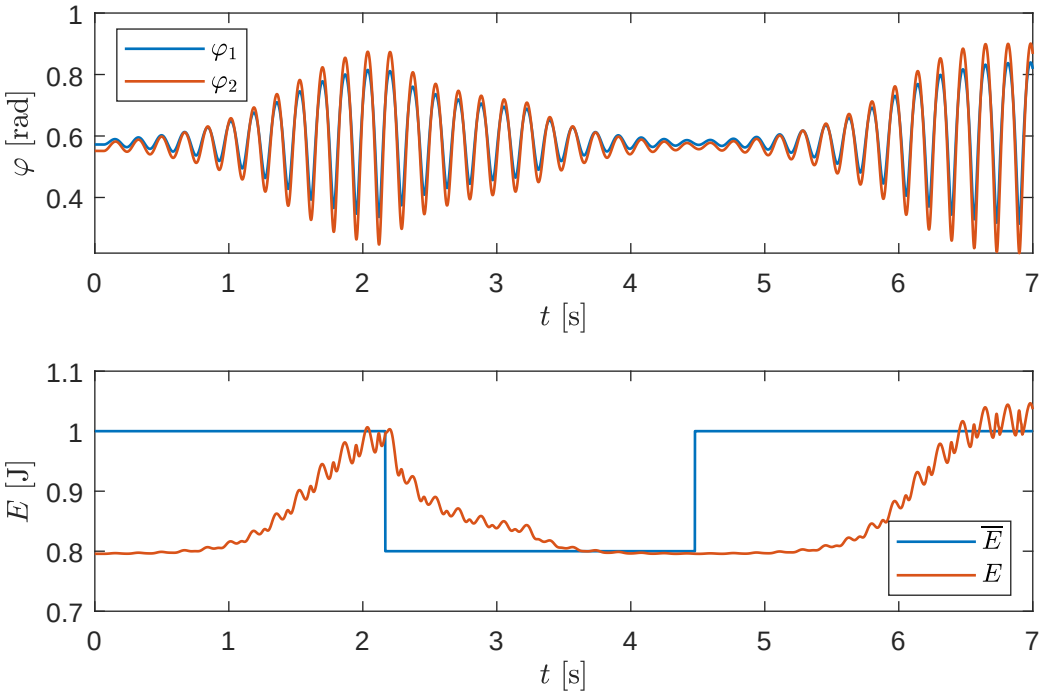

Figure 5-10: *Modal oscillation assured by the position mode controller with multiple changes in the desired energy resulting in smaller an larger oscillations of the angles dependent on the desired energy.*

In the upper plot, the decrease in the oscillation of the system is visible when decreasing the energy inbetween 2 s and 4.5 s. The lower plots indicates that at least 2 s are needed by the controller for an energy increase of 0.3 J. A decrease of the same amount of energy is faster with 1.5 s. Furthermore, it can be observed that it takes some time until the first changes of the energy occur resulting from the setting of the new desired energy. This is visible from 0 s to 1 s and from 4.5 s to 5.5 s. The decrease of energy does not need this lead time. This lead time behaviour for an energy increase might be caused by the controller parts counteracting. With the manifold stabilzer assuring the oscillation and the energy controller trying to increase the energy at a point where an increase would lead the trajecory far away from the manifold, this behaviour can be explained. Nevertheless, the controller is capable of establishing a given energy level for the system one after the other.

So far, only scenarios were analyzed where the state of the system has already been on the manifold. In real test scenarios it is possible though that the state of the Bert leg is far off the manifold. Therefore, it is now validated that the controller is capable of

assuring a modal oscillation with a given energy level when the system is released from a arbitrary configuration. The result for this test is shown in Figure 5-11. This figure shows the simulation trajectory on top of the normal mode and the generator at the top. The arbitrary release point is denoted by the black marker at the left top corner. The two lower plots show the energy time course and the time course of the distance of the state to the manifold.

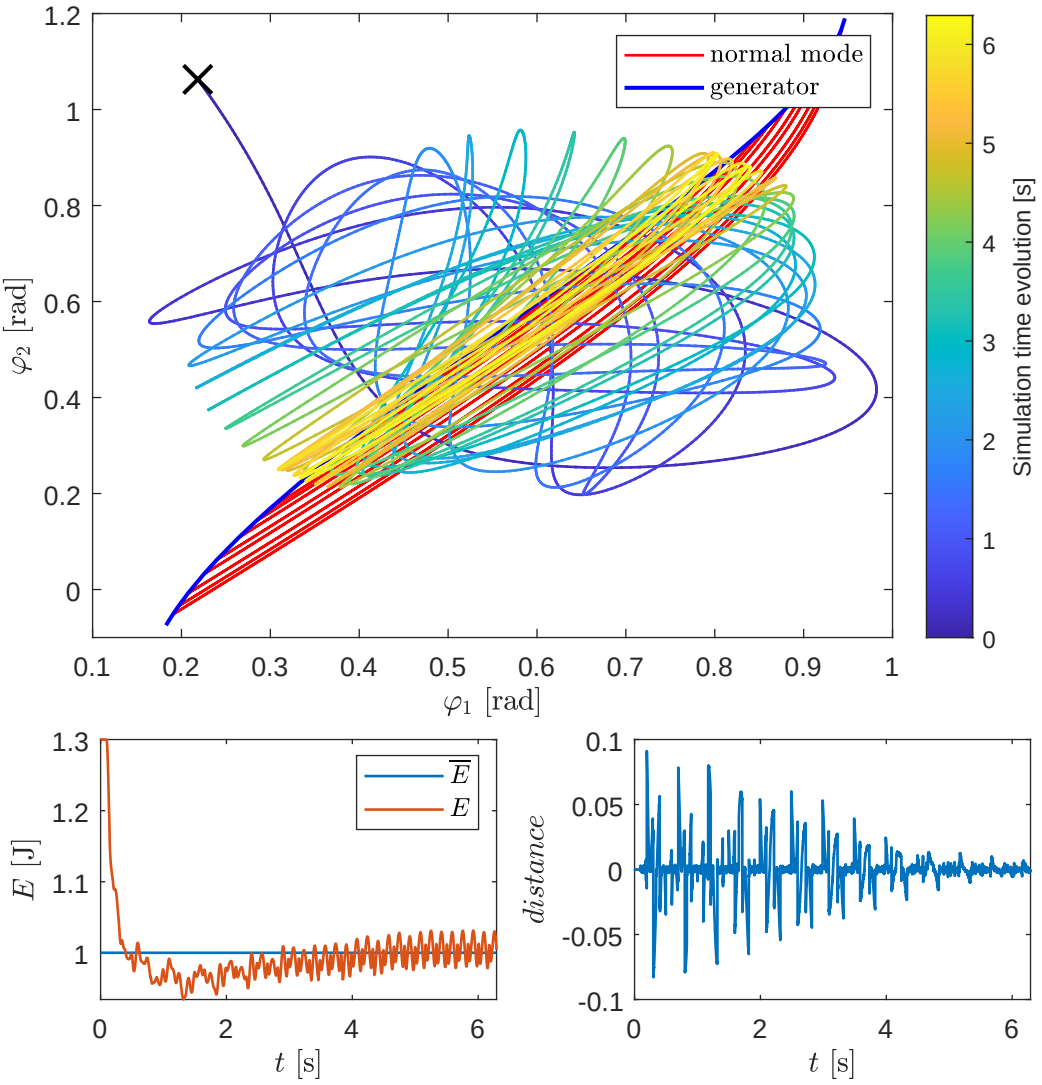

Figure 5-11: *Simulation result for a position mode controller test given the task to stabilize the desired modal oscillation from an arbitrary point far away from the nonlinear normal mode.*

The first observable behaviour of the system when released from this arbitrary point seems chaotic. Although the starting oscillations are far away from the mode, when looking at

the 5 s time mark, the modal oscillation is approached. This is among others indicated by the time course at the upper plot following the shape of the nonlinear normal mode. The two plots at the bottom indicate the steady approach of the desired modal oscillation as well. The distance to the manifold is continuously decreasing during the first 5 s reaching a low value almost equal to zero. Furthermore, the energy plot on the bottom left side shows a rapid decrease of the initially large energy of 1.3 J to the desired energy level of 1 J. However, there are some negative results such as the overshooting of the energy during the decrease and the ongoing steady oscillation around the desired target energy. The unsteady oscillation can also be observed in the mode plot at the top as the trajecory does not seem to approach a steady oscillation. To conclude, the controller was capable of shifting the state of the leg model to the manifold in a reasonable time of 5 s. Though, the resulting oscillation does not appear as steady on one modal oscillation of the mode as in the previous tests with the inital condition chosen to be a generator point.

Overall, it might cause problems that the trajectory is that chaotic when being shifted to the desired modal oscillation when released from an arbitrary point. To overcome this, the approach of an interception control as proposed in Section 3.4 could be used. By this, if a state far away from the manifold is detected, e.g. by a big *distance*, the controller could be switched to a trajectory tracking controller that leads the system to appoach and intercept the manifold with in a more desirable, i.e. less chaotic, way.

Other than choosing an arbitrary initial configuration for the system, the controller can also be investigated on choosing an initial configuration satisfying only one of the controller parts. This can be done by e.g. choosing a point with the desired energy but without matching the mode. This scenario is tested and presented in Figure 5-12. Here, the desired energy is added in the upper mode plot illustrating that the initial condition (black marker) already satisfied the energy controller. The only task for the position mode controller is in this case the shift to the mode. The lower plot shows the trajectory of the desired torques of both controller parts for joint one.

On the first view, the controller performed well on shifting the trajectory to the nonlinear normal mode as the trajectory is approaching the shape and the last oscillations end on the desired energy ellipse. By analysing the lower plot, the counteracting behaviour of the two controller parts is visible. At about 0.2 s, the trajectory of the manifold stabilizer part $\tau_{M,1}$ has a large peak in negative direction. Just about 0.01 s after this, the trajectory of the energy controller part $\tau_{E,1}$ has a peak in the positive direction. This behaviour of the manifold part giving a positive or negative peak torque with the energy part reacting in the opposite way slightly afterwards indicates counteracting. The energy was chosen correct at the beginning and as soon as the manifold stabilizer tries to shift the state to the manifold, the system is deviated from its (desired) energy level leading to a reaction of

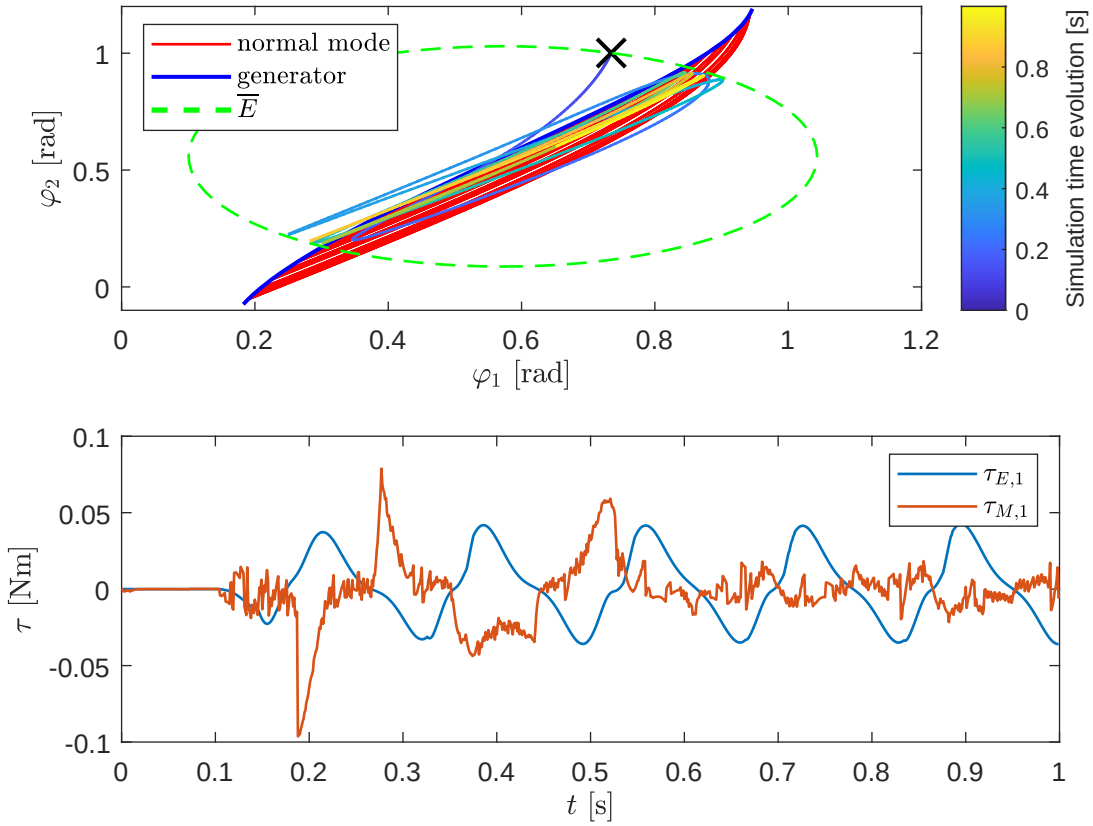

Figure 5-12: *Example situation where the initial condition was set to be on the desired energy level but the state is not on the nonlinear normal mode resulting in a trajectory adjustment towards the mode.*

the energy controller part. A solution to supress this behaviour would be a conservative manifold stabilizer. This means a adapted choosage of $\underline{\tau}_M$ in that way that it can not result in a change of the energy as this is only the task for the energy control part. With this restriction for the manifold stabilizer, in the scenario in the figure above, the system would never be deviated from its energy level by the manifold stabilizer. Resulting from this, the energy controller part does not desire any torques overall resulting in a improved energy efficiency. In summary, a conservative choosage of $\underline{\tau}_M$ could lead to an improved energy efficiency in situations where the state is already close to the desired energy level but not close to the nonlinear normal mode.

The last consideration of this thesis is the introduction of damping within the Gazebo leg model. So far, only the conservative leg model was taken into account but it is also interesting to investigate on the position mode controllers behaviour when damping is present. Therefore, a small damping coefficient of 0.003 $\mathrm{kgm^2s^{-1}}$ is chosen to evaluate on the controller. The results are plotted in Figure 5-13. Here, the modal oscillation is

illustrated in the top plot and the lower two plots show the energy trajectory and the torque trajectories of the controller parts for joint one.

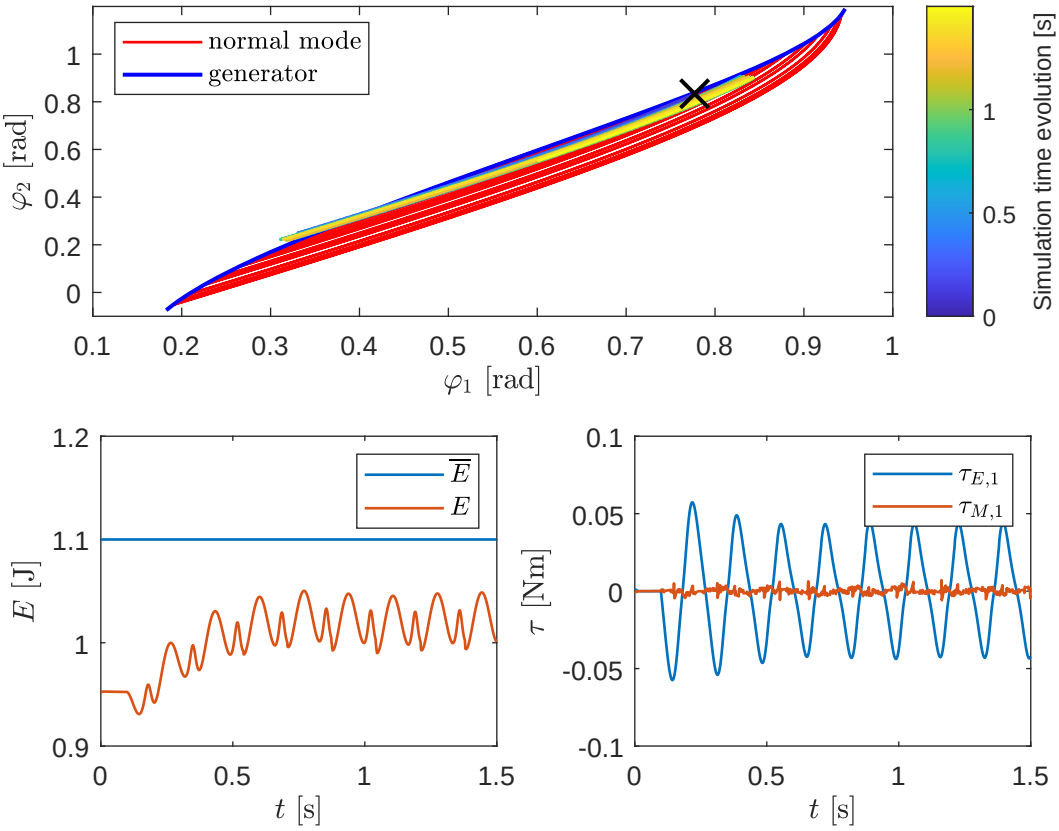

Figure 5-13: *Simulation result for an experiment with damping of* 0.003 $\mathrm{kgm^2s^{-1}}$ *being present within the leg model in Gazebo. The focus is on the evaluation of the controllers behaviour with the damping.*

As it can be seen in the figure, the controller increased the modal oscillation and stabilized it at a higher energy level. However, the energy level does not reach the desired level of 1.1 J in the lower left plot. This static offset is due to the damping and could be compensated by an increase in the energy controller integrator gain γ_I. The right plot shows that only the energy controller is giving a big torque which is reasonable as the trajectory is on the mode. By taking a deeper look it is visible that the energy controller is setteling a steady oscillation from 0.6 s on indicating that it is constantly acting agains the damping. These results appear to be reasonable and well explainable but also indicate that the controller framework needs extensions and adjustments to meet the requirement of full damping compensation. Furthermore, it does not seem to be enough to simply raise the controller gains as shown in the appendix A4. A raise of the controller gains results in an overshooting and vibrating behaviour. To overcome the damping, a feedforward

control should be used for a basic compensation. Though, this is not implemented in this thesis anymore. Overall, the controller is already capable to compensate damping until a certain extend, but if the damping is raised more realistically, the controller is reaching its limits without an addition to the control framework.

To conclude the validation of the position mode controller with the digital twin in Gazebo, it can be summarized that the controller is overall capable of initializing and keeping a modal oscillation. The computed nonlinear normal modes appear to be valid with minor deviations. A initialization of a modal oscillation out of the equlibrium was shown to be possible. Furthermore, changes of the desired energy were solved by the controller. In the end it was shown that the modal oscillation is ensured by the controller after a settling time when the system is released from an arbitrary configuration outside of the manifold. However, the oscillation was not perfectly steady anymore. Furthermore, some other improvements to the controller could be the conservative choosage of the manifold stabilizer torque and a feedforward damping compensation.

In summary, this chapter applied the torque mode controller, presented in Section 3.3 and developed in [BSAD22]. This controller showed a good performance on initializing and keeping a modal oscillation of the Bert leg model in Matlab. Furthermore, the control framework was extended to a position mode control framework to be able to output desired motor angles. The position mode controller was evaluated with the Matlab Bert leg model as well as with a digital twin in Gazebo. For both models, the controller performed well in the task to stabilize the desired modal oscillations. In future work, the controller could be extended by an interception control, a conservative controller part and a feedforward control to overcome its limitations.

6 Discussions and conclusions

The present thesis dealt with the problem of investigating the possibility to use intrinsic periodic motion patterns for a complex highly nonlinear system, the robotic test platform Bert. Within the work, the problem was specified to the consideration of one leg of the robot and framed with the definition of nonlinear normal modes. The first main part analyzed the nonlinear normal modes found for the Bert leg with a focus on parameter influences on the overall mode shapes and their usability. The second part established a position control framework for the Bert leg stabilizing modal oscillations on a desired energy level.

For the identification of the nonlinear normal modes, only a conservative system behaviour was considered. As damping and friction are present in hardware applications, the first analysis put special attention on the behaviour of the modal oscillation when damping is established in the model. As linear damping is smoothly decreasing the systems movement along the velocity, leading the system to its equilibrium, it was assumed priorly that the oscillation might stay on the normal mode until it stops at the equilibrium. This would have implied that no controller would be needed for some test rig experiments e.g. for observing nonlinear normal modes after releasing the system from its generator. However, it was shown by the distance plot in Figure 4-13 that the damping not only decreases the energy and leads the system to its equilibrium but it also deviates the system's trajectory from the normal mode. This result indicates that an oscillation on a normal mode, computed for a conservative system, needs to be ensured by a controller for a nonconservative system behaviour. It implies that observing a conservatively computed nonlinear normal mode in experiments with damping influenced test rigs can fail without a controller assuring the modal oscillation on every energy level. This underlines the need for a controller stabilizing the modal oscillations for the Bert leg.

Another important result of this thesis is the influence of the spring equilibria on the shape of the generators and normal modes with usability implications for the desired hopping motion of the leg. The spring equilibria were adjusted uniformly as well as independently and the resulting generator and mode shapes were analyzed. When changing the parameters of the system continuously with fixed step sizes, it was assumed that the shapes change continuously too. Though, the outcome of the analysis was different as the change of the generator and mode shapes appears to be volatile. For instance, the orientations of the generators in Figure 4-14 change by $\frac{\pi}{2}$ rad at some equilibrium points within one adjustment step. At the left bottom and right top edge the orientations suddenly change by π rad. Furthermore, especially for the last two mentioned example points, the overall shape (qualitative) differs from the previous points largely. This disproves the assump-

tion of a continuous change in the shape of the generators when continuously changing the spring equilibria. The sudden changes mostly appear when approaching the values of 0 rad, $\frac{\pi}{2}$ rad and π rad for at least one of the spring equilibria. One assumption is, that this behaviour might be caused by gravity when e.g. the overall equilibrium pose of the leg is shifted from the left to the right side of the base when adjusting the spring equilibria crossing 0 rad. Overall, when setting up experiments with different system parameters, a possible rapid change in the systems behaviour could be experienced and has to be kept in mind regarding expected outcomes.

Taking the aspect of changing generator shapes further, the resulting normal modes were analyzed concerning their usability for the desired hopping motion of the leg. For this, the spring equilibria were changed with equal values, respectively. It was expected to find one suitable normal mode out of Figure 4-16 for the hopping motion. Contrary to this assumption, when comparing the movement sequences of the five different shapes of normal modes emerged, it was found that for both manifolds, one normal mode could be found for each manifold that result in a hopping motion of the leg, respectively. For the choosage, the volatility can be applied as an argument, since the change of the normal mode shape is higher within Figure 4-16a compared to Figure 4-16b which implies the second manifold to be more suitable for experiments on the desired hopping motion. This analysis results in two outcomes: First, when comparing emerging manifolds of systems, it can be useful to evaluate the shapes of the manifolds regarding their volatility in parameter adjustments. But also second, even though one manifold appears to be more suitable and less volatil, it can still be reasonable to evaluate on the other manifold as the desired motions might also be found here, maybe in a smaller range of parameter sets and energy levels.

After the analysis of the nonlinear normal modes, the controller implementation and adjustment yielded valuable results in the stabilization of modes. The position controller successfully stabilized modal oscillations on a desired energy level with a given fast motor with a motor time constant of $T = 0.01$ s. However, the gains for the controller were adjusted optimally and the motor speed was chosen faster compared to realistic SEA motors. Both, the gain adjustment map in Figure **??** and the motor speed evaluation in Figure 5-5 show rapid increases in the objective function when choosing the gains or the motor constant suboptimal. In detail, the gain γ_P of the energy controller has a great impact on the control outcome when chosen higher or lower than the optimum leading the whole position control framework being highly dependent on the optimal choosage of the gain γ_P. For test rig experiments, this simulation result has to be carefully considered. Furthermore, a result is that the motor constant T has to be chosen less than 0.015 s to ensure a working position control. With regard to the real test rig and the slower motor constants

of the SEA motors, this result arises the feasibility question for the proposed position control when implemented at the real test rig with the currently used SEA motors.

As the Matlab position control framework showed the potential feasibility of the approach, next, a digital twin of the Bert leg was used in Gazebo. By connecting the position control to the leg in Gazebo, results emerged with the leg executing controlled modal oscillations, even with light linear damping of 0.003 kgm^2s^{-1}, validating the identified nonlinear normal modes as well as the overall position control approach. With the twin, a broader range of experiments was executed e.g., as shown in Figure 5-11, the inital condition was set with a big distance to the manifold which is realistic concerning the real test rig. Overall, it was assumed that the controller is capable of stabilizing a modal oscillation on a desired energy level. This assumption turned out to be correct. However, two problems occured that need to be adressed in further research. The first problem is the counteracting behaviour of the controller parts τ_M and τ_E. As shown in Figure 5-12, it could be observed that e.g. when starting at the right energy level but the state is not on the manifold, the manifold stabilizer part τ_M also changes the energy level of the system while adjusting the state to the manifold. This in turn results in the energy controller part τ_E reacting to the change of the energy level. If τ_M didn't change the energy level while adjusting the state, i.e. defining it as a conservative controller part, there would be no need of an additional energy input by τ_E. Therefore, in the future, τ_M has to be constrained to only provide input torques that don't change the energy level of the system as this is only the task for τ_E. Without the constraint, the behaviour of the two parts could be described as counteracting leading to a decrease of energy optimallity. The second problem that occured, is the overshooting behaviour of the controller. As the manifold stabilizer always uses the closest point of the manifold to calculate τ_M, the trajectory of the system is orthogonally shifted to the modal oscillation trajectories which leads to an overshooting of the desired mode. As an outlook, this problem could be adressed by an interception control as proposed in 3.4. By changing the mode control to a trajectory tracking control while the state has a big offset from the manifold, the state could be led to follow a desired trajectory approaching the normal mode with a suitable small angle and not orthogonally. Furthermore, an end point control could be set up, always guiding the state to the desired generator point with a velocity of zero, when the offset to the manifold is too big. Overall, with a conservative controller part τ_M and an additional interception control, the counteracting and overshooting behaviour of the mode controller can be adressed.

As the last part of the discussion and a further outlook, some aspects of the ongoing developement to the mode control of the whole robot are presented. This thesis ends with the sucessful validation of the position control approach with a digital twin of one leg of the robot Bert including light damping effects. To approach the overall goal of Bert

locomoting with its modal oscillations, adjustments and questions need to be made and answered. As mentioned in the beginning of the discussion, damping has a large influence on the modal oscillation. A solution for the damping difficulties of the position controller is a feedforward control, with the goal to eliminate disturbance quantities such as high damping. Though, this requires a precise model and measurement of the disturbance quantities which could be a goal for future work. As the friction and damping problems of the real one leg test rig are overcome, another evaluation has to be made on the flight phases of the leg when jumping. While in the air, the system characteristics are different in comparison to the setup with a foot fixed to the ground. Therefore, hybrid dynamics have to be considered leading to an increase in modelling and control complexity. If these problems are solved, the last step is the transition to the parallel usecase of the whole robot. Computing the nonlinear normal modes for parallel kinematics and developing a hybrid parallel position control approach for the alternating lifting of the legs further increases the overall complexity. Nevertheless, if the mentioned steps are done and the last transition to the parallel usecase is successful, the overall goal of using intrinsic periodic motion patterns for a complex highly nonlinear system as the robotic test platform Bert is reached.

Working towards this overall goal, this thesis contributed by identifying the nonlinear normal modes for one leg of the robot Bert. By analyzing the normal modes, advices were derived for choosing suitable parameters and deciding on the most usable modes for hopping motion. Furthermore, a position control framework was devloped for one leg of the robot Bert approaching the requirements of the one leg test rig and the whole robot. With continuing work and adjustments and by taking the mode analysis results and the position control framework into account, the research on the whole robot Bert was successfully further developed towards the use of intrinsic dynmaics, namely the nonlinear normal modes, for energy optimal robotic locomotion.

Bibliography

[AD20] Albu-Schäffer, A.; Della Santina, C.: A review on nonlinear modes in conservative mechanical systems. *Annual Reviews in Control* 50 (2020), pp. 49–71

[ALS21] Albu-Schaffer, A.; Lakatos, D.; Stramigioli, S.: Strict Nonlinear Normal Modes of Systems Characterized by Scalar Functions on Riemannian Manifolds. *IEEE Robotics and Automation Letters* 6 (2021), no. 2, pp. 1910–1917

[BSAD22] Bjelonic, F.; Sachtler, A.; Albu-Schäffer, A.; Della Santina, C.: Experimental Closed-Loop Excitation of Nonlinear Normal Modes on an Elastic Industrial Robot. *IEEE Robotics and Automation Letters* 7 (2022), no. 2, pp. 1689–1696

[CDGA22] Calzolari, D.; Della Santina, C.; Giordano, A. M.; Albu-Schaffer, A.: Single-Leg Forward Hopping via Nonlinear Modes. *2022 American Control Conference (ACC)*. 2022, pp. 506–513

[DA21] Della Santina, C.; Albu-Schaeffer, A.: Exciting Efficient Oscillations in Nonlinear Mechanical Systems Through Eigenmanifold Stabilization. *IEEE Control Systems Letters* 5 (2021), no. 6, pp. 1916–1921

[DCGA21] Della Santina, C.; Calzolari, D.; Giordano, A. M.; Albu-Schaffer, A.: Actuating Eigenmanifolds of Conservative Mechanical Systems via Bounded or Impulsive Control Actions. *IEEE Robotics and Automation Letters* 6 (2021), no. 2, pp. 2783–2790

[Del11] Deleanu, D.: The dynamics of a double pendulum: Classic and modern approach. *Dunarea De Jos - University of Galati* 3 (2011), pp. 203–212

[DLBA] Della Santina, C.; Lakatos, D.; Bicchi, A.; Albu-Schäffer, A.: *Using Nonlinear Normal Modes for Execution of Efficient Cyclic Motions in Articulated Soft Robots*

[DLBA19] Della Santina, C.; Lakatos, D.; Bicchi, A.; Albu-Schaeffer, A.: Exact Modal Characterization of the Non Conservative Non Linear Radial Mass Spring System. *2019 International Conference on Robotics and Automation (ICRA)*. 2019, pp. 3101–3107

[DLR22] DLR - Institut für Robotik und Mechatronik: *Bert*. 2022. `https://www.dlr.de/rm/desktopdefault.aspx/tabid-11826/#gallery/32812` (visited on 04/05/2022)

[Faj13] Fajen, B. R.: Guiding locomotion in complex, dynamic environments. *Frontiers in behavioral neuroscience* 7 (2013), p. 85

[Fli09] Fliessbach, T.: *Mechanik: Lehrbuch zur Theoretischen Physik*. 6. Aufl. 2009. Heidelberg: Spektrum Akademischer Verlag, 2009

[GH10] Geyer, H.; Herr, H.: A muscle-reflex model that encodes principles of legged mechanics produces human walking dynamics and muscle activities. *IEEE transactions on neural systems and rehabilitation engineering : a publication of the IEEE Engineering in Medicine and Biology Society* 18 (2010), no. 3, pp. 263–273

[GR14] Gan, Z.; Remy, C. D.: A passive dynamic quadruped that moves in a large variety of gaits. *IEEE/RSJ International Conference on Intelligent Robots and Systems (IROS), 2014*. Piscataway, NJ, 2014, pp. 4876–4881

[GR15] Gan, Z.; Remy, C. D.: *Passive Dynamic Quadrupedal Model Explain a Large Variety of Gaits*. Ed. by Roboticsand Motion Laboratory. 2015.

[HT81] Hoyt, D. F.; Taylor, C. R.: Gait and the energetics of locomotion in horses. *Nature* 292 (1981), no. 5820, pp. 239–240

[Kha00] Khalil, H. K.: *Nonlinear systems*. Internat. ed., 3. ed. Upper Saddle River, NJ: Pearson Education Internat, 2000

[LAH02] Lenord, O.; Albiez, J. C.; Hiller, M.: Virtual Prototyping of the Four-Legged Walking Machine BISAM. Ed. by International Conference on Climbing and Walking Robots. Vol. 5. 2002

[LFA17] Lakatos, D.; Friedl, W.; Albu-Schaffer, A.: Eigenmodes of Nonlinear Dynamics: Definition, Existence, and Embodiment into Legged Robots with Elastic Elements. *IEEE Robotics and Automation Letters* (2017)

[LP17] Lynch, K. M.; Park, F. C.: *Modern robotics: Mechanics, planning and control*. Cambridge UK: Cambridge University Press, 2017.

[LPL+18] Lakatos, D.; Ploeger, K.; Loeffl, F.; Seidel, D.; Schmidt, F.; Gumpert, T.; John, F.; Bertram, T.; Albu-Schaffer, A.: Dynamic Locomotion Gaits of a Compliantly Actuated Quadruped With SLIP-Like Articulated Legs Embodied in the Mechanical Design. *IEEE Robotics and Automation Letters* 3 (2018), no. 4, pp. 3908–3915

[LTA20] Li, L.; Tokuda, I.; Asano, F.: Energy-Efficient Locomotion Generation and Theoretical Analysis of a Quasi-Passive Dynamic Walker. *IEEE Robotics and Automation Letters* 5 (2020), no. 3, pp. 4305–4312

[Mat22] MathWorks: *Solve nonlinear least-squares (nonlinear data-fitting) problems - MATLAB lsqnonlin - MathWorks Deutschland*. 26.10.2022. `https://de.mathworks.com/help/optim/ug/lsqnonlin.html` (visited on 10/26/2022)

[McK90] McKenna, M. A.; Zeltzer, D. L. (supervisor): *A dynamic model of locomotion for computer animation*. Master Thesis. Cambridge, Massachusetts, USA: Massachusetts Institute of Technology, 1990.

[MLS94] Murray, R. M.; Li, Z.; Sastry, S. S.: *A mathematical introduction to robotic manipulation*. London: CRC Press, 1994.

[NGGP08] Naranjo, J. E.; Gonzalez, C.; Garcia, R.; Pedro, T. de: Lane-Change Fuzzy Control in Autonomous Vehicles for the Overtaking Maneuver. *IEEE Transactions on Intelligent Transportation Systems* 9 (2008), no. 3, pp. 438–450

[PD19] Pott, A.; Dietz, T.: *Industrielle Robotersysteme: Entscheiderwissen für die Planung und Umsetzung wirtschaftlicher Roboterlösungen*. Wiesbaden: Springer Vieweg, 2019

[Ros60] Rosenberg, R. M.: Normal Modes of Nonlinear Dual-Mode Systems. *Journal of Applied Mechanics* 27 (1960), no. 2, pp. 263–268

[RTLZ00] Rajamani, R.; Tan, H.-S.; Law, B. K.; Zhang, W.-B.: Demonstration of integrated longitudinal and lateral control for the operation of automated vehicles in platoons. *IEEE Transactions on Control Systems Technology* 8 (2000), no. 4, pp. 695–708

[SA22] Sachtler, A.; Albu-Schaffer, A.: Strict Modes Everywhere – Bringing Order Into Dynamics of Mechanical Systems by a Potential Compatible With the Geodesic Flow. *IEEE Robotics and Automation Letters* 7 (2022), no. 2, pp. 2337–2344

[SGSA22] Schmidt, A.; Gumpert, T.; Schreiber, S.; Albu-Schäffer, A.: *Practical Approach to Characterize Realistic Motor Dynamics for Robotic Simulation Independent of the Use Case*. 2022.

[Sha90] Shadwick, R. E.: Elastic energy storage in tendons: mechanical differences related to function and age. *Journal of applied physiology (Bethesda, Md. : 1985)* 68 (1990), no. 3, pp. 1033–1040

[Tay85] Taylor, C. R.: Force development during sustained locomotion: a determinant of gait, speed and metabolic power. *The Journal of experimental biology* 115 (1985), pp. 253–262

[TZFS04] Tedrake, R.; Zhang, T. W.; Fong, M.-f.; Seung, H. S.: Actuating a simple 3D passive dynamic walker. *IEEE International Conference on Robotics and Automation, 2004. Proceedings. ICRA '04. 2004*. 2004, 4656–4661 Vol.5

[WB05] Weck, M.; Brecher, C.: *Maschinenarten und Anwendungsbereiche*. 6., neu bearb. Aufl. Vol. 1. VDI-Buch. Berlin: Springer, 2005

[WSH04] Wisse, M.; Schwab, A. L.; Helm, F. C. T., van der: Passive dynamic walking model with upper body. *Robotica* 22 (2004), no. 6, pp. 681–688

[XYR16] Xi, W.; Yesilevskiy, Y.; Remy, C. D.: Selecting gaits for economical locomotion of legged robots. *The International Journal of Robotics Research* 35 (2016), no. 9, pp. 1140–1154

[ZSR19] Zhao, H.; Straub, D.; Rothkopf, C. A.: The visual control of interceptive steering: How do people steer a car to intercept a moving target? *Journal of vision* 19 (2019), no. 14, p. 11

[ZW17] Zhao, H.; Warren, W. H.: Intercepting a moving target: On-line or model-based control? *Journal of vision* 17 (2017), no. 5, p. 12

Appendix

Contents

A1 Slider crank simulation results

Figure A1-1 shows one simulation result of the Slider Crank with parameters from 4-1. The only difference is the spring stiffness that was chosen to be 100 here. The plots show the angel φ_1 on the left side which is directly obtained by the state vector. The plot in the middle shows the trajectory of φ_2 and the plot on the right shows s. Both variables can be expressed with φ_1 and are therefore calculated in a second step after the simulation.

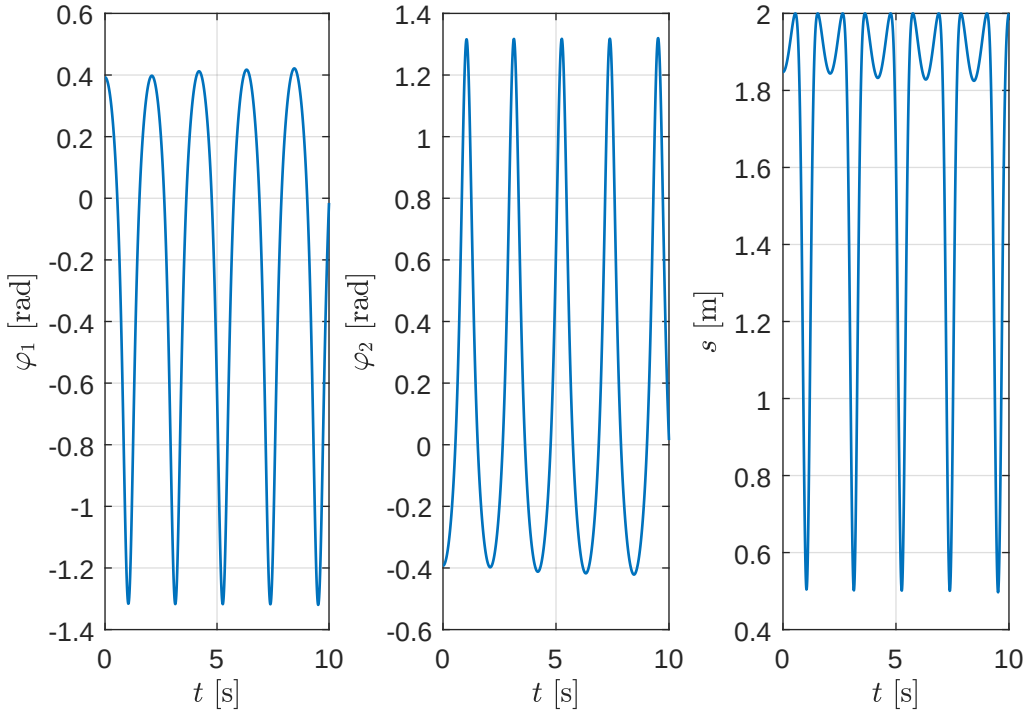

Figure A1-1: *Simulation results of the slider crank. They show the kinematic relations and the possiblity to obtain all variable trajectories even though the dynamics have been defined only with the angle* φ_1.

A2 Spring equilibrium, eigenmode shapes and resulting leg motion

The figures A2-1, A2-2 and A2-3 show the analysis of the mode shapes for different choices of the spring equilibrium position k_{eq}. The results shown here are not usable for the usecase of a translational hopping motion of the Bert leg.

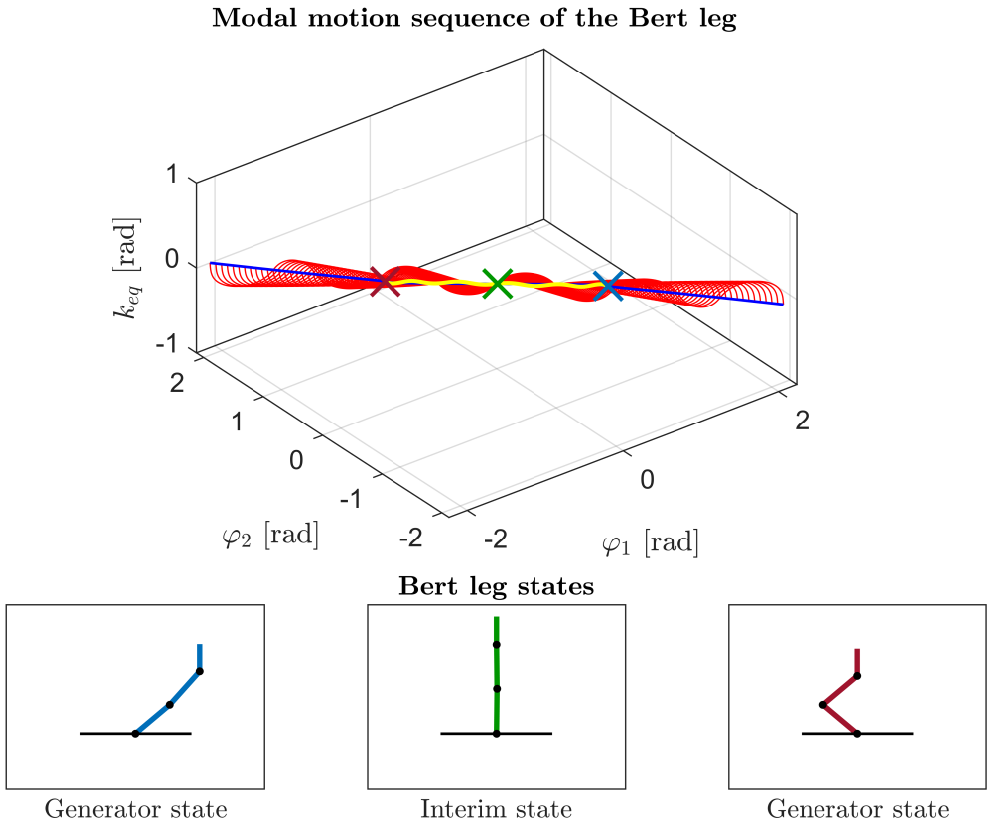

Figure A2-1: *Illustrational motion sequence of the one leg test rig oscillating on the eigenmode of manifold one resulting from choosing* $k_{eq} = 0\ \mathrm{kgs}^{-2}$.

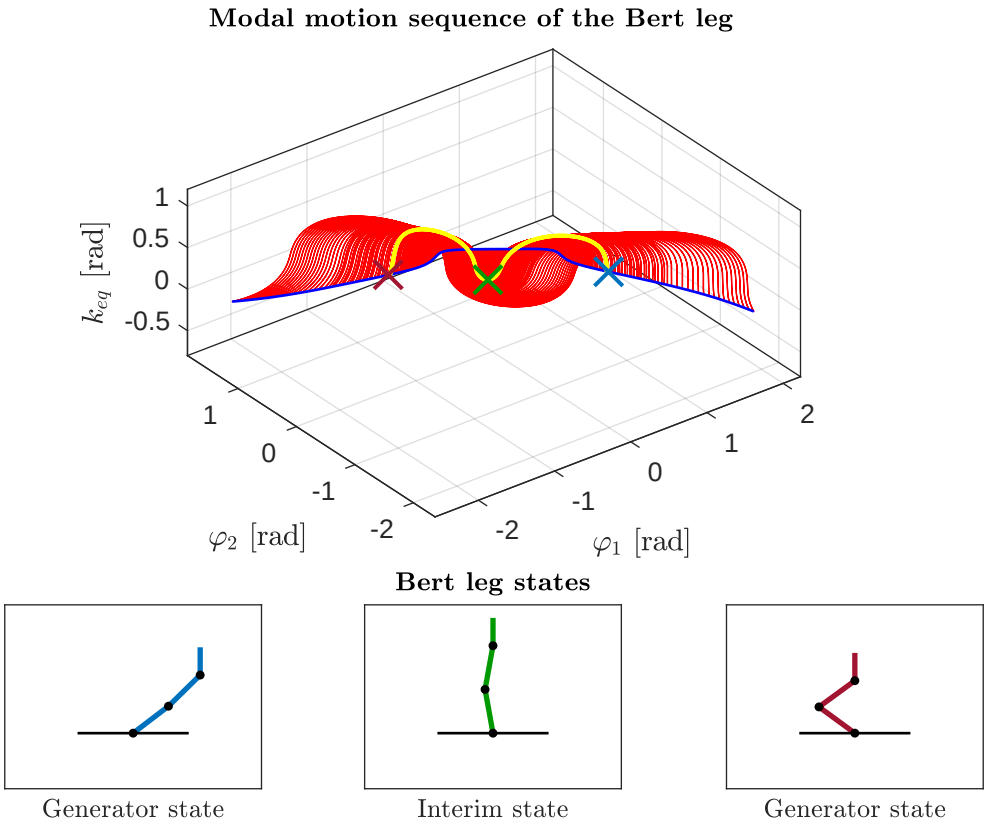

Figure A2-2: *Illustrational motion sequence of the one leg test rig oscillating on the eigenmode of manifold one resulting from choosing* $k_{eq} = 0.2\,\mathrm{kgs}^{-2}$.

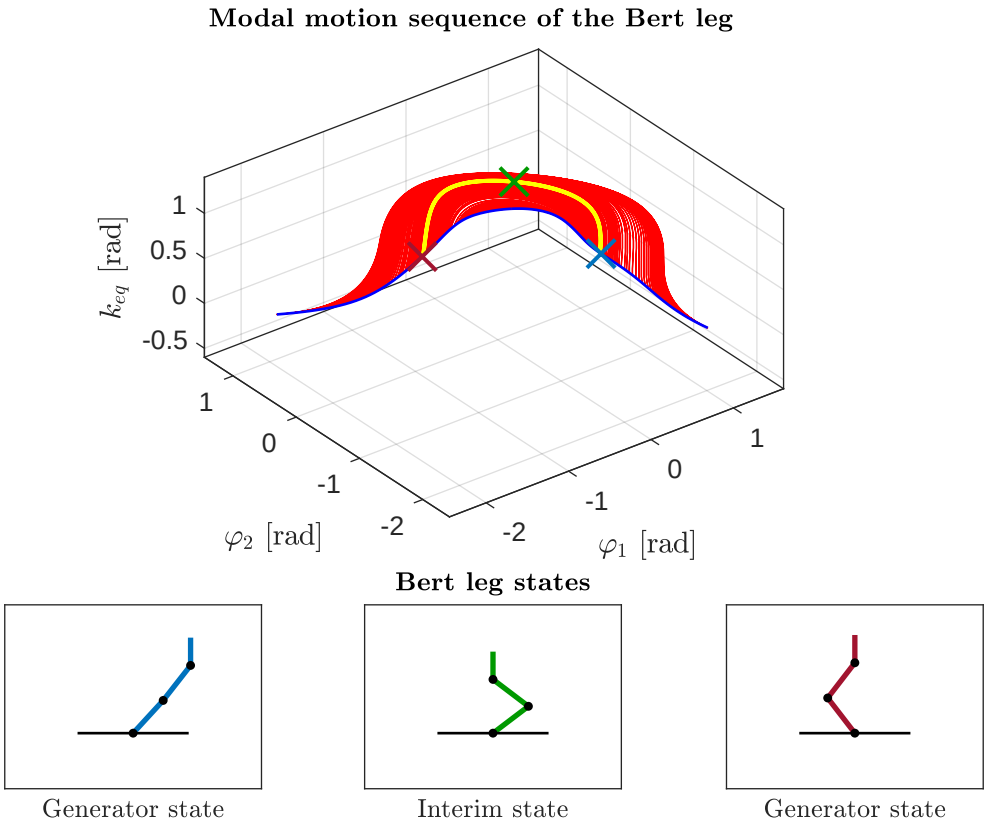

Figure A2-3: *Illustrational motion sequence of the one leg test rig oscillating on the eigenmode of manifold one resulting from choosing* $k_{eq} = 0.4\ \mathrm{kgs}^{-2}$.

A3 Controller gains map for the position mode controller

Figure A3-1 shows the controller gains map for the optimization of the position controller. The map supported the choice of suitable controller gains with the objective function. The objective function value is shown on the $z-$axis, the gain α_D is plotted on the $x-$axis and the gain γ_P is shown on the $y-$axis.

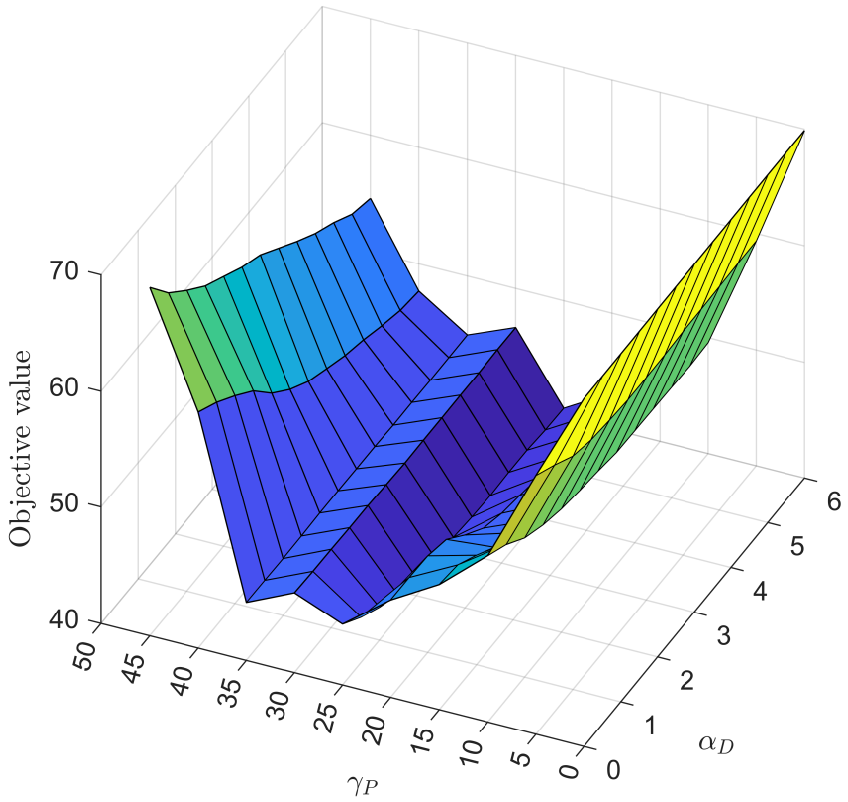

Figure A3-1: *The controller gains map with the objective function values resulting for the example situation when the position controller is used.*

A4 Controller limitation with the highly damped system

Figure A4-1 shows that the controller is not capable of stabilizing a modal oscillation for the highly damped system as the trajectory leaves the normal mode resulting in even higher input torques (bottom right plot). Furthermore, the desired energy is largely overshot.

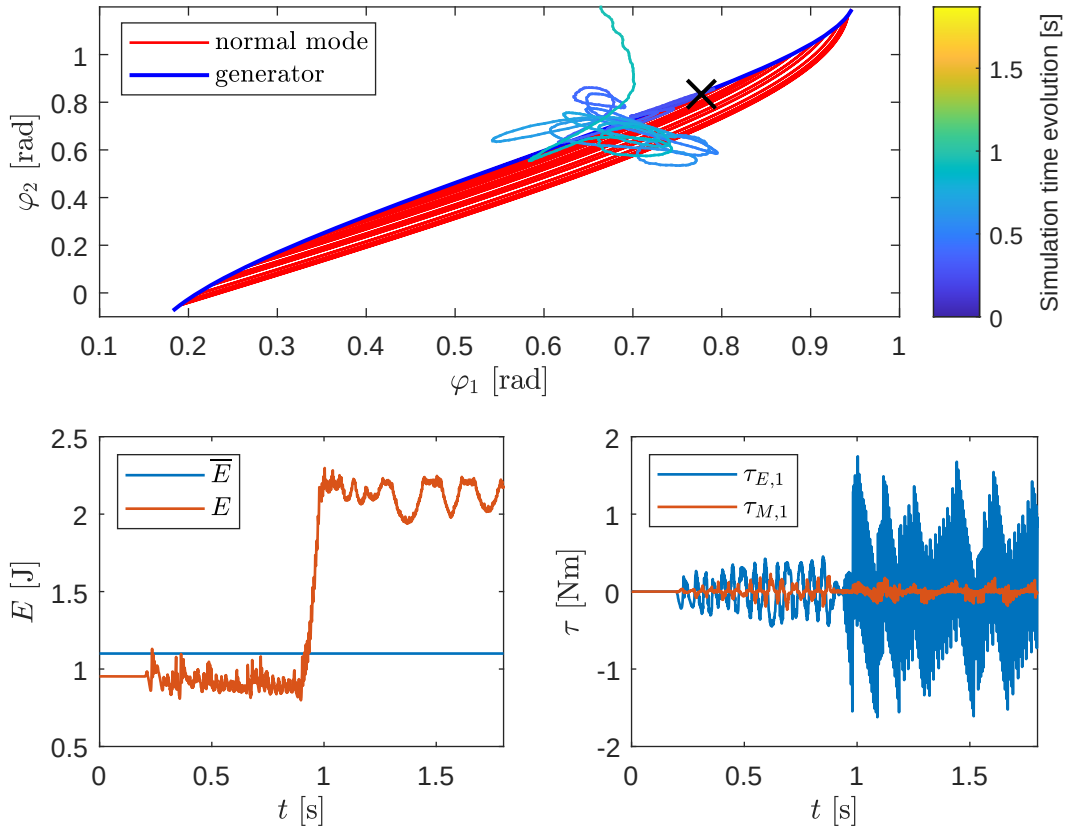

Figure A4-1: *Example simulation with increased gains resulting in a vibrating and highly overshooting behaviour of the highly damped system.*